NASA/CR—2001-211136/REV1

Broadband Noise of Fans—With Unsteady Coupling Theory to Account for Rotor and Stator Reflection/Transmission Effects

Donald B. Hanson, Consultant
Pratt & Whitney, East Hartford, Connecticut

December 2003

The NASA STI Program Office . . . in Profile

Since its founding, NASA has been dedicated to the advancement of aeronautics and space science. The NASA Scientific and Technical Information (STI) Program Office plays a key part in helping NASA maintain this important role.

The NASA STI Program Office is operated by Langley Research Center, the Lead Center for NASA's scientific and technical information. The NASA STI Program Office provides access to the NASA STI Database, the largest collection of aeronautical and space science STI in the world. The Program Office is also NASA's institutional mechanism for disseminating the results of its research and development activities. These results are published by NASA in the NASA STI Report Series, which includes the following report types:

- TECHNICAL PUBLICATION. Reports of completed research or a major significant phase of research that present the results of NASA programs and include extensive data or theoretical analysis. Includes compilations of significant scientific and technical data and information deemed to be of continuing reference value. NASA's counterpart of peer-reviewed formal professional papers but has less stringent limitations on manuscript length and extent of graphic presentations.

- TECHNICAL MEMORANDUM. Scientific and technical findings that are preliminary or of specialized interest, e.g., quick release reports, working papers, and bibliographies that contain minimal annotation. Does not contain extensive analysis.

- CONTRACTOR REPORT. Scientific and technical findings by NASA-sponsored contractors and grantees.

- CONFERENCE PUBLICATION. Collected papers from scientific and technical conferences, symposia, seminars, or other meetings sponsored or cosponsored by NASA.

- SPECIAL PUBLICATION. Scientific, technical, or historical information from NASA programs, projects, and missions, often concerned with subjects having substantial public interest.

- TECHNICAL TRANSLATION. English-language translations of foreign scientific and technical material pertinent to NASA's mission.

Specialized services that complement the STI Program Office's diverse offerings include creating custom thesauri, building customized data bases, organizing and publishing research results . . . even providing videos.

For more information about the NASA STI Program Office, see the following:

- Access the NASA STI Program Home Page at ***http://www.sti.nasa.gov***

- E-mail your question via the Internet to help@sti.nasa.gov

- Fax your question to the NASA Access Help Desk at 301–621–0134

- Telephone the NASA Access Help Desk at 301–621–0390

- Write to:
  NASA Access Help Desk
  NASA Center for AeroSpace Information
  7121 Standard Drive
  Hanover, MD 21076

NASA/CR—2001-211136/REV1

Broadband Noise of Fans—With Unsteady Coupling Theory to Account for Rotor and Stator Reflection/Transmission Effects

Donald B. Hanson, Consultant
Pratt & Whitney, East Hartford, Connecticut

Prepared under Contract NAS3–27727, AST Task 13

National Aeronautics and
Space Administration

Glenn Research Center

December 2003

Acknowledgments

This work was supported under Contract NAS3–27727 (AST Task 13) from NASA Glenn Research Center with Dennis Huff as contract monitor. The author wishes to thank NASA, Professor Stewart Glegg of Florida Atlantic University, and Dr. Ramons Reba of the United Technologies Research Center. Professor Glegg provided the harmonic cascade code used for the isolated blade row response calculations. In addition to his acoustic response theory, which had been supplied previously, he provided a new analysis that was required for the vortical wave response. Furthermore, Professor Glegg provided considerable support in assuring correct application of his theory. Dr. Reba gave invaluable help in adapting Professor Glegg's Matlab codes to Fortran, checking against available 2-D methods, and modifying the Wiener-Hopf techniques for improved efficiency in the present application.

Document Change History

This printing, numbered as **NASA/CR—2001-211136/REV1, December 2003,** replaces the previous version, **NASA/CR—2001-211136, November 2001**. It contains the following changes:

Equations 2.16, 6.2, and 7.19 were revised.

Equations 7.20 and 7.21 were added.

Equations 7.22, 7.38, 7.39, 7.40, 7.41, 7.42, 7.43, 7.44, and 7.45 equation numbers were changed and the contents revised.

Equations A-18, A-63, A-65, A-67, B-30, and B-31 were revised.

The text on pages 29, 45, and 48 was changed for clarity.

Figures 18–24 were revised.

Available from

NASA Center for Aerospace Information
7121 Standard Drive
Hanover, MD 21076

National Technical Information Service
5285 Port Royal Road
Springfield, VA 22100

Available electronically at http://gltrs.grc.nasa.gov/GLTRS

TABLE OF CONTENTS

SUMMARY

In the fan stage of a turbofan engine, broadband noise is generated by turbulent flow impinging on rotor and stator leading edges and by turbulence passing over trailing edges. This report provides an analytical model for prediction of the leading edge sources at both the rotor and stator. Whereas previous modeling treated rotors and stators as isolated blade rows (thereby ignoring reflection/transmission effects of neighboring blade rows), the analysis herein addresses broadband noise generation in a fully coupled environment. Modal scattering by the stator and mode/frequency scattering by the rotor are included in the acoustic/vortical coupling. This brings in the mode trapping physics previously included only in analyses of tone noise. Rotors and stators are treated as rectilinear cascades immersed in a mean flow that is constant in the spanwise direction. The cascade response theory recognizes 3D perturbations so that a true 3D turbulence spectrum can be used for excitation. Flow turning at both blade rows is handled by unsteady actuator disk theory based on the 4 linearized equations for conservation of mass and momentum.

If each acoustic mode/frequency combination were coupled to all others, the coupling analysis would be unmanageable. However, in developing the analysis, an important principle was discovered. The set of all participating modes divides itself naturally into many mode sub-sets that only couple within themselves. This property of "independent mode sub-sets" makes the broadband problem tractable and is the basis for the analysis. It was found that simple modal averaging techniques can be applied to eliminate many of these sub-sets from calculations and thereby save considerable computational effort.

This report presents the derivation of the coupling theory in detail and provides documentation for the associated computer code CupBB. Computed results show that accounting for coupling to adjacent blade rows adds considerably to downstream noise and increases the predicted split (or differential) between upstream and downstream sound power. Effects are large enough to indicate that absolute level predictions in the future should include the coupling physics.

The broadband coupling method developed here can be adapted to CFD procedures in the future. Lessons learned regarding modal sub-sets and modal averaging will carry over with little modification.

SECTION 1
INTRODUCTION

Fan noise is generated when flow non-uniformities interact with rotor blades and stator vanes as suggested in Figure 1. Sources can be classified into leading or trailing edge types. Leading edge sources include rotor inflow disturbances such as inlet distortion, atmospheric turbulence, and duct boundary layer turbulence. Stator inflow disturbances are primarily from the rotor wake and endwall flow. Trailing edge noise (also called self noise) is generated when turbulence in a blade or vane boundary layer interacts with a trailing edge. Fan noise can be further classified into tones or broadband as indicated in Figure 2. Tone noise is generated when the rotor interacts with a fixed flow distortion and when the stator interacts with the periodic

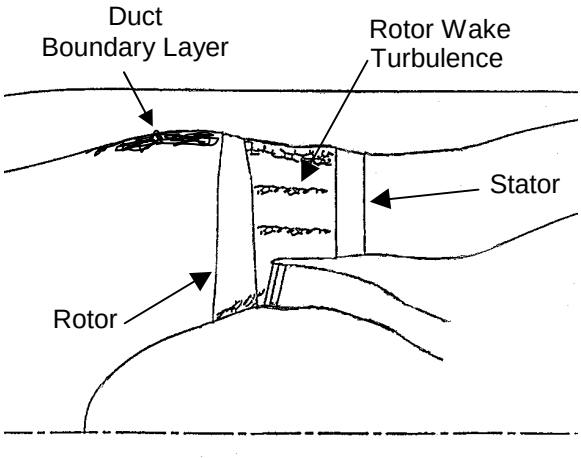

Fgure 1. Noise generation in a turbofan by turbulence in rotor wakes impinging on stator.

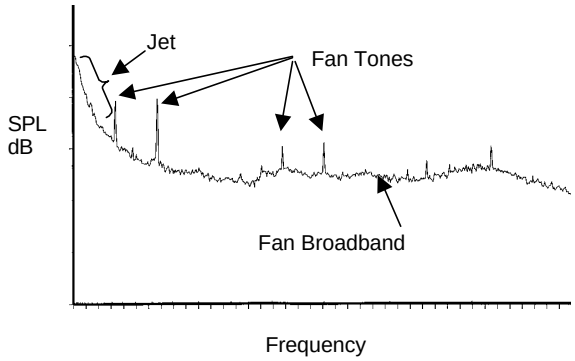

Figure 2. Fan noise spectrum showing major contributing sources.

component of the rotor wakes. This report is concerned with broadband noise caused by turbulence. The focus herein is on leading edge sources although the coupling methodology could be extended to trailing edge sources (self noise) as well.

Modeling for turbulence leading edge noise dates back at least to the early 1960's when simple estimates were made of overall noise based on turbulence intensity. No spectral distributions could be made with those early models. In the ensuing years, broadband modeling has become increasingly sophisticated with inclusion of spectral shapes, non-compactness, 3 dimensionality, and cascade effects. However, all of the preceding modeling treated noise generation by an isolated blade row only. For example, in noise generation at the stator in Figure 1, the only role of the rotor would be to generate turbulent wakes. Effects of acoustic reflection and transmission were ignored in earlier work.

The purpose of this report is to provide a first look at the effects a neighboring blade row on broadband noise generation. For noise generation at the stator, rotor reflection and transmission loss are obviously issues to consider. However, the report goes beyond that by including full unsteady coupling of the pressure and vortical waves between a rotor and stator. In addition to reflection and transmission losses at both blade rows, this accounts for mode and frequency scattering and mode trapping.

This report is an extension of previous work by the author: Reference 1 treats coupled rotor/stator tone interaction in 2D; References 2 and 3 analyze broadband noise generated by isolated rotors and stators. The present report combines these 2 methodologies in a coupled broadband model that has been coded as CupBB. This work has been enabled by the appearance of a harmonic cascade theory by Glegg (ref. 4) that this report adapts to the broadband problem. Glegg's theory accounts for inflow disturbances with wavenumber in all 3 coordinate directions; hence, 3D turbulence can be represented rigorously.

In the following, Section 2 presents background on the tone theory for coupled cascades and on the broadband theory for isolated cascades. It then outlines the strategy for combining these into the coupled broadband model. Section 3 summarizes the equations to be solved for the mean and unsteady flow. Section 4 develops the concept of "independent mode sub-sets" that facilitates the analysis. Sections 5 and 6 derive the coupling equations. Section 7 solves the coupled equations for the broadband application and shows how they are driven by a turbulence spectrum. Section 8 provides some verification of the new theory and presents sample calculations of sound power spectra to establish the importance of coupling effects. Section 9 gives some concluding remarks. Appendices A and B show how Glegg's theory is adapted to the current application. Appendix C derives equations for unsteady actuator disks used to represent flow turning at the rotor and stator. Finally, Appendix D provides a list of notation.

SECTION 2
BACKGROUND & STRATEGY FOR COUPLED BROADBAND THEORY

This section provides brief reviews of earlier theories for tone noise generation in a coupled rotor/stator environment and for broadband noise from an isolated rotor or stator. Then the strategy is outlined for combining these methodologies into the coupled broadband prediction scheme.

Review of Coupled Tone Method

Reference 1 presents a 2D scheme for coupling a rotor and stator modeled by flat plates as in Figure 3. The rotor sends acoustic and vortical waves to the stator and the stator sends acoustic waves to the rotor in a full unsteady coupling. Excitation of the system was via the periodic component of the rotor wake. It was found for certain vane/blade ratios that the blade passing frequency component of the wake produced high levels of 2×BPF and 3×BPF noise through frequency scattering at the rotor and trapping of the fundamental interaction mode between rotor and stator. After developing the coupling scheme via 2D modeling, it was extended to quasi 3D in Ref. 5 and is used at Pratt & Whitney for fan tone prediction in TFaNS, the Theoretical Fan Noise Prediction System. We will outline operation of the system in a 2 dimensional context but readers interested in details should consult Refs. 1 and 5. The coupling scheme is re-derived later in this report for broadband application so that this report does not depend on the references.

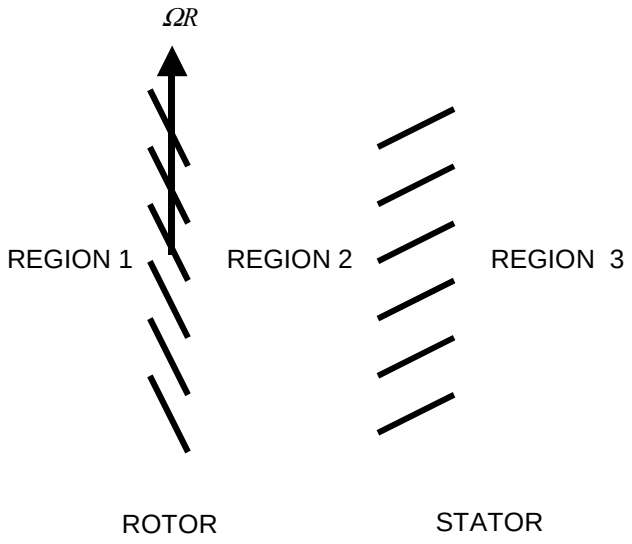

Figure 3. Flat plate representation for coupled rotor/ stator tone noise in Ref. 1.

Waves are considered in 3 *regions* per Figure 3 and counted by the index r. Also, there are 3 wave *types*: T=1, 2 for upstream/downstream propagating pressure waves and T = 3 for vortical waves in 2D. The pressure waveform for a type T wave in region r is written in a Fourier series as

$$p_T^r(\mathbf{x},t) = p_o \sum_n \sum_k A_T^r(n,k)\, e^{i[k_{xTnk}x + m\phi - nB_1\Omega t]}, \quad T = 1,2 \tag{2.1}$$

Coordinate x corresponds to the fan axis and ϕ is used for the transverse coordinate. Circumferential mode order given by the classic Tyler-Sofrin mode selection rule (Ref. 6):

$$m = nB_1 - kB_2 \tag{2.2}$$

B_1 and B_2 are the numbers of blades and vanes. The first summation is over the blade passing harmonics, counted by n. The second summation is over k, the stator scattering index. Vortical modes are represented by their transverse velocity component in parallel form

$$v_T^r(\mathbf{x},t) = a_o \sum_n \sum_k A_T^r(n,k)\, e^{i[k_{xTnk}\, x + m\phi - nB_1\Omega t]}, \qquad T = 3 \tag{2.3}$$

Scattering by the blade rows is denoted by coefficients defined in the following notation that relates modal amplitudes to each other

$$A_{T'}^{r'}(n',k') \Leftarrow S_{T'T}^{r'r}(n',k';n,k) A_T^r(n,k) \tag{2.4}$$

where $S_{T'T}^{r'r}(n',k';n,k)$ is the scattering coefficient giving the ratio of output wave amplitudes (with the primes) to input wave amplitudes (without primes). When all of these scattering coefficients are found from a cascade unsteady response theory, the resulting equations are arranged in matrix form as follows

$$\begin{bmatrix} A_1^1 \\ A_2^1 \\ A_3^1 \\ \hline A_1^2 \\ A_2^2 \\ A_3^2 \\ \hline A_1^3 \\ A_2^3 \\ A_3^3 \end{bmatrix} = \left[\begin{array}{ccc|ccc|ccc} \cdot & S_{12}^{11} & S_{13}^{11} & S_{11}^{12} & \cdot & \cdot & \cdot & \cdot & \cdot \\ S_{21}^{11} & \cdot & \cdot & \cdot & \cdot & \cdot & \cdot & \cdot & \cdot \\ S_{31}^{11} & \cdot & \cdot & \cdot & \cdot & \cdot & \cdot & \cdot & \cdot \\ \hline \cdot & \cdot & \cdot & \cdot & S_{12}^{22} & S_{13}^{22} & S_{11}^{23} & \cdot & \cdot \\ \cdot & S_{22}^{21} & S_{23}^{21} & S_{21}^{22} & \cdot & \cdot & \cdot & \cdot & \cdot \\ \cdot & S_{32}^{21} & S_{33}^{21} & S_{31}^{22} & \cdot & \cdot & \cdot & \cdot & \cdot \\ \hline \cdot & \cdot & \cdot & \cdot & \cdot & \cdot & \cdot & S_{12}^{33} & S_{13}^{33} \\ \cdot & \cdot & \cdot & \cdot & S_{22}^{32} & S_{23}^{32} & S_{21}^{33} & \cdot & \cdot \\ \cdot & \cdot & \cdot & \cdot & S_{32}^{32} & S_{33}^{32} & S_{31}^{33} & \cdot & \cdot \end{array}\right] \times \begin{bmatrix} A_1^1 \\ A_2^1 \\ A_3^1 \\ \hline A_1^2 \\ A_2^2 \\ A_3^2 \\ \hline A_1^3 \\ A_2^3 \\ A_3^3 \end{bmatrix} + \begin{bmatrix} B_1^1 \\ B_2^1 \\ B_3^1 \\ \hline B_1^2 \\ B_2^2 \\ B_3^2 \\ \hline B_1^3 \\ B_2^3 \\ B_3^3 \end{bmatrix} \tag{2.5}$$

This partially compressed notation suppresses the $n,\ k$ subscripts shown explicitly in Eq. 2.4. Dots in the matrix represent zero blocks. The notation can be further compressed so that Equation 2.5 reads

$$\mathbf{A} = \mathbf{S}\,\mathbf{A} + \mathbf{B} \tag{2.6}$$

$\mathbf{B}$ is the source vector or array of coefficients of prescribed waves that excite the system. Solution of this coupled system for the state vector $\mathbf{A}$ is given formally by

$$\mathbf{A} = (\mathbf{1} - \mathbf{S})^{-1}\,\mathbf{B} \tag{2.7}$$

For wake excitation, the only non-zero elements of $\mathbf{B}$ would be the $B_3^2(n,k)$'s to represent vortical waves (T = 3) from region #2. These coefficients, in an expression like Eq. 2.3 would define the rotor wake (only the k = 0 term is needed for convected disturbances).

When all of the elements of the state vector are found from Eq. 2.7, the entire wave field can be constructed from Equations 2.1 and 2.3.

Over a range of vane/blade ratios, the fundamental interaction mode can be trapped between rotor and stator. In this case, the tone coupling effect can be very strong and actually dominate noise generation. For example, Fig. 4, reproduced from Ref. 1, shows the downstream sound power in 3 BPF harmonics that results from exciting the stator with the BPF fundamental of the rotor wake in a coupled environment. Below BPF cuton in the aft duct, which is at $M_t = 0.80$, the noise is dominated by energy scattered up in frequency by the rotor. We now know how to avoid this situation by proper choice of vane count (and thereby, mode selection). However, since broadband noise generation includes all modes, mode trapping could also be a factor in that spectrum component and may be more difficult to control. One objective of the model developed this report is to determine the importance of mode trapping in broadband fan noise; however, further numerical studies are needed to resolve that issue.

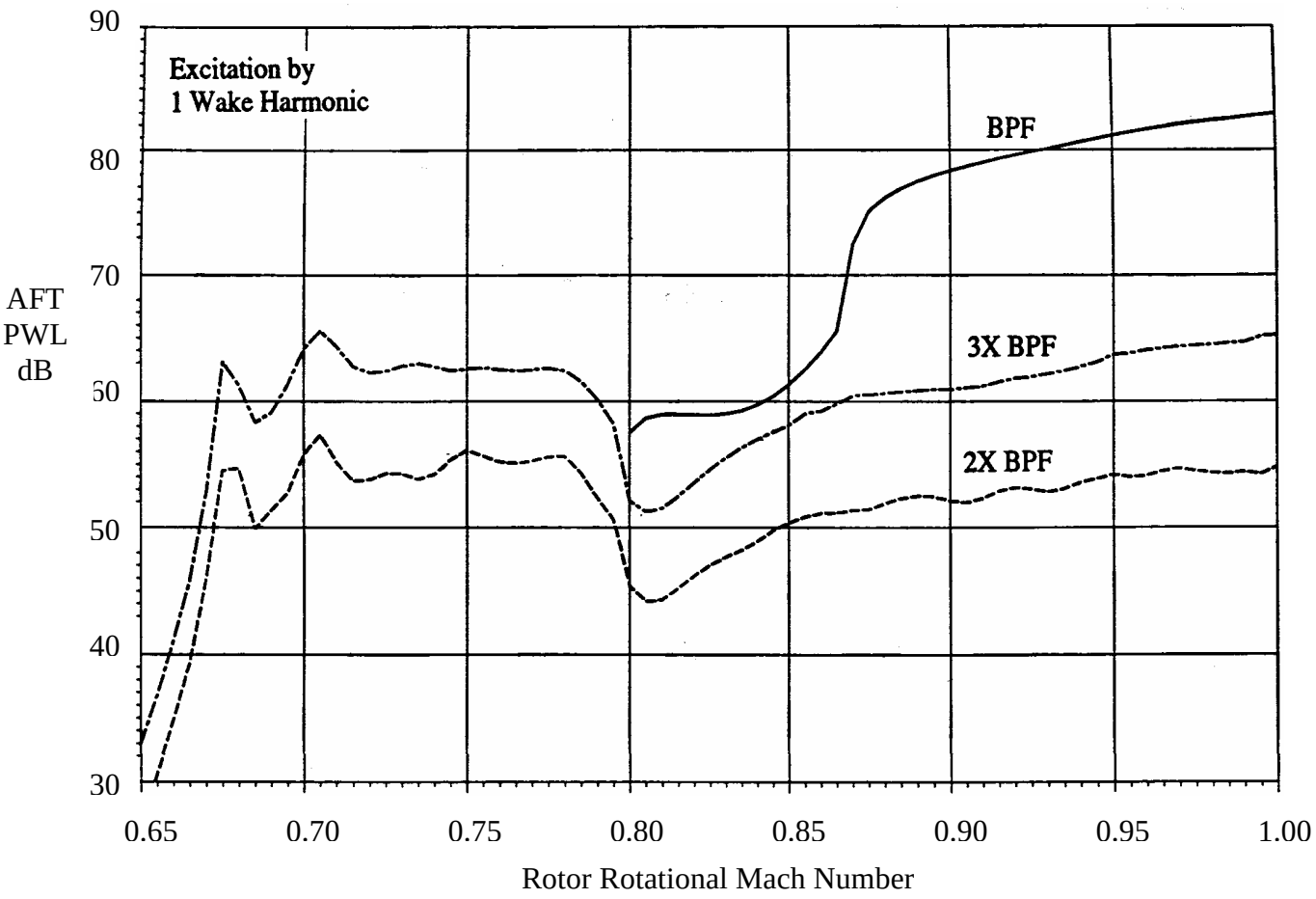

Figure 4. Coupled tone calculation from Ref. 1 showing 3 BPF harmonics resulting from excitation of the stator by the one harmonic of the wake at BPF.

Review of Broadband Method for Noise from an Isolated Stator

Here we review how the harmonic acoustic response of a cascade can be used in a broadband model for noise caused by inflow turbulence. This and the above coupled harmonic analysis will be used to explain how the coupled broadband formulation will be derived later in this report.

First, consider the cascade harmonic problem with mean flow and upwash as in Figure 5. We write the harmonic upwash waveform as

$$w(\mathbf{x},t) = w_q\, e^{i(k_{x3q}x + q\phi + \nu z - \omega t)} \tag{2.8}$$

In this notation, $\phi = y/R$ represents angle around an "unwrapped annulus" of effective radius R. z takes the role of the radial coordinate and ν is its associated wavenumber. With axial wavenumber

$$k_{x3q} = \frac{\omega - \frac{q}{R}V}{U} \tag{2.9}$$

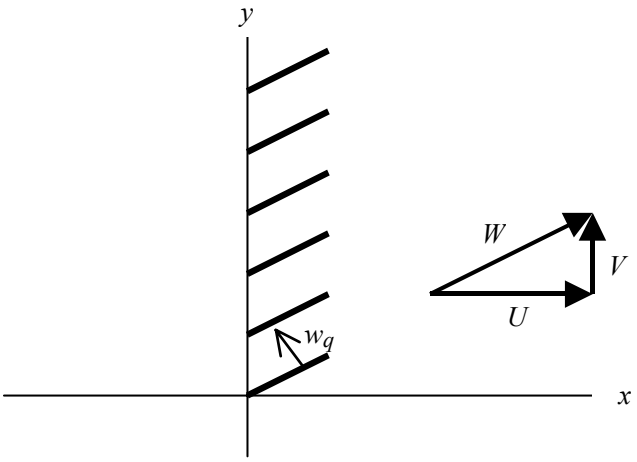

Figure 5. Sketch for cascade discussion.

Eq. 2.8 represents a convected wave (as in the frozen gust model of turbulence). Say we have a cascade response function $F_k(\omega,\nu)$ from an analysis like Glegg's (Ref. 4) that gives the upstream acoustic pressure resulting from the upwash as

$$p(\mathbf{x},t) = w_q \sum_k F_k(\omega,\nu)\, e^{i[k_{x1qk}x + (q - kB_2)\phi + \nu z - \omega t]} \tag{2.10}$$

where k is the scattering index for the stator and k_{x1qk} is the axial wavenumber for acoustic waves. With these equations, the harmonic acoustic pressure field can be computed from the inflow perturbation.

So far the discussion has related to harmonic excitation and response; w_q is a Fourier coefficient and Eq. 2.10 is a Fourier series. Now, we want to extend the above for application to broadband noise, in which case we deal with Fourier transforms and Fourier integrals. We generalize the inflow representation of Eq. 2.8 to aperiodic waves

$$w(\mathbf{x},t) = \sum_q \iint w_q(\omega,\nu)\, e^{i(k_{x3q}x + q\phi + \nu z - \omega t)}\, d\omega\, d\nu \tag{2.11}$$

which represents the upwash disturbance as a sum/integral over circumferential order q, radial order ν, and frequency ω. (In a more general type of flow, an integral over axial wavenumber would also be included. However, for convected waves, axial wavenumber and frequency are related through Eq. 2.9 and the fourth integral is not required.) There is an issue of existence of the Fourier transform w_q in Eq. 2.11. However, there are standard methods to deal with this, as applied later in the formal derivations.

With inflow represented by Eq. 2.11, the corresponding aperiodic response (generalizing Eq. 2.10) is

$$p(\mathbf{x},t) = \sum_k \sum_q \iint w_q(\omega,\nu)\, F_k(\omega,\nu)\, e^{i[k_{x1qk}x+(q-kB_2)\phi+\nu z-\omega t]}\, d\omega\, d\nu \tag{2.12}$$

Note that $w_q(\omega, \nu)$ is now a Fourier transform rather than a Fourier coefficient but that $F_k(\omega,\nu)$ is the same acoustic harmonic response function used for the tone analysis.

In principle, any non-periodic excitation and response fields could be represented in these forms. This is not actually possible in the case of turbulent flow, however, because $w(\mathbf{x},t)$ [and $w_q(\omega,\nu)$] cannot be known in sufficient detail. Instead we deal with statistical quantities (or expected values). In the following we review how the expected value of the pressure mean square (and its spectrum) can be related to the turbulence spectrum in an isolated cascade analysis. This is provided as a point of departure for the coupled broadband analysis.

To start, we square Eq. 2.12 and take the expected values of both sides, giving

$$\left\langle p^2(\mathbf{x},t)\right\rangle = \sum_k \sum_{k'} \sum_q \sum_{q'} \iint \iint \left\langle w_q(\omega,\nu)\, w^*_{q'}(\omega',\nu')\right\rangle F_k(\omega,\nu)\, F^*_{k'}(\omega',\nu') \times e^{i\{(k_{x1qk}-k'_{x1q'k'})x+[(q-kB_2)-(q'-k'B_2)]\phi+(\nu-\nu')z-(\omega-\omega')t\}}\, d\omega\, d\omega'\, d\nu\, d\nu' \tag{2.13}$$

where $\langle\ \rangle$ is the expected value operator. It can be shown that the expected value of the product of velocity transforms is related to the upwash component of the turbulence spectrum as follows

$$\left\langle w_q(\omega,\nu)\, w^*_{q'}(\omega',\nu')\right\rangle = \frac{1}{UR}\delta_{qq'}\,\delta(\omega-\omega')\,\delta(\nu-\nu')\,\Phi_{ww}(\mathbf{K}) \tag{2.14}$$

Turbulence wavenumber $\mathbf{K}$ has components

$$\mathbf{K} = (k_{x3q}, \frac{q}{R}, \nu) \tag{2.15}$$

The delta functions in Eq. 2.14 eliminate 2 integrals and a summation, reducing Eq. 2.13 to

$$\left\langle p^2(\mathbf{x},t)\right\rangle = \frac{1}{UR}\sum_k \sum_{k'} \sum_q \iint \Phi_{ww}(\mathbf{K})\, F_k(\omega,\nu)\, F^*_{k'}(\omega,\nu)\, e^{i[(k_{x1qk}-k_{x1qk'})x-(k-k')B_2\phi]}\, d\omega\, d\nu \tag{2.16}$$

This result for the mean square pressure varies with position via the ϕ variable. If we limit our interest to the average over ϕ, the averaging process produces another delta, $\delta_{kk'}$. This enables the sum over k' and we arrive at our final form for the mean square pressure integrated over all frequencies

$$\overline{\left\langle p^2(\mathbf{x},t)\right\rangle} = \frac{1}{UR}\sum_k \sum_q \iint \Phi_{ww}(\mathbf{K})\left|F_k(\omega,\nu)\right|^2 d\omega\, d\nu \tag{2.17}$$

where it can be seen that the x dependence has disappeared. (Actually, this is true only for the propagating waves.) Usually, we want the sound spectrum or power spectral density of the pressure; this is just the frequency integrand:

$$S_{pp}(\omega) = \frac{1}{UR}\sum_k \sum_q \int \Phi_{ww}(\mathbf{K})\left|F_k(\omega,\nu)\right|^2 d\nu \tag{2.18}$$

This establishes a very simple relation between the spectrum of turbulence and the sound spectrum through the square of the magnitude of the acoustic response function. There is no phase information; only magnitudes appear. We are generally not interested in phase information for the sound spectrum and this is fortunate since turbulence models do not include phase.

Figure 6 compares computed results from this theory with scaled data from an ADP fan model. In applying the 2D geometry and mean flow, conditions at the 85% radius were used. Turbulence intensity and scale were the only free parameters and they were adjusted for a good fit to the data. Further detail is given in Ref. 2. The fit is reasonably satisfactory: overall shape, including high frequency roll off, is good and the upstream/downstream split matches that of the data. However, it will be seen that the match to the upstream/downstream split was fortuitous since the more complete analysis shows that the rotor blocks much of the upstream noise from the stator.

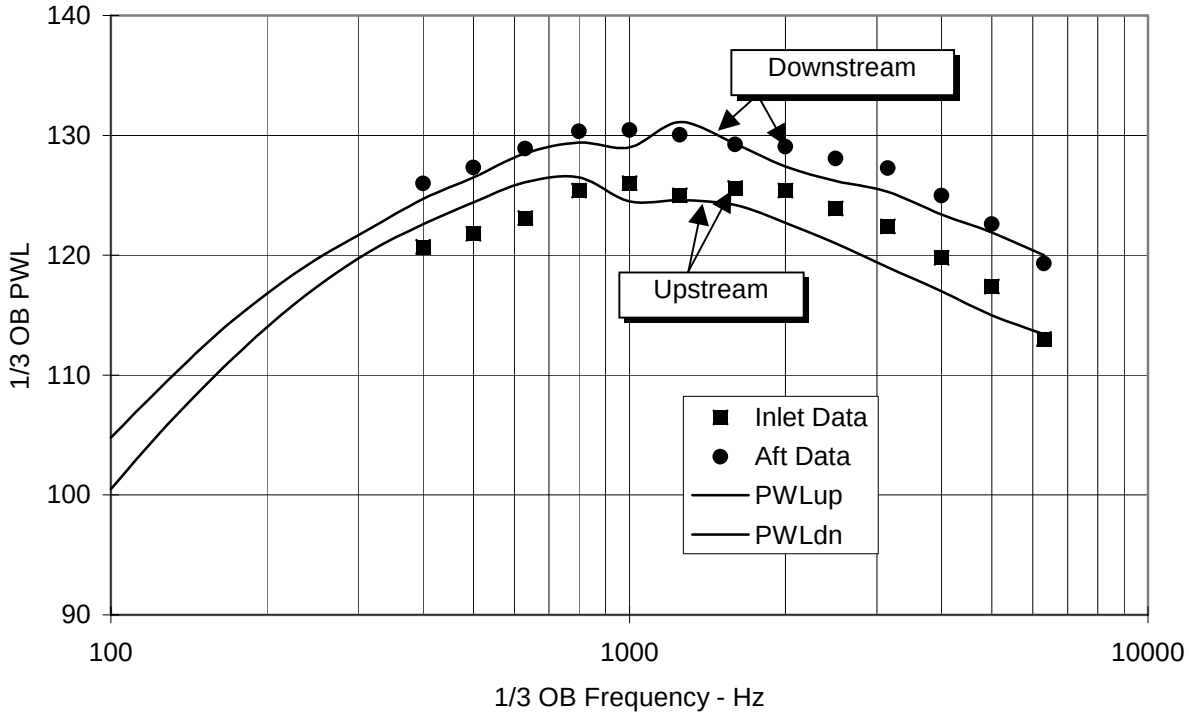

Figure 6. Calculations from BBCascade compared with scaled test data. Plot reproduced from Ref. 2.

Broadband Coupling

Now we ask how to combine the 2 types of analysis above into a coupled broadband model. The key is Eq. 2.18: think of the turbulence spectrum $\Phi_{ww}(\mathbf{K})$ as excitation for the system and think of $|F_k(\omega,\nu)|^2$ as the system response function. There is a parallel with the harmonic solution found in Eqs. 2.1 and 2.7; in this case the system response function $(\mathbf{1}\text{-}\mathbf{S})^{-1}$ is the inverse of a large matrix of Fourier coefficients. In Section 6 we will see that $(\mathbf{1}\text{-}\mathbf{S})^{-1}$ takes the role of $F_k(\omega, \nu)$ in Eq. 2.10. An integral/summation like Eq. 2.18 will be wrapped around this entire matrix system. In the broadband analysis, the elements of $\mathbf{S}$ will be Fourier transforms instead of Fourier coefficients. This approach rigorously retains all of the phase information in the frequency and mode scattering between the blade rows but then gives up the phase information in the final working formulas, as was the case with Eq. 2.18. Again, the sound spectrum will be driven by the turbulence spectrum.

The analysis is simpler than might be expected because of the property of "independent mode sets" mentioned in the Summary and Introduction. Sections 3 to 6 establish the coupling matrix system, Section 7 connects the matrix system to the turbulence spectrum and gives the final working equations for the computer code CupBB, and Section 8 shows some computed examples.

SECTION 3
MEAN FLOW AND GENERAL WAVE CHARACTERISTICS

In this section we define the environment for the coupled blade row analysis. This includes the duct boundaries, mean flow, and boundary conditions. It also gives the general properties of the perturbation waves consistent with this ducted flow environment (but without yet accounting for the presence of blades and vanes).

In later sections, we use Glegg's unsteady cascade analysis (Ref. 4) for the acoustic and vortical responses of the blade rows. Since this treats waves with 3 independent wavenumbers, it permits a completely general representation of turbulent flow. However, it is based on rectilinear geometry and a uniform background flow. Because of this, we represent flow in a fan duct annulus by "unwrapping" it and enforcing periodic boundary conditions in the tangential direction. I.e., variables at $\phi = \pm\pi$ are the same. We introduce an "effective radius" R, which is used for scaling and to make the equations look more like the true 3D acoustic equations in cylindrical coordinates. R relates the tangential angular and linear coordinates through $y = \phi R$.

Geometry and Mean Flow

The x, y, z coordinates are shown in Figure 7. x is parallel to the machine axis, y is the tangential coordinate (parallel to the direction of rotor rotation), and z corresponds to the radial coordinate. Inner and outer duct walls are represented by the $z = 0$ and $z = h$ planes. Periodic

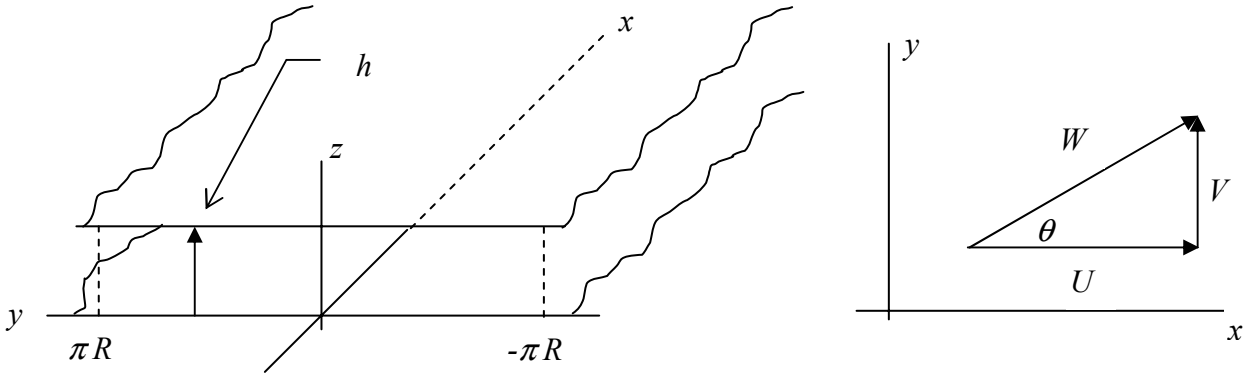

Figure 7. Definition of boundaries and mean flow

boundaries are at $y = \pm\pi R$. Mean flow is the same everywhere with axial component U and tangential (or swirl) component V. Represented in vector form, the mean velocity is

$$\mathbf{U} = U\hat{\mathbf{i}} + V\hat{\mathbf{j}} + 0\hat{\mathbf{k}} \tag{3.1}$$

Perturbation Equations

Here we follow the general approach and notation of Smith (Ref. 7) but extend it to 3 dimensions. Unsteady flow satisfies the linearized continuity and momentum equations

$$\frac{Dp}{Dt} + \rho_r a_r^2 \nabla \cdot \mathbf{u} = 0 \tag{3.2}$$

$$\rho_r \frac{D\mathbf{u}}{Dt} = -\nabla p \tag{3.3}$$

where the convective derivative is

$$\frac{D}{Dt} = \frac{\partial}{\partial t} + \mathbf{U} \cdot \nabla \tag{3.4}$$

and subscript r implies mean value in a region designated by r. For perturbations periodic in space and time, solutions have the general form

$$\begin{bmatrix} p \\ u \\ v \\ w \end{bmatrix} = \begin{bmatrix} \overline{p} \\ \overline{u} \\ \overline{v} \\ \overline{w} \end{bmatrix} e^{i(k_x x + k_y y + k_z z - \omega t)} \tag{3.5}$$

Note that the convective derivative yields

$$\frac{D}{Dt} = i(-\omega + U k_x + V k_y) \tag{3.6}$$

and, accordingly, define a parameter that occurs frequently in the analysis

$$\lambda = -\omega + U k_x + V k_y \tag{3.7}$$

When we substitute the solutions from Eq. 3.5 into the continuity and momentum equations, the exponentials cancel and we can write

$$\begin{bmatrix} \lambda & a_r^2 \rho_r k_x & a_r^2 \rho_r k_y & a_r^2 \rho_r k_z \\ k_x / \rho_r & \lambda & 0 & 0 \\ k_y / \rho_r & 0 & \lambda & 0 \\ k_z / \rho_r & 0 & 0 & \lambda \end{bmatrix} \begin{bmatrix} \overline{p} \\ \overline{u} \\ \overline{v} \\ \overline{w} \end{bmatrix} = 0 \tag{3.8}$$

Non-trivial solutions are obtained from

$$\lambda^2 [\lambda^2 - a_r^2 (k_x^2 + k_y^2 + k_z^2)] = 0 \tag{3.9}$$

This permits 4 wave types. For periodicity in y, we require m to be an integer in $k_y y = m\phi$. This, with $\phi = y/R$, gives $k_y = m/R$. Also, for hard wall boundary conditions, we use linear combinations of Eqs. 3.5 to give sines and cosines for z dependence. Thus, μ is an integer and $k_z = (\mu\pi/h)$. The following form fits all 4 wave types

$$\begin{aligned} p_T &= \bar{p}_T \; e^{i(k_{xT}x + m\phi - \omega t)} \cos(\tfrac{\mu\pi z}{h}) \\ u_T &= \bar{u}_T \; e^{i(k_{xT}x + m\phi - \omega t)} \cos(\tfrac{\mu\pi z}{h}) \\ v_T &= \bar{v}_T \; e^{i(k_{xT}x + m\phi - \omega t)} \cos(\tfrac{\mu\pi z}{h}) \qquad T = 1,2,3,4 \\ w_T &= \bar{w}_T \; e^{i(k_{xT}x + m\phi - \omega t)} \sin(\tfrac{\mu\pi z}{h}) \end{aligned} \tag{3.10}$$

These, with the correct relationships between the pressure and velocity magnitudes (given below), satisfy the governing equations, the periodicity conditions in the y direction, and zero radial velocity at the duct walls at $z = 0$ and h. Characteristics of the different wave types will be discussed below.

Pressure Waves

In Eq. 3.9 pressure waves are associated with

$$[\lambda^2 - a_r^2(k_x^2 + k_y^2 + k_z^2)] = 0 \tag{3.11}$$

This can be solved for the axial wavenumber k_x:

$$k_x = \frac{1}{a_r^2 - U^2}\left[U(-\omega + Vk_y) \pm a_r\sqrt{(-\omega + Vk_y)^2 - (a_r^2 - U^2)(k_y^2 + k_z^2)}\right] \tag{3.12}$$

As in Smith's analysis, we identify upstream-going pressure (or acoustic) waves as Type 1 waves:

$$k_{x1} = \frac{1}{a_r^2 - U^2}\left[U(-\omega + mV/R) - a_r\sqrt{(-\omega + mV/R)^2 - (a_r^2 - U^2)[(m/R)^2 + (\mu\pi/h)^2]}\right] \tag{3.13}$$

and downstream-going pressure waves as Type 2 waves:

$$k_{x2} = \frac{1}{a_r^2 - U^2}\left[U(-\omega + mV/R) + a_r\sqrt{(-\omega + mV/R)^2 - (a_r^2 - U^2)[(m/R)^2 + (\mu\pi/h)^2]}\right] \tag{3.14}$$

Depending on frequency and mode orders m and μ, the argument of the square root can be positive or negative. If it is positive, the axial wavenumber is pure real and waves propagate without decay. If the argument is negative, the axial wavenumber is complex and waves decay. The signs of the square roots must be chosen so that waves decay exponentially away from the blade row in the x direction.

For the pressure waves we use the momentum equation to relate the complex velocity magnitudes to the complex magnitude defining the pressure waves:

$$\begin{aligned} \bar{u}_T &= -\frac{k_{xT}}{\rho_r \lambda_T} \bar{p}_T \\ \bar{v}_T &= -\frac{m/R}{\rho_r \lambda_T} \bar{p}_T \qquad T = 1,2 \\ \bar{w}_T &= -\frac{i\mu\pi/h}{\rho_r \lambda_T} \bar{p}_T \end{aligned} \tag{3.15}$$

Vortical Waves

In Eq. 3.9 vortical waves are associated with $\lambda = 0$. i.e.

$$-\omega + U k_x + V k_y = 0 \tag{3.16}$$

which can be solved for their axial wavenumber. Since λ was squared, there are 2 independent vortical waves with the same wavenumber

$$k_{xT} = \frac{\omega - mV/R}{U} \qquad T = 3,4 \tag{3.17}$$

Substitution into the momentum equation confirms that the vortical waves have no pressure

$$\bar{p}_T = 0 \qquad T = 3,4 \tag{3.18}$$

Also, substitution of Eq. 3.17 into the exponentials of Eq. 3.10 verifies that the type 3 and 4 waves are purely convected. The relationships between the velocity components depend on continuity and the actual families to be used in the modeling. These will be defined in Section 5.

SECTION 4
PERMITTED MODES AND THE SCATTERING RULES

We intend to build a rotor/stator coupling scheme based on matching modal output of the stator to modal input of the rotor and *vice versa*. The usual tool for studying modal behavior in the fan environment is the "mode order/frequency plot" schematically shown below in Figure 8. In our convention, modes with positive m are co-rotating (rotating in the same direction as the rotor). Such plots permit us to locate mode orders at various frequencies and to determine whether they propagate (are cut on) or decay (cut off). Modes in the shaded area are cut on; hence, we can see that that there are more modes propagating at higher frequencies. The cutoff boundaries are given by the square root in Eqs. 3.13 and 3.14. When the argument is positive, modes propagate. Test data shown in Figure 9 were plotted in the same format. Acoustic power can be found at all integer mode orders in the cuton area. When the radial modes are included, we find that thousands of modes must be accounted for to get a complete representation of the noise field.

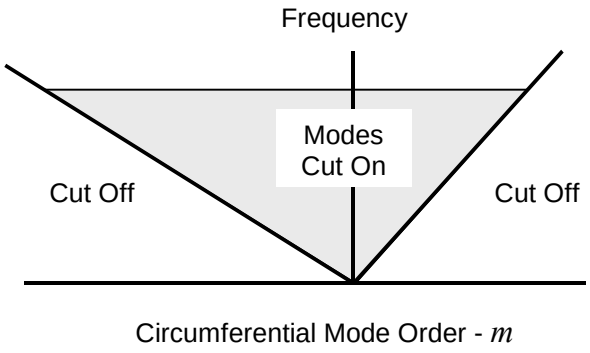

Figure 8. Mode order/frequency plot for $\mu = 0$

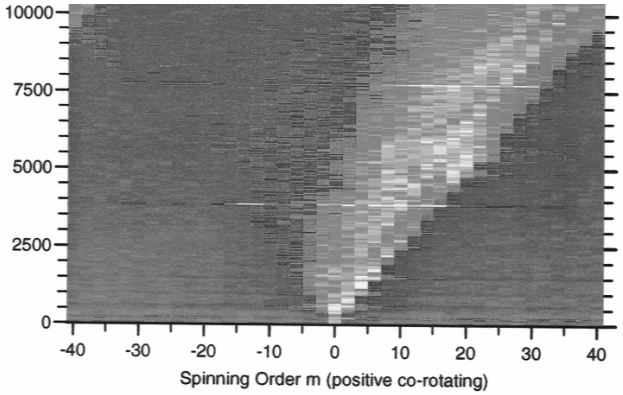

Figure 9. Experimental mode order-frequency plot from Boeing's 18 inch research fan, Ref. 8.

We will see that, when a mode impinges on the stator, it scatters out a series of modes of different circumferential order. When each of these impinges on the rotor, scattering there produces modes of different orders *and* frequencies. If any mode could scatter into any other mode and frequency, the modal accounting scheme would be unmanageable. We will soon see that this is *not* the case but that only modes within certain sub-sets of the total mode count are connected with each other; there is no scattering from one sub-set to another. Once this is understood, the fan broadband analysis can be set up as a series of "small", independent coupling problems and the situation becomes manageable. This section is devoted to explaining the kinematics of broadband scattering/coupling and establishing the independent modal sub-sets just mentioned.

Permitted Modes

Modal scattering by a stator will already be understood in the tone context to readers familiar with the Tyler-Sofrin fan noise theory (Ref. 6). In the tone case, the frequencies and modes are restricted to

$$\begin{aligned} &\text{frequency}: \quad \omega = nB_1\Omega, \qquad && n = \ldots -1,\ 0,\ 1,\ 2, \ldots \\ &\text{mode order}: \quad m = nB_1 - kB_2 \qquad && k = \ldots -1,\ 0,\ 1,\ 2, \ldots \end{aligned} \tag{4.1}$$

i.e. frequencies are restricted to multiples of blade passing frequency (counted by n) and circumferential mode orders are restricted to the values of m resulting from integer values of the rotor and stator scattering indices, n and k. Furthermore, it was shown in Ref. 1 that, even after scattering back and forth between rotor and stator, waves are still restricted the frequencies and mode orders in Eq. 4.1. Thus, Eq. 4.1 is a mode set that can scatter only among its members but not to other orders and frequencies. Broadband scattering is more general: any frequency and any integer mode order can occur. In the following, we will find how Eq. 4.1 is generalized for the broadband problem.

The space-time dependence of the pressure waves in Equation 3.10 is given by

$$e^{i(k_x x + m\phi - \omega t)} \cos(\mu\pi z / h) \tag{4.2}$$

where we can identify circumferential mode order m and radial mode order μ. A major simplification in the analysis arises when we note that there is no scattering from one radial mode to another. This is an artifact of using rectilinear geometry and constant mean flow and is true because the pressure modes and upwash components of the vortical modes (see Eq. 3.10) have cosine dependence on the radial (z) coordinate. A cosine input produces a cosine output with the same μ. This simplification would not apply strictly in a situation with real geometry and flow but, even there, the radial coupling should be weak and may not be a major factor in noise generation. Thus, radial order μ becomes a parameter and, for coupling at any x plane, we can focus on circumferential orders via the exponential $e^{i(m\phi - \omega t)}$. To establish the scattering rules, we define $m\phi$ - ωt to be the kinematic phase, i.e.

$$\psi = m\phi - \omega t \tag{4.3}$$

and track its behavior as waves scatter back and forth between the rotor and stator.

To start the discussion, we must define interblade phase angle σ and show what happens to it upon scattering by a cascade. Since σ is the phase shift from $y = 0$ to $y = g$ (the blade gap), it follows (using the exponential form in Eq. 3.5) that $\sigma = k_y g$. In our rectilinear geometry the tangential wavenumber $k_y = m/R$. Cascade theory (see Ref. 4 or 7) teaches us that, for an input wave with frequency ω and circumferential wave number $k_y = \sigma/g$, the scattered waves have the same frequency ω and their circumferential wavenumbers are

$$k_y' = \frac{\sigma - 2\pi k}{g} \tag{4.4}$$

where k is an integer that we call the scattering index and the prime indicates a scattered wave. Consider a wave input to the stator with circumferential order q and frequency ω_0. The circumferential wavenumber of the input wave is $k_y = \sigma/g = q/R$. And since $B_2\, g = 2\pi R$, it follows that

$$\sigma = \frac{2\pi q}{B_2} \tag{4.5}$$

And for $k_y' = m/R$, it can be seen from Eq. 4.4 that the orders of the scattered modes are given by

$$m = q - kB_2 \tag{4.6}$$

Thus, from Eq. 4.3 the kinematic phases of the waves scattered by the stator with input $\psi = q\phi - \omega_o t$ are

$$\psi' = (q - kB_2)\phi - \omega_o t \tag{4.7}$$

To consider scattering at the rotor, shift to rotor coordinates via

$$\phi = \phi_r + \Omega t \tag{4.8}$$

Then, the same mode viewed in the rotor frame has phase

$$\psi' = (q - kB_2)\phi_r - [\omega_o - (q - kB_2)\Omega]t \tag{4.9}$$

It can be seen that the frequency in that frame is

$$\omega_r = \omega_o - (q - kB_2)\Omega \tag{4.10}$$

For scattering by the rotor, we use the index n (with the opposite sign for convenience) so that the waves scattered by the rotor have kinematic phase

$$\psi'' = (q + nB_1 - kB_2)\phi_r - [\omega_o - (q - kB_2)\Omega]t \tag{4.11}$$

Scattering does not change frequency in the rotor frame. When this expression is shifted back to the stator frame via $\phi_r = \phi - \Omega t$, we find that the same waves have the form

$$\psi'' = (q + nB_1 - kB_2)\phi - (\omega_o + nB_1\Omega)t \tag{4.12}$$

Mode orders have been shifted from the input order q by $nB_1 - kB_2$ and frequencies have been scattered up and down from the input frequency ω_0 by multiples of blade passing frequency $nB_1\Omega$.

This process of following the scattering from stator to rotor and back can be repeated indefinitely but it turns out that the waves, when represented in the stator frame, always have the form given by Eq. 4.12. Furthermore, we could have started with a wave impinging on the rotor and found the same form. Thus, to summarize, a wave in the stator frame having frequency ω_0 and mode order q scatters as follows

$$\begin{array}{lllll} \text{frequency}: & \omega_o & \Rightarrow & \omega = \omega_o + nB_1\Omega, & n = \ldots -1, 0, 1, 2, \ldots \\ \text{mode order}: & q & \Rightarrow & m = q + nB_1 - kB_2 & k = \ldots -1, 0, 1, 2, \ldots \end{array} \tag{4.13}$$

This result establishes the scattering "independent mode sub-set" property asserted above: if we input a set of modes with frequencies $\omega_o + nB_1\Omega$ and orders $m = q + nB_1 - kB_2$, those modes only scatter among themselves and not to other frequencies and not to other mode orders. In particular, at any frequency, only one out of every B_2 modes is involved in the scattering.

We can consider ω_0 and q to be frequency and mode offsets from the tone interaction set of Eq. 4.1. The set of modes and frequencies resulting from a choice of ω_0, μ, and q is independent of sets with other values of these indices. Thus, in the computer code, we can set up loops on ω_0, μ, and q and solve a relatively small coupled problem for scattering on n and k for each of these combinations. In each case, the input is a vector of turbulence modes for all n and k and the response is found simultaneously for the acoustic modes for the same ranges of n and k. Both n and k take on positive and negative values. Fortunately, the required range of k is limited by acoustic cutoff and by decay of the turbulence spectrum. The range of n to be included could be limited by the frequency content of the turbulence; however, practically speaking, this range may be limited by computer resources. What we hope is that the n (frequency) range can be truncated at a reasonable value without significantly sacrificing accuracy for the frequencies included in the analysis. This did turn out to be the case for the tone problem (Ref. 1) and will be verified later in the broadband case.

This independent mode sub-set property (including the absence of coupling between radial orders) changes the broadband coupling problem from one that appeared intractable to one quite manageable, at least in terms of the rectilinear geometry used herein. The operation of the independent sub-set property will be made clearer below with illustrations in terms of mode order/frequency plots.

As an historical note, recall that excitation of pressure waves by blades vibrating at non-integer multiples of blade passing frequency is of great interest in the field of rotor blade flutter and has been studied extensively in the past. In several publications, Owczarek tracked pressure pulses bouncing from rotor to stator in a time domain approach and found expressions for the allowed frequencies (e.g., ref. 9). Mengle, ref. 10, studied rotor blades vibrating at given frequency and interblade phase in the presence of adjacent stators. He found that, after successive reflections between rotor and stator, the same limited set of frequencies and mode orders keeps being generated. Mengle's analysis was in the frequency domain and led to formulas similar to those derived below for broadband application. Hall & Silkowski, ref. 11, went beyond Mengle's kinematics with the flutter problem and computed actual rotor blade loading levels with accounting for reflections from adjacent stators.

Mode Order/Frequency Plots

The plot shown in Figure 9 was constructed for a fan with 18 blades and 45 vanes and applies to the axial flow regions upstream of the rotor and downstream of the stator. In general, the cuton boundaries can be determined by setting the argument of the root in Equation 3.13 to zero:

$$(-\hat{\omega} + mM_y)^2 - \beta_x^2(m^2 + \hat{\nu}^2) = 0 \tag{4.14}$$

where $\hat{\omega} = \omega R/a_r$ and $\hat{\nu} = \mu\pi R/h$. This can be re-arranged as follows

$$\beta_x^2 \hat{\omega}^2 = (\hat{\omega} M_y + \beta^2 m)^2 + \beta^2 \beta_x^2 \hat{\nu}^2 \tag{4.15}$$

which is the equation of a conical surface enclosing the cut on values of m and $\hat{\nu}$ for any frequency. (To visualize the cone, recognize in Figure 9 that the cone axis is the $\hat{\omega}$ coordinate, the $\hat{\nu}$ axis is out of the paper, and that the plot is a cut through the $\hat{\nu}$=0 plane.) Note that the lower half of the conical surface is included in the analysis but is not shown in Figure 9.

In the $\hat{\nu}$=0 plane, Eq. 4.15 reduces to equations for straight lines with slopes $M_y \pm \beta_x$.

$$\hat{\omega} = (M_y \pm \beta_x) m \ , \qquad \hat{\nu} = 0 \tag{4.16}$$

In Figure 9, the slopes are $\pm\beta_x$ since $M_y = 0$. The large dots on the plot represent permitted modes according to Eq. 4.13, for a particular values of ω_0 and q. Scattering at the stator is along the dashed lines; this is at constant frequency (constant n) and varying k . Scattering at the rotor is along the dotted lines; this is at constant k and varying n . It is easily deduced that these lines have slope M_T and that this slope is less than that of the co-rotating cutoff boundary, $M_y + \beta_x$, for cases where the flow is subsonic relative to the rotor blades.

Figure 10 has exactly the same information as Figure 9 but presented in the rotor reference frame. Frequency at the rotor is given by Eq. 4.10. Changing reference frames does not change what modes are cut on; it only changes their apparent frequencies.

Behavior of the independent modal sub-set is now established in Figure 9: with the stator scattering along horizontal lines and the rotor scattering along the diagonal lines, any mode inside the cuton limits can communicate with any other such mode through multiple reflections between rotor and stator. However, only those modes and frequencies are connected with each other. Figure 9 was plotted with $q = 0$ and the broadband frequencies half way between the BPF harmonics ($\omega_0 = B_1\Omega/2$). Other independent mode sets can be found by taking the dashed and dotted scattering lines as a rigid pattern and moving the pattern vertically on the page to cover different frequencies and horizontally to cover different q's. Each new position (each new q and ω_o) generates a new set of modes that scatters only among themselves. Furthermore, for radial orders greater than zero, the pattern of dashed and dotted scattering lines can be held above the plane of Figure 9 to represent cutting the conical surface for μ = 1, 2, 3, … for more independent mode sets. Note, with this example for 45 vanes, q can take on all integer values from 0 to 44. The broadband frequency variable is continuous so that any number of ω_0's could be used; however, a broadband spectrum could be reasonably well defined by frequencies at the BPF multiples and halfway in between.

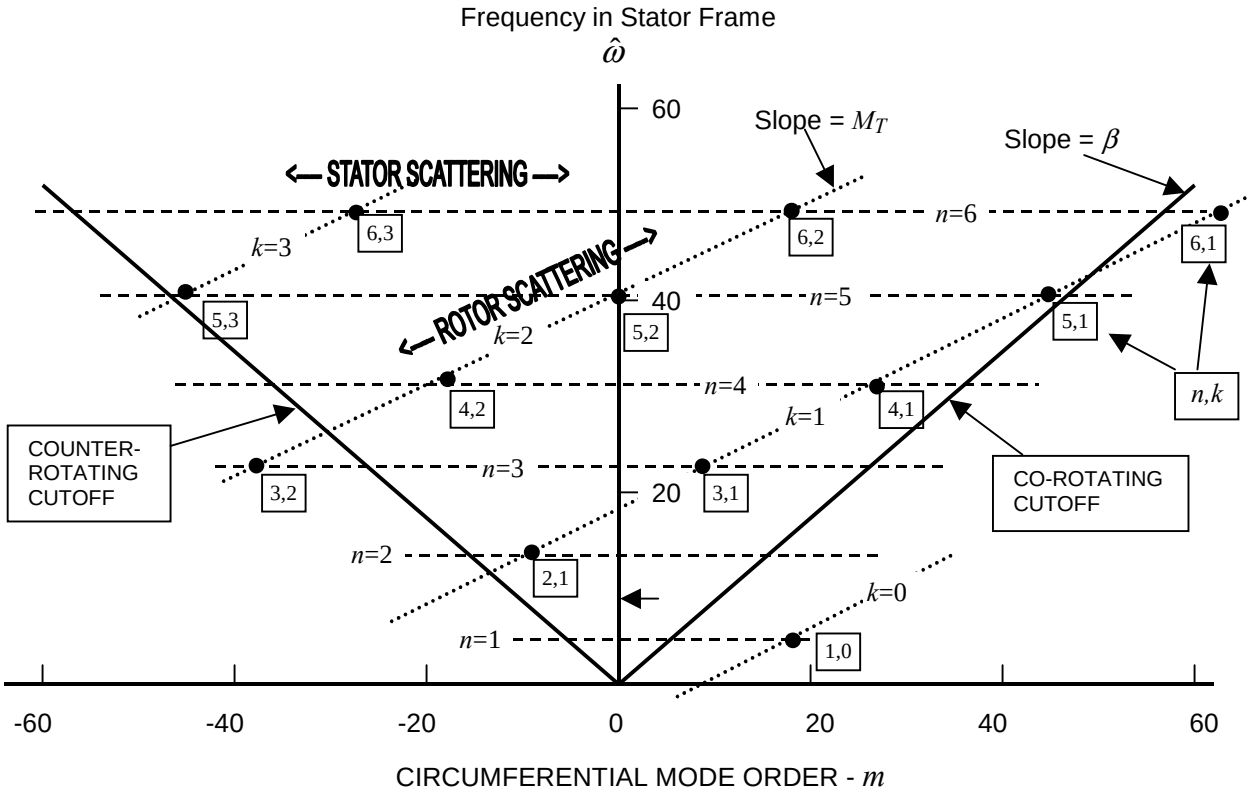

Figure 9. Mode order/frequency plot for fan in axial flow at M_x = 0.5. B_1 = 18, B_2 = 45, and M_T = 0.5. Also, q = 0 and ω_0 = BPF/2. Presented in stator reference frame.

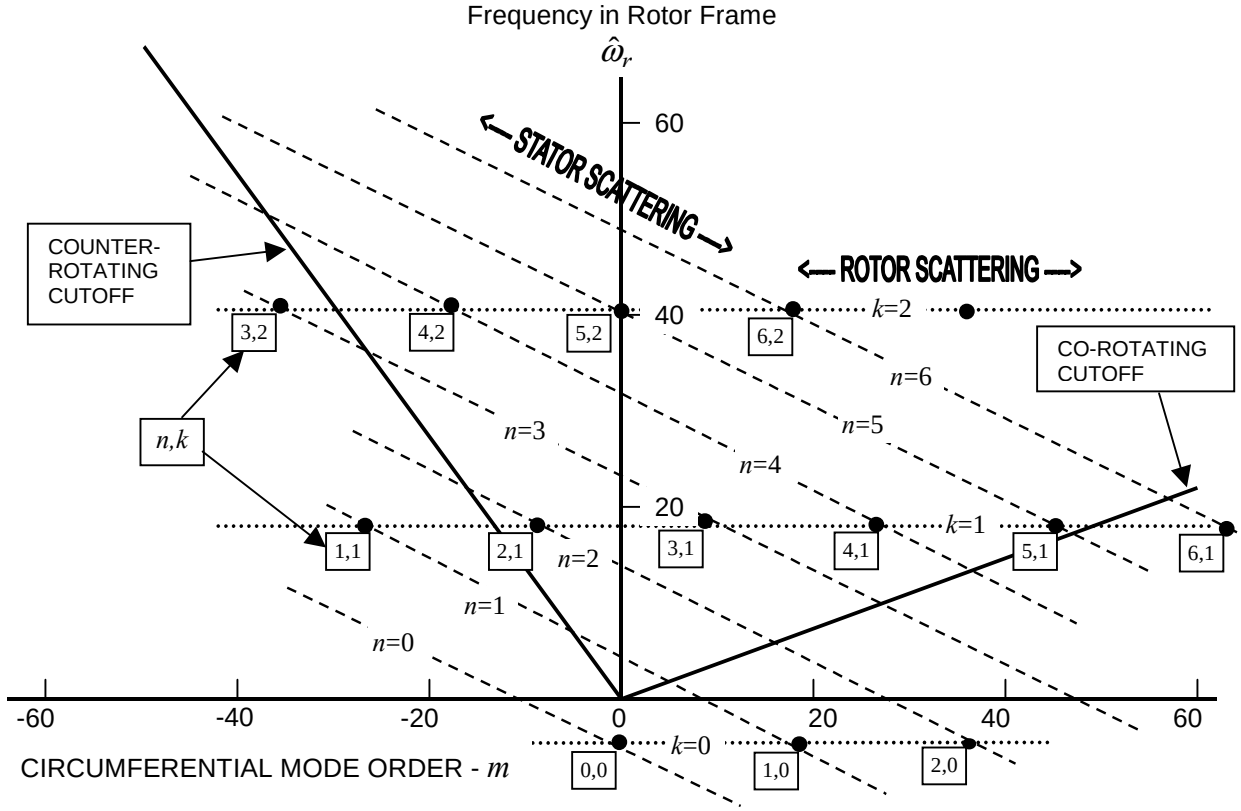

Figure 10. Same information as above but presented in rotor reference frame.

The plots just discussed were generated for axial flow, which would apply upstream of the rotor and downstream of the stator. Between blade rows, swirl affects the cuton boundaries as shown in Figure 11. Both the swirl flow and axial flow boundaries are plotted. The gray region in the plot indicates modes that propagate between rotor and stator but are cut off upstream and downstream. These modes are "trapped"; that is they can bounce back and forth between blade rows, possibly amplifying, but cannot escape. However, they do scatter to higher mode orders and frequencies that do propagate and contribute to the radiated noise. This mode trapping and up-scattering was first noted in the context of tone noise by Topol, Mathews, and Holheubner (Ref. 12), studied and modeled extensively by Hanson (Ref. 1), and incorporated in a quasi 3D prediction scheme (TFaNS) by Topol (Ref. 5). For certain vane/blade ratios, mode trapping/frequency scattering dominates tone generation in fans. In the future, numerical studies are planned to find how important this mode trapping phenomenon is for broadband fan noise.

The next 3 sections of this report are devoted to building a broadband noise prediction scheme using the modal scattering kinematics described above. Section 5 develops a notation for modes (via Fourier transforms) compatible with the scattering rules of this section. Then Section 6

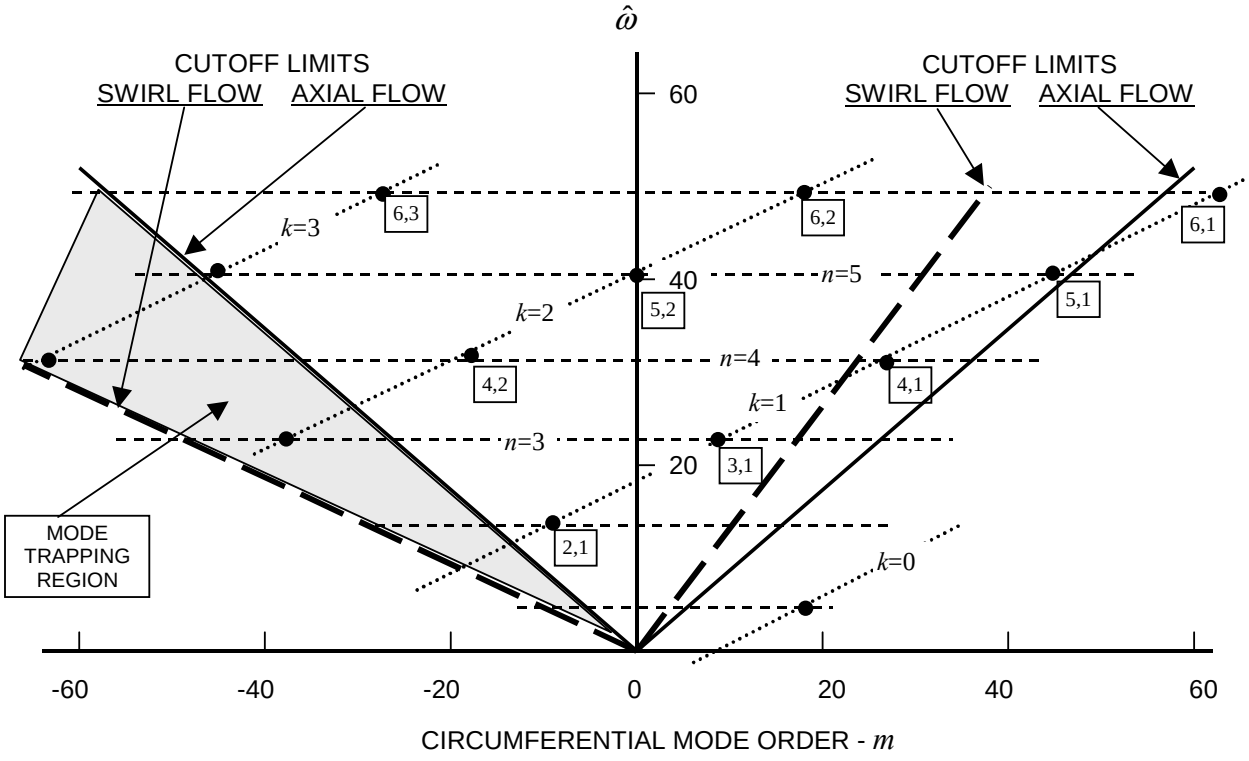

Figure 11. Mode order/frequency plot showing cutoff limits for both the axial flow region (upstream of rotor and downstream of stator) and for the swirl region (between rotor and stator). In the swirl region, M_y = 0.4. In the shaded region, modes can reflect back and forth between rotor and stator but cannot propagate beyond the blade rows.

derives equations for coupling rotor and stator using a matrix of scattering coefficients and vectors of modal amplitudes for the scattered waves. Section 7 relates a standard turbulence spectrum to a source vector, which drives the coupled equations, and presents working equations used in the prediction code CupBB. Sample calculations are shown in Section 8.

The prediction scheme is based on the independent mode set property described above so as to minimize the required computer resources. Rather than treating broadband prediction as one very large coupling problem, it is broken down into many small coupling problems via loops on frequency ω_0, radial mode order μ, and the mode order shift index q. Each of these smaller analyses finds amplitudes of all of the modes and frequencies in a mode subset (as shown, for example, in Figure 9) by solving a series of simultaneous equations (derived in Section 6) for blade row scattering. Excitation for the system is given by modes of the turbulence input at all the same orders and frequencies simultaneously.

SECTION 5
FOURIER TRANSFORMS AND STANDARD WAVESET NOTATION

The preceding section established the scattering rules for broadband rotor/stator interaction. In this section, we develop a notation system for Fourier transforms tailored to those rules and designed to facilitate development of the code for noise prediction.

Recall that the totality of modes that participate in the interaction can be broken down into independent sub-sets that scatter only among themselves. And recall from Section 4 that for excitation with a given frequency offset ω_0, mode offset q, and radial order μ, the set of permitted frequencies and circumferential mode orders is given by

$$\begin{aligned} &\text{frequency :} \quad \omega = \omega_o + nB_1\Omega, && n = \ldots -1,\ 0,\ 1,\ 2, \ldots \\ &\text{mode order :} \quad m = q + nB_1 - kB_2 && k = \ldots -1,\ 0,\ 1,\ 2, \ldots \end{aligned} \tag{5.1}$$

i.e. frequencies are separated by blade passing frequency and circumferential mode orders are restricted to the values of m resulting from integer values of the rotor and stator scattering indices, n and k as shown in Figure 9. Thus, in the computer code, we can set up loops on ω_0, μ, and q and solve a relatively small coupling problem for scattering on n and k for each of these combinations. In each case, the input is a vector of turbulence modes for all n and k and the response is found simultaneously for the acoustic modes with the same n's and k's .

The pressure and vortical wave systems are treated separately below.

Pressure Waves

Background flow for the unsteady interactions will be divided into 3 distinct regions as shown in Figure 3 and counted by the index r :

r = 1: upstream of rotor
r = 2: between rotor and stator
r = 3: downstream of stator

Furthermore, in each region, there are 4 distinct wave types (or families) counted by index T :

T = 1: Upstream-going pressure waves
T = 2: Downstream-going pressure waves
T = 3 and 4: Two independent sets of vortical (convected) waves

These indices are used to express pressure waves (T = 1 or 2) in region r as a typical Fourier integral

$$p_T^r(\mathbf{x}, t) = \int_{-\infty}^{+\infty} P_T^r(\mathbf{x}, \omega)\, e^{-i\omega t}\, d\omega \tag{5.2}$$

To coordinate with the frequency scattering rule, we break the frequency axis into segments each BPF long

$$p_T^r(\mathbf{x},t) = \sum_{n=-\infty}^{\infty} \int_0^{B_1\Omega} P_T^r(\mathbf{x},\omega_o + nB_1\Omega)\; e^{-i(\omega_o + nB_1\Omega)t}\, d\omega_o \tag{5.3}$$

and then further expand the Fourier transform as follows to coordinate with the radial and circumferential scattering rules

$$P_T^r(\mathbf{x},\omega_o + nB_1\Omega) = p_o \sum_{\mu=0}^{\infty} \sum_{q=0}^{B_2-1} \sum_{k=-\infty}^{\infty} P_{T\mu qk}^r(\omega_o + nB_1\Omega)\; e^{i[k_{xTnk}^r (x - x_T^r) + m\phi]} \cos(\frac{\mu\pi z}{h}) \tag{5.4}$$

where p_o is a reference pressure taken to be the sea level, standard day value. x_T^r is the x reference location for the type T waves in region r. We have an independent scattering problem for each combination of ω_0 , μ , q. The solution to each of those scattering problems gives $P_{T\mu qk}^r(\omega_o + nB_1\Omega)$ for a range of n's and k's as shown in the mode/frequency plot of Figure 9.

We will solve for only a small number of ω_o's and they will be discretized as ω_j . For example, if we are satisfied to discretize the frequency axis with points at the BPF harmonics and points midway between, we would use

$$\begin{aligned} \omega_1 &= 0.5B_1\Omega \\ \omega_2 &= \quad B_1\Omega \end{aligned} \tag{5.5}$$

Along the frequency axis represented below, the simultaneous solution for ω_1 would find the spectral levels for all frequencies marked by × and the solution for ω_2 would find the levels for the frequencies marked by • .

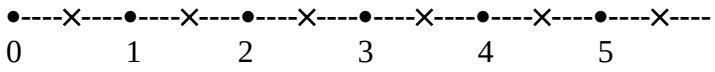

The velocity components for the 2 pressure wave types (and the vortical waves) can be written in form parallel to Eq. 5.3 as follows.

$$\begin{aligned} u_T^r(\mathbf{x},t) &= \sum_{n=-\infty}^{\infty} \int_0^{B_1\Omega} U_T^r(\mathbf{x},\omega_o + nB_1\Omega)\; e^{-i(\omega_o + nB_1\Omega)t}\, d\omega_o \\ v_T^r(\mathbf{x},t) &= \sum_{n=-\infty}^{\infty} \int_0^{B_1\Omega} V_T^r(\mathbf{x},\omega_o + nB_1\Omega)\; e^{-i(\omega_o + nB_1\Omega)t}\, d\omega_o \\ w_T^r(\mathbf{x},t) &= \sum_{n=-\infty}^{\infty} \int_0^{B_1\Omega} W_T^r(\mathbf{x},\omega_o + nB_1\Omega)\; e^{-i(\omega_o + nB_1\Omega)t}\, d\omega_o \end{aligned} \tag{5.6}$$

where

$$U_T^r(\mathbf{x},\omega_o+nB_1\Omega)=a_o\sum_{\mu=0}^{\infty}\sum_{q=0}^{B_2-1}\sum_{k=-\infty}^{\infty}U_{T\mu qk}^r(\omega_o+nB_1\Omega)\;e^{i[k_{xTnk}^r(x-x_T^r)+m\phi]}\cos(\frac{\mu\pi z}{h})$$

$$V_T^r(\mathbf{x},\omega_o+nB_1\Omega)=a_o\sum_{\mu=0}^{\infty}\sum_{q=0}^{B_2-1}\sum_{k=-\infty}^{\infty}V_{T\mu qk}^r(\omega_o+nB_1\Omega)\;e^{i[k_{xTnk}^r(x-x_T^r)+m\phi]}\cos(\frac{\mu\pi z}{h}) \qquad (5.7)$$

$$W_T^r(\mathbf{x},\omega_o+nB_1\Omega)=a_o\sum_{\mu=0}^{\infty}\sum_{q=0}^{B_2-1}\sum_{k=-\infty}^{\infty}W_{T\mu qk}^r(\omega_o+nB_1\Omega)\;e^{i[k_{xTnk}^r(x-x_T^r)+m\phi]}\sin(\frac{\mu\pi z}{h})$$

Later, we will need to express the velocity transforms in terms of the velocity perturbations to represent turbulence (i.e. to invert Eq. 5.6 for T = 3, 4). These can be found in the usual manner from Eqs. 5.6 and 5.7 by exploiting the orthogonality of sinusoidal and exponential functions. For example, the transverse velocity transform is

$$V_{T\mu qk}^r(\omega_o+nB_1\Omega)=\frac{1}{4\pi^2Ra_ohU\varepsilon_\mu}\int_{-\infty}^{\infty}\int_{-\pi R}^{\pi R}\int_0^{h_D}\tilde{v}_T^r(\tilde{\mathbf{x}})e^{-i(k_{xTnk}\tilde{x}+\frac{m}{R}\tilde{y})}\cos(\frac{\mu\pi z}{h})\,d\tilde{x}\,d\tilde{y}\,dz \qquad (5.8)$$

where $\varepsilon_\mu = 1$ for $\mu = 0$ and = ½ for $\mu > 0$. $\tilde{\mathbf{x}} = (\tilde{x}, \tilde{y}, z)$ is the fluid-fixed coordinate. $\tilde{v}_T^r$ is the velocity represented in the fluid-fixed frame, i.e. $\tilde{v}_T^r(\tilde{\mathbf{x}}) = v_T^r(\tilde{\mathbf{x}}+\mathbf{U}t,t)$. The transform $U_{T\mu qk}^r(\omega_o+nB_1\Omega)$ of the axial velocity is the same but with $\tilde{v}_T^r$ replaced by $\tilde{u}_T^r$.

[Note that in this type of waveform analysis, the integral in Eq. 5.8 will not converge if the extent of the velocity field is infinite in the x direction. One procedure for dealing with this is to set the perturbation velocity to zero outside of a region given by $-U\tau < x < U\tau$ where 2τ is the time for the block of flow to pass the cascade. This guarantees convergence of the integral. When the desired energy spectrum is found, it can be divided by 2τ to find the power spectrum. Then we can take the limit as τ approaches infinity.]

In the following, we define some non-dimensional quantities based on a representative radius R. Parameter R is a constant for the problem and can be thought of as a scaling parameter that brings the notation for our rectilinear representation of the fan closer to notation used in full 3D annular representations. Thus, from Eqs. 3.13 and 3.14 the axial wavenumber becomes

$$\hat{k}_{xTnk}^r \equiv k_{xTnk}^r R=\frac{1}{\beta_x^2}\left[M_x^r(-\hat{\omega}+mM_y^r)\mp\sqrt{(-\hat{\omega}+mM_y^r)^2-\beta_x^2(m^2+\hat{\nu}^2)}\right] \qquad (5.9)$$

with the upper,lower sign going with T = 1,2 and from Eq. 3.7

$$\Lambda_{Tnk}^r \equiv \frac{\lambda_T R}{a_r}=-\hat{\omega}+M_x^r\,\hat{k}_{xTnk}^r+M_y^r\,m \qquad (5.10)$$

with $\hat{\omega}=\omega R/a_r=\left(\frac{\omega_o}{B_1\Omega}+n\right)B_1M_t^r$ where $M_t^r=\Omega R/a_r$ is the tip rotational Mach number and M_x^r and M_y^r are the axial and swirl Mach numbers. All Mach numbers are based on local sound speed a_r in the regions counted by r.

In defining the standard wave sets, we deal with *defining* components and *associated* components. The pressure waves are *defined* in terms of the pressure amplitude coefficients on the right hand side of Eq. 5.4. The *associated* acoustic velocity components can be related to the pressure coefficients by inspection of Eqs. 3.15:

$$
\begin{aligned}
&P^r_{T\mu qk}(\omega_o + nB_1\Omega) = \text{defining coefficient for pressure waves} \\
&U^r_{T\mu qk}(\omega_o + nB_1\Omega) = \frac{p_o}{\rho_r a_o a_r}\left(\frac{-\hat{k}^r_{xTnk}}{\Lambda^r_{Tnk}}\right) P^r_{T\mu qk}(\omega_o + nB_1\Omega) \\
&V^r_{T\mu qk}(\omega_o + nB_1\Omega) = \frac{p_o}{\rho_r a_o a_r}\left(\frac{-m}{\Lambda^r_{Tnk}}\right) P^r_{T\mu qk}(\omega_o + nB_1\Omega) \qquad T = 1,2 \\
&W^r_{T\mu qk}(\omega_o + nB_1\Omega) = \frac{p_o}{\rho_r a_o a_r}\left(\frac{-i\mu\pi/H_D}{\Lambda^r_{Tnk}}\right) P^r_{T\mu qk}(\omega_o + nB_1\Omega)
\end{aligned}
\tag{5.11}
$$

Thus, if $P^r_{T\mu qk}(\omega_o + nB_1\Omega)$ were known, the pressure field could be constructed from Eqs. 5.3 and 5.4 . In fact, in Section 6, the $P^r_{T\mu qk}(\omega_o + nB_1\Omega)$ transforms with ranges of the indices *r, T, n, k* will be used as elements of the system state vector similar to the Fourier coefficients in the state vector for the tone problem in Eq.2.5.

Vortical Waves (*T* = 3, 4)

Since vorticity is a 3D vector, it might appear that 3 components could be specified independently. However, because the convected field satisfies the continuity equation $\nabla \cdot \mathbf{u} = 0$, only 2 are independent. In fact, for the $\mu = 0$ case, which corresponds to 2D flow, there is only one component.

We deal with the $\mu > 0$ cases first and define 2 families as follows

T = 3 family: has v and w components but no u
T = 4 family: has u and w components but no v

The T = 3 family is defined via the transverse velocity component in a form parallel to the pressure wave families. Thus, the $V^r_{3\mu qk}(\omega_o + nB_1\Omega)$'s are the defining coefficients (that go into the state vector). Again, the associated $W^r_{3\mu qk}(\omega_o + nB_1\Omega)$'s are related through the continuity equation, $\partial w/\partial z = -\partial v/\partial y$. Hence,

$$
\begin{aligned}
&\text{for } \mu > 0, \qquad P^r_{3\mu qk}(\omega_o + nB_1\Omega) = 0 \\
&U^r_{3\mu qk}(\omega_o + nB_1\Omega) = 0 \\
&V^r_{3\mu qk}(\omega_o + nB_1\Omega) = \text{Defining component} \\
&W^r_{3\mu qk}(\omega_o + nB_1\Omega) = \left(\frac{-im}{\mu\pi/H_D}\right) V^r_{3\mu qk}(\omega_o + nB_1\Omega)
\end{aligned}
\tag{5.12}
$$

The T = 4 family is defined via the axial velocity. Thus, the $U^r_{4\mu qk}(\omega_o + nB_1\Omega)$'s are the defining coefficients (that go into the state vector). The $W^r_{4\mu qk}(\omega_o + nB_1\Omega)$'s are related through the continuity equation, $\partial w/\partial z = -\partial u/\partial x$,

$$\text{for } \mu > 0, \qquad \begin{aligned} &P^r_{4\mu qk}(\omega_o + nB_1\Omega) = 0 \\ &U^r_{4\mu qk}(\omega_o + nB_1\Omega) = \text{Defining component} \\ &V^r_{4\mu qk}(\omega_o + nB_1\Omega) = 0 \\ &W^r_{4\mu qk}(\omega_o + nB_1\Omega) = \left(\frac{-i\hat{k}^r_{x4nk}}{\mu\pi/H_D}\right) U^r_{4\mu qk}(\omega_o + nB_1\Omega) \end{aligned} \tag{5.13}$$

Finally, we define the vortical waves for μ = 0. They only exist for the T = 3 type. We still choose to define these by the transverse component but now the associated component is the axial velocity via $\partial u/\partial x = -\partial v/\partial y$ and the radial velocity is 0.

$$\text{for } \mu = 0, \qquad \begin{aligned} &P^r_{3\mu qk}(\omega_o + nB_1\Omega) = 0 \\ &U^r_{3\mu qk}(\omega_o + nB_1\Omega) = \left(\frac{-m}{\hat{k}^r_{x3nk}}\right) V^r_{3\mu qk}(\omega_o + nB_1\Omega) \\ &V^r_{3\mu qk}(\omega_o + nB_1\Omega) = \text{Defining component} \\ &W^r_{3\mu qk}(\omega_o + nB_1\Omega) = 0 \end{aligned} \tag{5.14}$$

The reader can verify that the wave families defined above satisfy the continuity and momentum equations in each of the 3 flow regions and that the boundary conditions of periodicity in ϕ and flow tangency at z = 0 and h are satisfied.

In the above, wavenumbers for the convected waves are normalized (from Eq. 3.17) as follows

$$\hat{k}^r_{x3nk} = \hat{k}^r_{x4nk} \equiv \frac{\hat{\omega} - mM_y}{M_x} \tag{5.15}$$

In the next section, we will show how the defining components established above are used in the state vector and coupling equations.

SECTION 6

SCATTERING COEFFICIENTS AND THE COUPLING EQUATIONS

In this section, we develop the rotor/stator system coupling equations; these match the modal output of the stator to the modal input of the rotor and *vice versa* and show how the turbulence enters as a source, i.e. excitation, for the system. This is all in terms of Fourier transforms of the acoustic and vortical perturbations – as if they were known. Since, in fact, they are knowable only in a statistical sense, both the turbulence and resulting noise must be treated in terms of expected values of magnitudes of the Fourier transforms. That subject is treated in Section 7 where we show how to compute the power spectral density of the sound from the turbulence spectrum.

In the preceding section, we developed expressions for all permitted perturbations in the 3 regions under consideration:

Region $r = 1$ - upstream of rotor
Region $r = 2$ - between rotor and stator
Region $r = 3$ - downstream of stator

The waves are of 4 types:

Type $T = 1$ - upstream going pressure waves
Type $T = 2$ - downstream going pressure waves
Type $T = 3$ - vortical waves (first independent set based on v – velocity component)
Type $T = 4$ - vortical waves (second independent set based on u – velocity component)

Perturbations were expressed in Fourier expansions. If the Fourier coefficients were known, the flow would be completely defined from Eqs. 5.3 to 5.14. The coefficients defining the waves are of the form $P^r_{T\mu qk}(\omega_o + nB_1\Omega)$. We form a state vector of these coefficients and compress the notation for convenience. Thus, for each region r,

$$\begin{aligned} A^r_1(n,k) &= P^r_{1\mu qk}(\omega_o + nB_1\Omega) \\ A^r_2(n,k) &= P^r_{2\mu qk}(\omega_o + nB_1\Omega) \\ A^r_3(n,k) &= V^r_{3\mu qk}(\omega_o + nB_1\Omega) \\ A^r_4(n,k) &= U^r_{4\mu qk}(\omega_o + nB_1\Omega) \end{aligned} \tag{6.1}$$

The ordered array of the $A^r_T(n,k)$'s is the state vector **A .** The n's run over user-specified frequency limits (from $-NH$ to $+NH$). The k's run over ranges determined by cuton of the acoustic waves and decay of the turbulence spectrum. The μ's , q's , and ω_o's are not needed in the state vector notation because they are constant parameters for each coupling sub-problem.

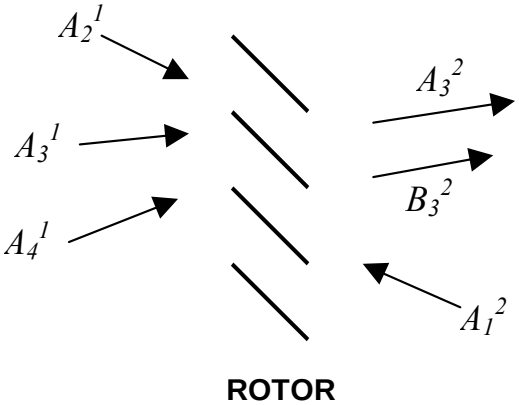

Figure 12. Sketch to explain rotor scattering

To help understand the structure of the coupling equations, consider the scattering of modes by the rotor shown in Figure 12. First, note in general that output waves are the sum of scattered waves and prescribed waves (the source, or turbulence waves). We focus on the output vortical waves (Type 3) in region 2 (to the right of the rotor) and what contributes to them. These can be scattered into from each of the 4 input wave types and that action is denoted by scattering coefficients as follows.

$$A_3^2(n',k) = \sum_n \Big[\; S_{31}^{22}(n',k;n,k)A_1^2(n,k) + S_{32}^{21}(n',k;n,k)A_2^1(n,k) + S_{33}^{21}(n',k;n,k)A_3^1(n,k) + S_{34}^{21}(n',k;n,k)A_4^1(n,k) \; \Big] + B_3^2(n',k) \tag{6.2}$$

This meaning of this equation is that the Type 3 vortical waves in region 2 come from scattering of the up-going pressure waves (T = 1) in region 2 and scattering of the Types 2, 3, and 4 waves in region 1. The summation is on the n index since we found in Section 4 that rotors scatter on n and not on k. We have also added $B_3^2(n',k)$. These are source waves that are to be prescribed as excitation for the system. Notation for the scattering coefficients is

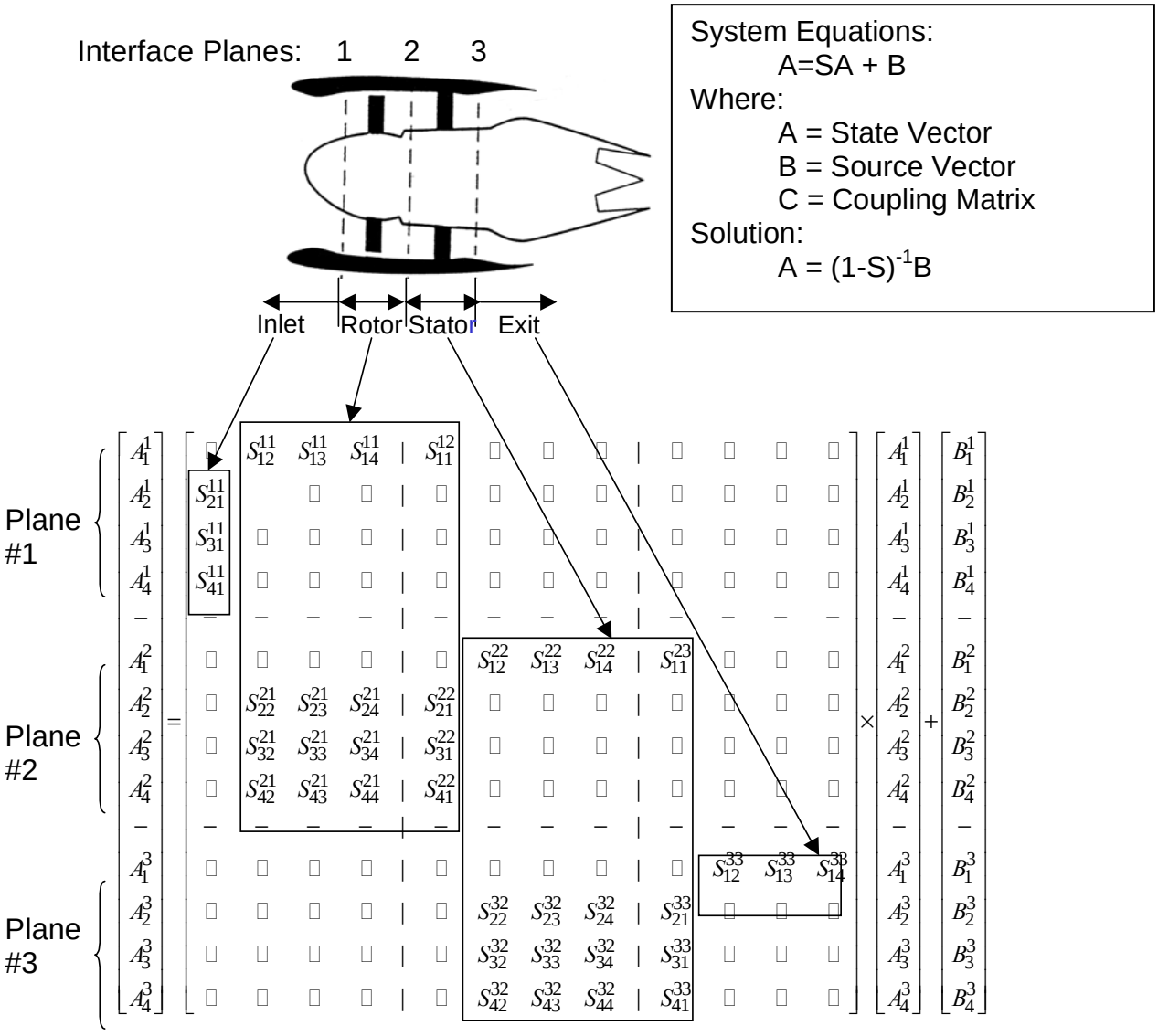

Figure 13. System coupling matrix

$S_{T'T}^{r'r}(n',k';n,k)$ with the unprimed indices denoting input modes scattered from and the primed indices denoting output modes scattered into.

Equation 6-2 can be generalized to treat the entire inlet/rotor/stator/nozzle problem as shown in Figure 13. Equation 6.2 can be seen as the 7th line of the matrix equation. All of the other scattering coefficients are shown as well. Dots indicate empty elements, or no scattering. The next sections show how the stator and rotor scattering coefficients are computed. (We ignore scattering from inlet and nozzle in this report but expect to address it in the future.)

Computation of Stator Scattering Coefficients

The stator acoustic element consists of the stator vanes themselves and an actuator disk which represents turning of the mean flow. The jump in mean flow properties across the disk determines jumps in perturbation quantities via conservation of mass and momentum. In this section we first treat scattering by the vanes and then later show how the actuator disk effect is added.

To compute scattering by the stator vanes, note that the connection between input modes and output modes is through the upwash at the stator. Thus, we need to find the upwash associated with each of the 4 input wave types. Then, we need to find the amplitudes of each of the 4 response modes to unit upwash. The required scattering coefficients are formed from the 16 combinations of input and output. The upwashes associated with various wave types follow from the wave kinematics of Section 5 and are shown on the right in Table 1 under "Excitation". The output mode amplitudes due to unit upwash are found using Glegg's Wiener-Hopf cascade method (as explained later in this section) and are shown on the left in the table under "Response". Notation $S_{T'T}^{r'r}(n,k';n,k)$ is used for scattering by the vanes. Its meaning is given by

$$A_{T'}^{r'}(n,k') \leftarrow S_{T'T}^{r'r}(n,k';n,k)\,A_T^r(n,k) \tag{6.3}$$

When the actuator disk is added, the coefficients will be modified and placed in the scattering matrix with the same notation. For example, scattering of vortical waves into downstream pressure waves is given by

$$A_2^{3'}(n,k') \leftarrow S_{23}^{3'2}(n,k';n,k)\,A_3^2(n,k) \tag{6.4}$$

The prime on the superscript on the LHS indicates that the coefficient does not yet apply to Region 3; this will be dropped when the actuator disk is included. This coefficient for scattering of the type 3 vortical waves (with μ = 0) into down-going pressure waves can be constructed from elements of Table 1,

$$S_{23}^{3'2}(n,k';n,k) = \left(\frac{1.4i\pi\hat{c}_2}{\bar{g}_2}\frac{P_2}{A_2}\frac{\Lambda_{2nk'}^2\hat{\zeta}_{2nk'}D_{2nkk'}}{R_{nk'}}\right)\left(\frac{m}{\hat{k}_{x3nk}^2}\sin\theta_2+\cos\theta_2\right) \tag{6.5}$$

Derivations of the excitation and response factors in Table 1 are discussed in the next 2 sections.

TABLE 1

FACTORS FOR STATOR SCATTERING COEFFICIENTS

T'	Response	T	Excitation
1	$A_1^2(n,k') = \dfrac{-1.4i\pi\hat{c}_2}{\bar{g}_2}\dfrac{P_2}{A_2}\dfrac{\Lambda_{1nk'}^2\hat{\zeta}_{1nk'}D_{1nkk'}}{R_{nk'}}\dfrac{w_{nk}}{a_o}$	1	$\dfrac{w_{nk}}{a_o} = \dfrac{A_2}{1.4P_2}\dfrac{\hat{k}_{x1nk}^2\sin\theta_2 - m\cos\theta_2}{\Lambda_{1nk}^2}A_1^{3'}(n,k)$
2	$A_2^{3'}(n,k') = \dfrac{+1.4i\pi\hat{c}_2}{\bar{g}_2}\dfrac{P_2}{A_2}\dfrac{\Lambda_{2nk'}^2\hat{\zeta}_{2nk'}D_{2nkk'}}{R_{nk'}}\dfrac{w_{nk}}{a_o}$	2	$\dfrac{w_{nk}}{a_o} = \dfrac{A_2}{1.4P_2}\dfrac{\hat{k}_{x2nk}^2\sin\theta_2 - m\cos\theta_2}{\Lambda_{2nk}^2}A_2^2(n,k)$
3	<u>all μ</u> $A_3^{3'}(n,k') = \dfrac{-2\pi i}{\bar{g}_2\cos\theta_2}\left(\dfrac{\hat{\alpha}_{nk'}\hat{\gamma}_c\sin\theta_2 + \hat{\zeta}_c^2\cos\theta_2}{\hat{\gamma}_c^2 + \hat{\alpha}_{nk'}^2 + \hat{\nu}^2}\right)K_{nk}\dfrac{w_{nk}}{a_o}$	3	<u>μ=0</u> $\dfrac{w_{nk}}{a_o} = \left(\dfrac{m}{\hat{k}_{x3nk}^2}\sin\theta_2 + \cos\theta_2\right)A_3^2(n,k)$ <u>μ>0</u> $\dfrac{w_{nk}}{a_o} = (\cos\theta_2)A_3^2(n,k)$
4	<u>μ>0</u> $A_4^{3'}(n,k') = \dfrac{-2\pi i}{\bar{g}_2\cos\theta_2}\left(\dfrac{\hat{\alpha}_{nk'}\hat{\gamma}_c\cos\theta_2 - \hat{\zeta}_c^2\sin\theta_2}{\hat{\gamma}_c^2 + \hat{\alpha}_{nk'}^2 + \hat{\nu}^2}\right)K_{nk}\dfrac{w_{nk}}{a_o}$	4	<u>μ>0</u> $\dfrac{w_{nk}}{a_o} = (-\sin\theta_2)A_4^2(n,k)$

Above, $D_{T'nkk'}$ is the potential jump across the wake from Glegg's theory (see Appendix A). Subscripts nkk' indicate input waves with interblade phase

$$\sigma = \frac{2\pi m}{B_2}\ , \qquad m = q + nB_1 - kB_2$$

and output waves with interblade phase

$$\sigma' = \frac{2\pi m'}{B_2}\ , \qquad m' = q + nB_1 - k'B_2$$

Also,

$$\Lambda_{T'nk'}^2 = -\hat{\omega} + M_x\hat{k}_{xT'nk'}^2 + M_y m'$$

and in

$$\hat{\zeta}_{T'nk'} = \frac{1}{\beta_x^2}\left[R_{nk'}\sin\theta_2 \pm (\beta^2 m' + \hat{\omega}M_y)\cos\theta_2\right]$$

the upper, lower sign goes with T' = 1,2. K_{nk} is Glegg's vorticity factor (K(χ_c) in Appendix B), which depends only on n and k (not on k'). The wavenumbers required for vortical response are

$$\hat{\gamma}_c = \hat{\omega}/M \qquad \hat{\alpha}_{nk'} = -\hat{k}_{x3nk'}^2\sin\theta_2 + m'\cos\theta_2 \qquad \hat{\nu} = \mu\pi/H_D \qquad \hat{\zeta}_c^2 = -(\hat{\gamma}_c^2 + \hat{\nu}^2)$$

Excitation Factors

Here, as an example, we show how the excitation factor for down-going pressure waves at the stator is derived; this is the second item in the right column of Table 1. The remaining excitation factors can be derived in similar fashion.

The upwash at the stator due to the down-going pressure waves in region 2 is given by

$$w(\mathbf{x},t) = -u_2^2(\mathbf{x},t)\sin\theta_2 + v_2^2(\mathbf{x},t)\cos\theta_2 \tag{6.6}$$

By using Eqs. 5.6 and 5.7, it can be shown that the coefficient of the upwash is

$$w_{nk} = a_o\left[-U_{2\mu qk}^2(\omega_o + nB_1\Omega)\sin\theta_2 + V_{2\mu qk}^2(\omega_o + nB_1\Omega)\cos\theta_2\right] \tag{6.7}$$

The U and V coefficients are related by Eqs. 5.11 to the P coefficient that defines the pressure wave. When these are substituted into Eq. 6.7, the result is

$$\frac{w_{nk}}{a_o} = \frac{p_o}{\rho_2 a_2 a_o}\left[\frac{\hat{k}_{x2nk}^2\sin\theta_2 - m\cos\theta_2}{\Lambda_{2nk}^2}\right]P_{2\mu qk}^2(\omega_o + nB_1\Omega) \tag{6.8}$$

The factor before the square brackets can be modified using $\rho_2 a_2^2 = \gamma p_2$ where γ is the ratio of specific heats (γ= 1.4 for air). Using this and replacing $P_{2\mu qk}^2(\omega_o + nB_1\Omega)$ with $A_2^2(n,k)$ lead to

$$\frac{w_{nk}}{a_o} = \frac{A_2}{1.4\,P_2}\left[\frac{\hat{k}_{x2nk}^2\sin\theta_2 - m\cos\theta_2}{\Lambda_{2nk}^2}\right]A_2^2(n,k) \tag{6.9}$$

which is the second item on the right in Table 1, as desired. A_2 and P_2 are speed of sound and pressure in region 2 normalized to sea level, standard day conditions.

Response Factors

These are the factors in the left column of Table 1 and are computed using Glegg's Wiener-Hopf cascade method. As an example, we derive the modal coefficient for upgoing waves from the stator due to unit upwash (the first item in column 1 of Table 1).

Appendix A adapts Glegg's equations to duct coordinates and to our modal indices n, k, and μ. Equation A-43 gives the pressure wave scattered into mode n,k' due to upwash in mode n,k as

$$p_{nkk'} = \frac{-i\pi\,\rho_2\,a_2\,\hat{c}_2}{\bar{g}_2}\,w_{nk}\,\frac{\Lambda_{1nk'}^2\,\hat{\xi}_{1nk'}^2\,D_{1nkk'}}{R_{nk'}}\,e^{i[k_{x1nk'}^2 x + m'\phi - \omega t]}\cos\left(\frac{\mu\pi z}{h}\right) \tag{6.10}$$

where we have replaced Glegg's $\pm$ superscript notation indicating up/down going waves with a subscript 1, since we are addressing upstream going waves. Upon comparison with Eq. 5.4, we can write for the modal coefficient of the upgoing wave, at frequency $\omega = \omega_o + nB_1\Omega$

$$P^2_{1\mu qk}(\omega_o + nB_1\Omega) = \frac{-i\pi\,\rho_2\,a_2\,\hat{c}_2}{p_o\,\bar{g}_2}\;\frac{\Lambda^2_{1nk'}\,\hat{\zeta}^2_{1nk'}\,D_{1nkk'}}{R_{nk'}}\,w_{nk} \tag{6.11}$$

Note that the phase in Eq. 6.11 is based on an x-origin at the leading edge. In code CupBB, origins are shifted to the appropriate reference planes after coupling to the actuator disks.

In Eq. 6.11, we again apply $\rho_2 a_2^2 = 1.4 p_2$ and replace $P^2_{1\mu qk'}(\omega_o + nB_1\Omega)$ with $A^2_1(n,k')$, leading to

$$A^2_1(n,k') = \frac{-1.4\,i\pi\,\hat{c}_2}{\bar{g}_2}\;\frac{P_2}{A_2}\,\frac{\Lambda^2_{1nk'}\,\hat{\zeta}^2_{1nk'}\,D_{1nkk'}}{R_{nk'}}\,\frac{w_{nk}}{a_o} \tag{6.12}$$

This is the response factor giving the modal coefficients for up-going waves from the stator due to unit upwash. It is the first item in the left column of Table 1, which was to be found. The factor relating to downstream pressure wave response follows immediately. The response of the vortical waves can be found from Equations in Appendix B.

Rotor Scattering Coefficients

Derivation of the rotor scattering coefficients proceeds in the same manner as that for the stator. The 16 groups of coefficients are formed from factors in Table 2. The 4 inputs in the right column drive the 4 responses in the left column. The resulting coefficients are denoted by $S^{r'r}_{T'T}(n',k;n,k)$. They are then modified by the effect of the rotor actuator disk and placed in the system scattering matrix $\mathbf{S}$.

TABLE 2
FACTORS FOR ROTOR SCATTERING COEFFICIENTS

T'	Response	T	Excitation
1	$A_1^{1'}(n',k) = \dfrac{-1.4i\pi\hat{c}_1}{\bar{g}_1}\dfrac{P_2}{A_2}\dfrac{\Lambda_{1n'k}^2\,\hat{\xi}_{1n'k}\,D_{1nkn'}}{R_{n'k}}\dfrac{w_{nk}}{a_o}$	1	$\dfrac{w_{nk}}{a_o} = \dfrac{A_2}{1.4P_2}\dfrac{\hat{k}_{x1nk}^2\sin\theta_1 - m\cos\theta_1}{\Lambda_{1nk}^2}A_1^{2}(n,k)$
2	$A_2^{2}(n',k) = \dfrac{+1.4i\pi\hat{c}_1}{\bar{g}_1}\dfrac{P_2}{A_2}\dfrac{\Lambda_{2n'k}^2\,\hat{\xi}_{2n'k}\,D_{2nkn'}}{R_{n'k}}\dfrac{w_{nk}}{a_o}$	2	$\dfrac{w_{nk}}{a_o} = \dfrac{A_2}{1.4P_2}\dfrac{\hat{k}_{x2nk}^2\sin\theta_1 - m\cos\theta_1}{\Lambda_{2nk}^2}A_2^{1'}(n,k)$
3	<u>all μ</u> $A_3^{2}(n',k) = \dfrac{-2\pi i}{\bar{g}_1\cos\theta_1}\left(\dfrac{\hat{\alpha}_{n'k}\hat{\gamma}_c\sin\theta_1 + \hat{\xi}_c^2\cos\theta_1}{\hat{\gamma}_c^2 + \hat{\alpha}_{n'k}^2 + \hat{\nu}^2}\right)K_{nk}\dfrac{w_{nk}}{a_o}$	3	<u>μ=0</u> $\dfrac{w_{nk}}{a_o} = \left(\dfrac{m}{\hat{k}_{x3nk}^2}\sin\theta_1 + \cos\theta_1\right)A_3^{1'}(n,k)$ <u>μ>0</u> $\dfrac{w_{nk}}{a_o} = (\cos\theta_1)A_3^{1'}(n,k)$
4	<u>μ>0</u> $A_4^{2}(n',k) = \dfrac{-2\pi i}{\bar{g}_1\cos\theta_1}\left(\dfrac{\hat{\alpha}_{n'k}\hat{\gamma}_c\cos\theta_1 - \hat{\xi}_c^2\sin\theta_1}{\hat{\gamma}_c^2 + \hat{\alpha}_{n'k}^2 + \hat{\nu}^2}\right)K_{nk}\dfrac{w_{nk}}{a_o}$	4	<u>μ>0</u> $\dfrac{w_{nk}}{a_o} = (-\sin\theta_1)A_4^{1'}(n,k)$

Above, $D_{T'nkn'}$ is the potential jump across the wake from Glegg's theory (see Appendix A). Subscripts nkn' indicate input waves with interblade phase

$$\sigma = \frac{2\pi m}{B_2}, \qquad m = q + nB_1 - kB_2$$

and output waves with interblade phase

$$\sigma' = \frac{2\pi m'}{B_2}, \qquad m' = q + n'B_1 - kB_2$$

$$\Lambda_{T'n'k}^2 = -\hat{\omega} + M_x\hat{k}_{xT'n'k}^2 + M_y m'$$

and

$$\hat{\xi}_{T'n'k} = \frac{1}{\beta_x^2}\left[R_{n'k}\sin\theta_1 \pm (\beta_1^2 m' + \hat{\omega}_r(M_y - M_T))\cos\theta_1\right]$$

where $\beta_1^2 = 1 - M_1^2$ and M_1 is relative Mach number at the rotor and the upper, lower sign goes with the T=1,2 wave. K_{nk} is Glegg's vorticity factor ($K(\gamma_c)$ in Appendix B), which depends only on n and k (not on n'). And the wavenumbers required for vortical response are

$$\hat{\gamma}_c = \hat{\omega}_r / M_1 \qquad \hat{\alpha}_{n'k} = -\hat{k}_{x3n'k}^2\sin\theta_1 + m'\cos\theta_1 \qquad \hat{\nu} = \mu\pi/H_D \qquad \hat{\zeta}_c^2 = -(\hat{\gamma}_c^2 + \hat{\nu}^2)$$

Combining Blade and Vane Elements with Their Actuator Disks

The coupling scheme shown in Figure 13 treats 4 acoustic elements: Inlet, Rotor, Stator, and Nozzle. Only the rotor and stator are addressed in this report; inlet and nozzle reflection and transmission must be treated in a separate study. Figure 14 shows the mean flow entering the fan stage axially, turning at the rotor, and straightening back to axial at the stator. To deal with this turning, actuator disks are combined with the rotor and stator blade rows. Appendix C derives the actuator disk equations based on linearized equations for conservation of mass and momentum; jumps in background flow properties cause jumps in the wave modal amplitudes.

Code CupBB models the background flow via 1D isentropic (lossless) flow equations and the standard equation for action of the rotor

$$\Delta(\text{tangential velocity}) = \frac{C_p}{\text{wheel speed}} \times \Delta(\text{total temperature}) \tag{6.13}$$

Ambient conditions correspond to a standard day at sea level. The user inputs inlet axial Mach number, rotor rotational Mach number, and stage pressure ratio; the code calculates the remaining mean flow quantities based on isentropic flow and Eq. 6.13 assuming axial flow out of the stator.

This section shows how the actuator disk scattering factors are combined with the scattering factors just found for the blade rows to produce a combined rotor/actuator disk element and a combined stator/actuator disk element. These are the elements that are used in the coupling matrix of Figure 13.

Figure 14 shows the rotor with its actuator disk, the stator with its actuator disk, and all of the wave families included in the coupling scheme. As described earlier, the A's are elements of the state vector (to be found) and the B's are elements of the source vector (to be prescribed from a turbulence model). The A's and B's are further subscripted on the scattering indices n and k. The derivation below is in the context of the stator but the method of combining a blade row with its actuator disk is the same for the rotor as for the stator.

The lower part of Figure 14 shows the stator element broken down into the vane row and the actuator disk. Scattering equations for the vane row are

$$\begin{aligned}
A_1^a &= S_{12}^{aa} A_2^a + S_{13}^{aa} A_3^a + S_{14}^{aa} A_4^a + S_{11}^{ab} A_1^b + B_1^a \\
A_2^b &= S_{22}^{ba} A_2^a + S_{23}^{ba} A_3^a + S_{24}^{ba} A_4^a + S_{21}^{bb} A_1^b + B_2^b \\
A_3^b &= S_{32}^{ba} A_2^a + S_{33}^{ba} A_3^a + S_{34}^{ba} A_4^a + S_{31}^{bb} A_1^b + B_3^b \\
A_4^b &= S_{42}^{ba} A_2^a + S_{43}^{ba} A_3^a + S_{44}^{ba} A_4^a + S_{41}^{bb} A_1^b + B_4^b
\end{aligned} \tag{6.14}$$

and for the actuator disk are

$$
\begin{aligned}
A_1^b &= S_{12}^{bb} A_2^b + S_{13}^{bb} A_3^b + S_{14}^{bb} A_4^b + S_{11}^{bc} A_1^c \\
A_2^c &= S_{22}^{cb} A_2^b + S_{23}^{cb} A_3^b + S_{24}^{cb} A_4^b + S_{21}^{cc} A_1^c \\
A_3^c &= S_{32}^{cb} A_2^b + S_{33}^{cb} A_3^b + S_{34}^{cb} A_4^b + S_{31}^{cc} A_1^c \\
A_4^c &= S_{42}^{cb} A_2^b + S_{43}^{cb} A_3^b + S_{44}^{cb} A_4^b + S_{41}^{cc} A_1^c
\end{aligned}
\tag{6.15}
$$

These can be placed into a matrix system similar to that in Figure 13 as follows

$$
\begin{bmatrix} A_1^a \\ A_2^a \\ A_3^a \\ A_4^a \\ \hline A_1^b \\ A_2^b \\ A_3^b \\ A_4^b \\ \hline A_1^c \\ A_2^c \\ A_3^c \\ A_4^c \end{bmatrix}
=
\left[\begin{array}{cccc|cccc|cccc}
 & S_{12}^{aa} & S_{13}^{aa} & S_{14}^{aa} & S_{11}^{ab} & & & & & & & \\
 & & S_{AA} & & & & S_{AB} & & & & S_{AC} & \\
 & & & & & & & & & & & \\
\hline
 & & & & & S_{12}^{bb} & S_{13}^{bb} & S_{14}^{bb} & S_{11}^{bc} & & & \\
S_{BA} & & & & & & & & & & & \\
 & S_{22}^{ba} & S_{23}^{ba} & S_{24}^{ba} & S_{21}^{bb} & & S_{BB} & & & & S_{BC} & \\
 & S_{32}^{ba} & S_{33}^{ba} & S_{34}^{ba} & S_{31}^{bb} & & & & & & & \\
 & S_{42}^{ba} & S_{43}^{ba} & S_{44}^{ba} & S_{41}^{bb} & & & & & & & \\
\hline
 & & & & & & & & & & & \\
 & & & & S_{CB} & & & & & & & \\
 & & S_{CA} & & & S_{22}^{cb} & S_{23}^{cb} & S_{24}^{cb} & S_{21}^{cc} & & S_{CC} & \\
 & & & & & S_{32}^{cb} & S_{33}^{cb} & S_{34}^{cb} & S_{31}^{cc} & & & \\
 & & & & & S_{42}^{cb} & S_{43}^{cb} & S_{44}^{cb} & S_{41}^{cc} & & &
\end{array}\right]
\times
\begin{bmatrix} A_1^a \\ A_2^a \\ A_3^a \\ A_4^a \\ \hline A_1^b \\ A_2^b \\ A_3^b \\ A_4^b \\ \hline A_1^c \\ A_2^c \\ A_3^c \\ A_4^c \end{bmatrix}
=
\begin{bmatrix} B_1^a \\ B_2^a \\ B_3^a \\ B_4^a \\ \hline B_1^b \\ B_2^b \\ B_3^b \\ B_4^b \\ \hline B_1^c \\ B_2^c \\ B_3^c \\ B_4^c \end{bmatrix}
\tag{6.16}
$$

With the block matrix notation indicated by the shaded boxes Eq. 6.16 reduces to

$$
\begin{aligned}
A^a &= S_{AA} A^a + S_{AB} A^b &&+ B^a \\
A^b &= S_{BA} A^a + S_{BB} A^b + S_{BC} A^c &&+ B^b \\
A^c &= \qquad\quad S_{CB} A^b + S_{CC} A^c &&+ B^c
\end{aligned}
\tag{6.17}
$$

The middle line of Equation 6.17 can be written

$$
(1 - S_{BB}) A^b = S_{BA} A^a + S_{BC} A^c + B^b \tag{6.18}
$$

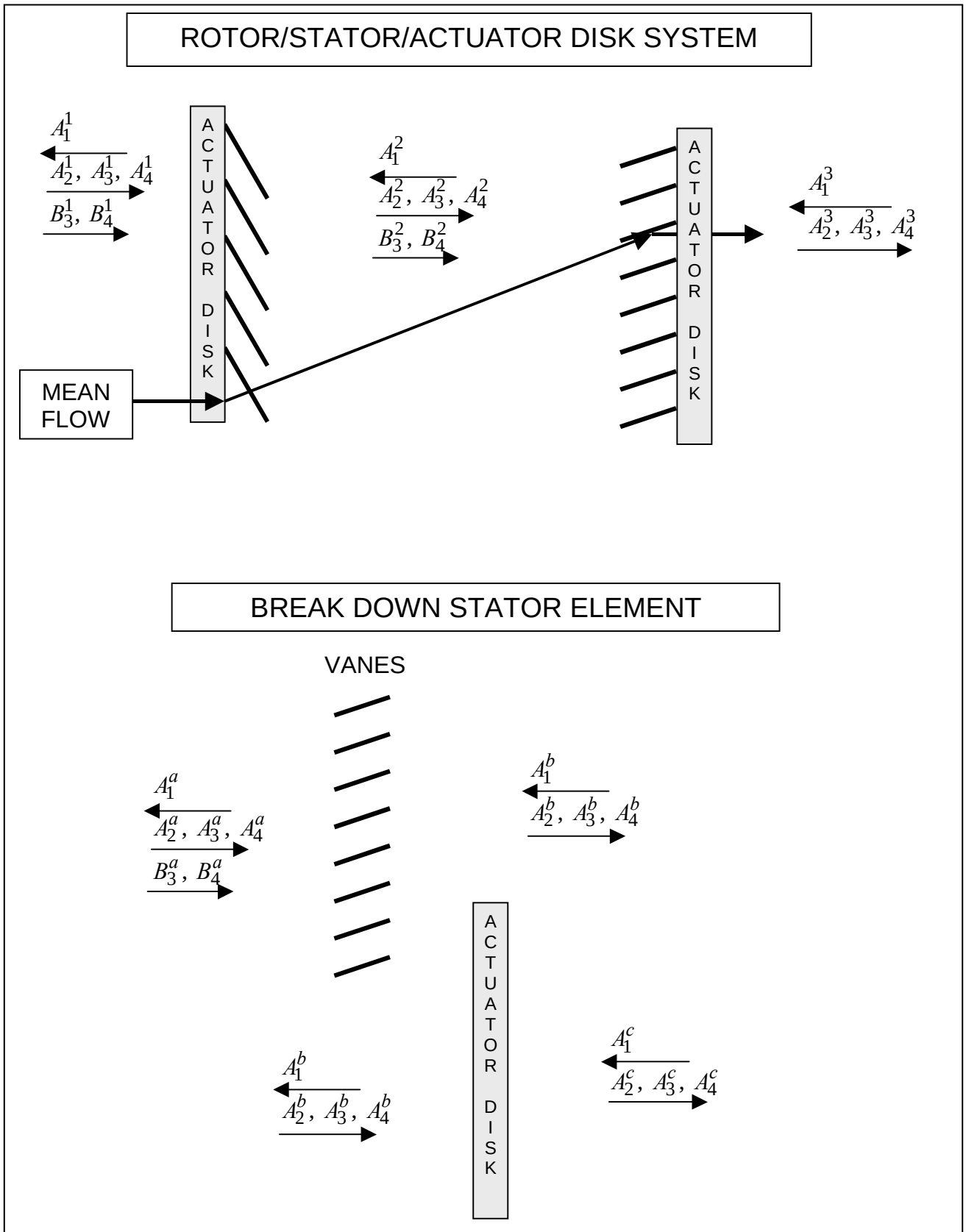

Figure 14. Rotor/stator actuator disk system.

and solved for A^b via

$$A^b = E\,S_{BA}A^a + E\,S_{BC}A^c + E\,B^b \tag{6.19}$$

where

$$E = (1 - S_{BB})^{-1} \tag{6.20}$$

Substitution of Equation 6.19 into the first and last lines of Equation 6.17 eliminates the scattered waves in the middle (b) region

$$\begin{aligned} A^a &= (S_{AA} + S_{AB}\,E\,S_{BA})A^a + S_{AB}\,E\,S_{BC}A^c + B^a + S_{AB}\,E\,B^b \\ A^c &= S_{CB}\,E\,S_{BA}A^a + (S_{CC} + S_{CB}\,E\,S_{BC})A^c + S_{CB}\,E\,B^b + B^c \end{aligned} \tag{6.21}$$

or

$$\begin{bmatrix} A^a \\ \hline A^c \end{bmatrix} = \left[\begin{array}{c|c} S_{AA} + S_{AB}\,E\,S_{BA} & S_{AB}\,E\,S_{BC} \\ \hline S_{CB}\,E\,S_{BA} & S_{CC} + S_{CB}\,E\,S_{BC} \end{array}\right] \times \begin{bmatrix} A^a \\ \hline A^c \end{bmatrix} + \begin{bmatrix} B^a + S_{AB}\,E\,B^b \\ \hline S_{CB}\,E\,B^b + B^c \end{bmatrix} \tag{6.22}$$

In the current application, we will not prescribe any source waves in the "b" region so that finally

$$\begin{bmatrix} A^a \\ \hline A^c \end{bmatrix} = \left[\begin{array}{c|c} S_{AA} + S_{AB}\,E\,S_{BA} & S_{AB}\,E\,S_{BC} \\ \hline S_{CB}\,E\,S_{BA} & S_{CC} + S_{CB}\,E\,S_{BC} \end{array}\right] \times \begin{bmatrix} A^a \\ \hline A^c \end{bmatrix} + \begin{bmatrix} B^a \\ \hline B^c \end{bmatrix} \tag{6.23}$$

This is the desired form for combining the stator vanes and the stator actuator disk into a single acoustic element. The scattered waves in the region between the vanes and the disk have been eliminated from the equations so that the input/output properties of the stator element are completely specified by the A^a and A^c state vector components. To apply this scheme in the computer code CupBB, we first compute the scattering coefficients for the vanes with uniform background flow corresponding to region 2 (between blade rows) and place these into the S array as in the example of Eq. 6.5. Then we compute the scattering coefficients for the actuator disk according to theory in Appendix C and place them in array D. Next, elements of S are placed into block matrices S_{AA}, S_{AB}, S_{BA}, S_{BB} and elements of D are placed into S_{BB}, S_{BC}, S_{CB}, S_{CC} per Eq. 6-16. Equation 6-23 is applied to find an array to replace the old array S. Finally, sections of S are placed into the stator location of the system scattering matrix of Figure 13. The same procedure is applied to the rotor blades and their actuator disk to complete the system scattering matrix.

SECTION 7
EQUATIONS FOR SOUND POWER SPECTRA

This section develops equations required to compute spectra of sound power propagating upstream and downstream from the coupled blade rows. The development is in 5 stages:

1. Derive equations for sound power in terms of the Fourier transforms defining the standard wave sets in Section 5.
2. Derive equations to compute those Fourier transforms in terms of the inverted coupling matrix and the source vector elements.
3. Develop equations for the source vector expected values in terms of 3D turbulence spectra.
4. Adapt a standard turbulence spectrum (the Liepmann spectrum) to the ducted flow environment.
5. Assemble the working equations for programming.

Sound Power Equations in Terms of Standard Wave Set Coefficients

Power associated with acoustic perturbations is evaluated according to the energy flux vector given by Goldstein (Ref. 13).

$$\mathbf{I} = \left(\frac{p}{\rho_r} + \mathbf{u} \cdot \mathbf{U} \right) (\rho_r \mathbf{u} + \rho \mathbf{U}) \tag{7.1}$$

This is the instantaneous energy per unit area per unit time in the direction given by $\mathbf{I}$. The perturbation pressure, density, and velocity are p, ρ, and $\mathbf{u}$. ρ_r and $\mathbf{U}$ are the density and velocity of the background flow in Region r. The energy flux vector is space and time dependent. We are interested in its component in the x direction. Forming $I_x = \mathbf{I} \cdot \mathbf{i}_x$ and applying $\rho = p / a_r^2$ lead to

$$I_x = (1 + M_x^2) pu + \frac{M_x}{\rho_r a_r} p^2 + \rho_r a_r M_x u^2 + \rho_r a_r M_y uv + M_x M_y pv \tag{7.2}$$

for the power flux in the x direction. M_x and M_y are Mach number components in the axial and tangential directions relating to the background velocity $\mathbf{U} = (U, V, 0)$.

Recall from Section 5 that the expressions for perturbation acoustic quantities are

$$\begin{bmatrix} p_T^r(\mathbf{x},t) \\ u_T^r(\mathbf{x},t) \\ v_T^r(\mathbf{x},t) \end{bmatrix} = p_o \sum_{n=-\infty}^{\infty} \int_0^{B_1\Omega} \sum_{\mu=0}^{\infty} \sum_{q=0}^{B_2-1} \sum_{k=-\infty}^{\infty} \begin{bmatrix} 1 \\ \dfrac{-\hat{k}_{xTnk}^r}{\rho_r a_r \Lambda_{Tnk}^r} \\ \dfrac{-m}{\rho_r a_r \Lambda_{Tnk}^r} \end{bmatrix} P_{T\mu qk}^r(\omega_o + nB_1\Omega) \times e^{i[k_{xTmk}(x - x_T^r) + m\phi - (\omega_o + nB_1\Omega)t]} \cos\left(\frac{\mu\pi z}{h} \right) d\omega_o \tag{7.3}$$

Before substituting these into Eq. 7.2, note that, in our convention, the pressure and velocity are pure real by virtue of using 2-sided series. I.e. imaginary parts in the upper and lower halves of the n series cancel. Thus, $p^2 = pp^*$, and we use pp^*, for convenience in the manipulations that follow.

$$I_x = \frac{p_o^2}{\rho_r a_r} \sum_n \sum_{n'} \iint \sum_\mu \sum_q \sum_k \sum_{\mu'} \sum_{q'} \sum_{k'} \left[(1+M_x^2)\left(\frac{-\hat{k}'^r_{xTn'k'}}{\Lambda'^r_{Tn'k'}}\right) + M_x + M_x\left(\frac{-\hat{k}^r_{xTnk}}{\Lambda^r_{Tnk}}\right)\left(\frac{-\hat{k}'^r_{xTn'k'}}{\Lambda'^r_{Tn'k'}}\right) \right.$$
$$\left. + M_y\left(\frac{-\hat{k}^r_{xTnk}}{\Lambda^r_{Tnk}}\right)\left(\frac{-m'}{\Lambda'^r_{Tn'k'}}\right) + M_x M_y\left(\frac{-m'}{\Lambda'^r_{Tn'k'}}\right)\right] P^r_{T\mu qk}(\omega_o + nB_1\Omega)\, P^{r*}_{T\mu' q'k'}(\omega'_o + n'B_1\Omega)$$
$$\times e^{i\{(k_{xTnk} - k'_{xTn'k'})(x - x^r_T) + (m-m')\phi - [(\omega_o + nB_1\Omega) - (\omega'_o + n'B_1\Omega)]t\}} \cos\left(\frac{\mu\pi z}{h}\right)\cos\left(\frac{\mu'\pi z}{h}\right) d\omega_o\, d\omega'_o \tag{7.4}$$

We need to average this over time and then over the space variables z and ϕ. For the time average, recall that the Fourier transforms apply to a block of flow passing through the cascades in the period $-\tau < t < \tau$. Outside of that time range, the perturbations are temporarily set to 0. We still integrate over all time since it produces a Dirac delta function

$$\int_{-\infty}^{\infty} e^{i[(\omega_o + nB_1\Omega) - (\omega'_o + n'B_1\Omega)]t}\, dt = 2\pi\, \delta_{nn'}\, \delta(\omega_o - \omega'_o) \tag{7.5}$$

This gives the energy due to that block of flow. Then we divide by 2τ to get the average energy/unit time, i.e. power. Similarly, the average over z requires

$$\frac{1}{h}\int_0^h \cos\left(\frac{\mu\pi z}{h}\right)\cos\left(\frac{\mu'\pi z}{h}\right) dz = \delta_{\mu\mu'}\, \varepsilon_\mu \tag{7.6}$$

where $\varepsilon_\mu = 1$ for $\mu = 0$ and $= ½$ for $\mu > 0$. Also, the average over ϕ yields $\delta_{qq'}\delta_{kk'}$. These operations eliminate all the cross terms in Eq. 7.4 with the result

$$\bar{I}_x = \frac{p_o^2}{\rho_r a_r} \sum_n \int \sum_\mu \sum_q \sum_k F_{nk}\, \frac{\pi\varepsilon_\mu}{\tau} \left| P^r_{T\mu qk}(\omega_o + nB_1\Omega) \right|^2 d\omega_o \tag{7.7}$$

where

$$F_{nk} = (1+M_x^2)\left(\frac{-\hat{k}^r_{xTnk}}{\Lambda^r_{Tnk}}\right) + M_x + M_x\left(\frac{\hat{k}^r_{xTnk}}{\Lambda^r_{Tnk}}\right)^2 + M_y\left(\frac{\hat{k}^r_{xTnk}}{\Lambda^r_{Tnk}}\right)\left(\frac{m}{\Lambda^r_{Tnk}}\right) + M_x M_y\left(\frac{-m}{\Lambda^r_{Tnk}}\right) \tag{7.8}$$

By applying definitions of the wavenumbers in Eqs. 5.9 and 5.10, F_{nk} can be reduced to

$$F_{nk} = \frac{\mp\beta_x^4 \hat{\omega}\sqrt{E}}{\left[(-\hat{\omega} + mM_y) \mp M_x\sqrt{E}\right]^2} \tag{7.9}$$

where E is the cuton discriminator

$$E = (-\hat{\omega} + mM_y)^2 - \beta_x^2(m^2 + \hat{\nu}^2) \tag{7.10}$$

This is positive for this application, since only cut on waves carry power. The $\mp$ sign in the numerator of Eq. 7.10 indicates that energy upstream travels in the negative x direction and downstream travels in the positive x direction. This sign is dropped henceforth.

Now, since the expression for $\bar{I}_x$ is an integral over frequency, we identify the integrand as the power spectral density of acoustic intensity. (We still have to multiply by duct area and bandwidth to get sound power.) We define the area averaged intensity spectra upstream and downstream as

$$\begin{aligned}
\Pi^1_{\mu q}(\omega_o + nB_1\Omega) &= \frac{p_o^2}{\rho_1 a_1}\sum_k F_{nk}\,\frac{\pi\varepsilon_\mu}{\tau}\left|P^1_{1\mu qk}(\omega_o + nB_1\Omega)\right|^2 \\
\Pi^3_{\mu q}(\omega_o + nB_1\Omega) &= \frac{p_o^2}{\rho_3 a_3}\sum_k F_{nk}\,\frac{\pi\varepsilon_\mu}{\tau}\left|P^3_{2\mu qk}(\omega_o + nB_1\Omega)\right|^2
\end{aligned} \tag{7.11}$$

for each independent mode sub-set defined by ω_o, q, and μ. Next, we will find the required expressions for $\left|P^1_{1\mu qk}(\omega_o + nB_1\Omega)\right|^2$ and $\left|P^3_{2\mu qk}(\omega_o + nB_1\Omega)\right|^2$ in terms of the source vector elements.

Fourier Coefficients in Terms of the Coupling Matrix and Source

The terms $P^1_{1\mu qk}(\omega_o + nB_1\Omega)$ and $P^3_{2\mu qk}(\omega_o + nB_1\Omega)$ are elements of the state vector developed in Section 6. Specifically,

$$\begin{aligned}
P^1_{1\mu qk}(\omega_o + nB_1\Omega) &= A^1_1(n,k) \\
\text{and} \qquad & \\
P^3_{2\mu qk}(\omega_o + nB_1\Omega) &= A^3_2(n,k)
\end{aligned} \tag{7.12}$$

are the coefficients for upstream-going pressure waves in region 1 and downstream-going pressure wave in region 3. The coupling equation was shown to be

$$\mathbf{A} = \mathbf{S}\,\mathbf{A} + \mathbf{B} \tag{7.13}$$

where $\mathbf{A}$ is the source vector, $\mathbf{S}$ is the scattering matrix, and $\mathbf{B}$ is the source vector. This could be inverted to find $\mathbf{A}$ as a function of $\mathbf{B}$

$$\mathbf{A} = (\mathbf{1} - \mathbf{S})^{-1}\mathbf{B} \tag{7.14}$$

although a more efficient solver has been developed. In this section, we write out the equations for the desired elements of the state vector in terms of the elements of $\mathbf{B}$ that relate to turbulent

flow into the rotor and stator. In the following section, we will express those elements from **B** in terms of the turbulence spectrum.

We treat turbulence entering the rotor and stator as the source. The relevant elements in the source vector are

$$\begin{aligned} B_3^1(n,k) &= V_{3\mu qk}^1(\omega_o + nB_1\Omega) \\ B_4^1(n,k) &= U_{4\mu qk}^1(\omega_o + nB_1\Omega) \end{aligned} \tag{7.15}$$

which are coefficients of the 2 vortical wave types (3 and 4) in region 1 (entering the rotor) and

$$\begin{aligned} B_3^2(n,k) &= V_{3\mu qk}^2(\omega_o + nB_1\Omega) \\ B_4^2(n,k) &= U_{4\mu qk}^2(\omega_o + nB_1\Omega) \end{aligned} \tag{7.16}$$

which are the same for vortical flow entering the stator from region 2. (For radial mode index μ = 0, the Type 4 waves are absent.) We denote the matrix of the inverted system by **C** where

$$\mathbf{C} = (\mathbf{1} - \mathbf{S})^{-1} \tag{7.17}$$

In terms of the elements of **C** , the coefficients for the upstream-going pressure waves become

$$\begin{aligned} P_{1\mu qk'}^1(\omega_o + n'B_1\Omega) = \sum_n \sum_k \{ & C(1,1,n',k';1,3,n,k)B_3^1(n,k) + C(1,1,n',k';1,4,n,k)B_4^1(n,k) \\ & + C(1,1,n',k';2,3,n,k)B_3^2(n,k) + C(1,1,n',k';2,4,n,k)B_4^2(n,k)\} \end{aligned} \tag{7.18}$$

Rather than using conventional matrix notation, we denote the matrix elements by *C(R',T',n',k';R,T,n,k)* . We have returned to the convention where primed indices denote waves scattered into and unprimed indices denote waves scattered from. Hence, indices *R'* and *R* are the *regions* scattered to and from (see page 29) and *T'* and *T* are the *wave types* scattered to and from (again, see page 29). In Eq. 7.18, the B_4 terms are absent in the case of $\mu = 0$. We will not bother to write out the corresponding form for downstream going waves until the end of this section. We can not know $\left|P_{T\mu qk'}^1(\omega_o + n'B_1\Omega)\right|^2$ in general but we can deal with its expected value (or ensemble average) $\left\langle \left|P_{T\mu qk'}^1(\omega_o + n'B_1\Omega)\right|^2 \right\rangle$. Squaring the magnitude of Eq. 7.18 and taking expected values results in many cross terms which we will justify eliminating. The cross terms between regions 1 and 2 vanish because we assume the turbulence entering the rotor to be independent of that entering the stator. This leaves

$$\left\langle \left| P^1_{T\mu qk'}(\omega_o + n' B_1 \Omega) \right|^2 \right\rangle =$$

$$\sum_n \sum_k \sum_{n''} \sum_{k''} \Big[C(1,1,n',k';1,3,n,k) C^*(1,1,n',k';1,3,n'',k'') \left\langle B^1_3(n,k) B^{1*}_3(n'',k'') \right\rangle$$
$$+ C(1,1,n',k';1,4,n,k) C^*(1,1,n',k';1,4,n'',k'') \left\langle B^1_4(n,k) B^{1*}_4(n'',k'') \right\rangle$$
$$+ C(1,1,n',k';1,3,n,k) C^*(1,1,n',k';1,4,n'',k'') \left\langle B^1_3(n,k) B^{1*}_4(n'',k'') \right\rangle$$
$$+ C(1,1,n',k';1,4,n,k) C^*(1,1,n',k';1,3,n'',k'') \left\langle B^1_4(n,k) B^{1*}_3(n'',k'') \right\rangle$$
$$+ C(1,1,n',k';2,3,n,k) C^*(1,1,n',k';2,3,n'',k'') \left\langle B^2_3(n,k) B^{2*}_3(n'',k'') \right\rangle$$
$$+ C(1,1,n',k';2,4,n,k) C^*(1,1,n',k';2,4,n'',k'') \left\langle B^2_4(n,k) B^{2*}_4(n'',k'') \right\rangle$$
$$+ C(1,1,n',k';2,3,n,k) C^*(1,1,n',k';2,4,n'',k'') \left\langle B^2_3(n,k) B^{2*}_4(n'',k'') \right\rangle$$
$$+ C(1,1,n',k';2,4,n,k) C^*(1,1,n',k';2,3,n'',k'') \left\langle B^2_4(n,k) B^{2*}_3(n'',k'') \right\rangle \Big] \tag{7.19}$$

In the following section, we will see that the n,n'' and k,k'' cross terms also vanish so that Eq. 7.19 can be written

$$\left\langle \left| P^1_{T\mu qk'}(\omega_o + n' B_1 \Omega) \right|^2 \right\rangle =$$

$$\sum_n \sum_k \Big[\left| C(1,1,n',k';1,3,n,k) \right|^2 \left\langle \left| B^1_3(n,k) \right|^2 \right\rangle + \left| C(1,1,n',k';1,4,n,k) \right|^2 \left\langle \left| B^1_4(n,k) \right|^2 \right\rangle$$
$$+ C(1,1,n',k';1,3,n,k) C^*(1,1,n',k';1,4,n,k) \left\langle B^1_3(n,k) B^{1*}_4(n,k) \right\rangle$$
$$+ C(1,1,n',k';1,4,n,k) C^*(1,1,n',k';1,3,n,k) \left\langle B^1_4(n,k) B^{1*}_3(n,k) \right\rangle$$
$$+ \left| C(1,1,n',k';2,3,n,k) \right|^2 \left\langle \left| B^2_3(n,k) \right|^2 \right\rangle + \left| C(1,1,n',k';2,4,n,k) \right|^2 \left\langle \left| B^2_4(n,k) \right|^2 \right\rangle$$
$$+ C(1,1,n',k';2,3,n,k) C^*(1,1,n',k';2,4,n,k) \left\langle B^2_3(n,k) B^{2*}_4(n,k) \right\rangle$$
$$+ C(1,1,n',k';2,4,n,k) C^*(1,1,n',k';2,3,n,k) \left\langle B^2_4(n,k) B^{2*}_3(n,k) \right\rangle \Big] \tag{7.20}$$

In Eq. 7.20, it can be seen that the 2nd and 3rd lines on the right are conjugates of each other. The same is true of the 5th and 6th lines. Hence, Eq. 7.20 reduces to

$$\left\langle \left| P^1_{T\mu qk'}(\omega_o + n' B_1\Omega) \right|^2 \right\rangle =$$

$$\sum_n \sum_k \left\{ \left| C(1,1,n',k';1,3,n,k) \right|^2 \left\langle \left| B^1_3(n,k) \right|^2 \right\rangle + \left| C(1,1,n',k';1,4,n,k) \right|^2 \left\langle \left| B^1_4(n,k) \right|^2 \right\rangle \right.$$
$$+ 2\,\mathrm{Re}\left[C(1,1,n',k';1,3,n,k) C^*(1,1,n',k';1,4,n,k) \left\langle B^1_3(n,k) B^{1*}_4(n,k) \right\rangle \right]$$
$$+ \left| C(1,1,n',k';2,3,n,k) \right|^2 \left\langle \left| B^2_3(n,k) \right|^2 \right\rangle + \left| C(1,1,n',k';2,4,n,k) \right|^2 \left\langle \left| B^2_4(n,k) \right|^2 \right\rangle$$
$$\left. + 2\,\mathrm{Re}\left[C(1,1,n',k';2,3,n,k) C^*(1,1,n',k';2,4,n,k) \left\langle B^2_3(n,k) B^{2*}_4(n,k) \right\rangle \right] \right\} \tag{7.21}$$

Source Elements in Terms of Turbulence Spectra

We will treat one of the source expectations on the right of Eq. 7.19 in detail and then write down the rest by inspection. [We are going back to Eq. 19 because we still need to show that the n,n'' and k,k'' cross terms cancel.] Including the $\pi\varepsilon_\mu/\tau$ from Eq. 7.7, we use A to denote

$$A = \frac{\pi\varepsilon_\mu}{\tau} \left\langle B^1_3(n,k) B^{1*}_3(n'',k'') \right\rangle = \frac{\pi\varepsilon_\mu}{\tau} \left\langle V^1_{3\mu qk}(\omega_o + nB_1\Omega)\, V^{1*}_{3\mu qk''}(\omega_o + n''B_1\Omega) \right\rangle \tag{7.22}$$

and we proceed by inserting the inverse transform of the V's given in Eq. 5.8.

$$A = \left[\frac{1}{4\pi^2 Ra_o h U \varepsilon_\mu} \right]^2 \frac{\pi\varepsilon_\mu}{\tau} \iiint \iiint \left\langle \tilde{v}^1_3(\tilde{\mathbf{x}}) \tilde{v}^1_3(\tilde{\mathbf{x}}') \right\rangle e^{-i\left(k_{x3nk}\tilde{x} - k''_{x3n''k''}\tilde{x}' + \frac{m}{R}\tilde{y} - \frac{m''}{R}\tilde{y}'\right)}$$
$$\times \cos\left(\frac{\mu\pi z}{h}\right) \cos\left(\frac{\mu\pi z'}{h}\right) d\tilde{x}\, d\tilde{y}\, dz\, d\tilde{x}'\, d\tilde{y}'\, dz' \tag{7.23}$$

Recall that $\tilde{v}^1_3(\tilde{\mathbf{x}})$ is the y turbulence velocity component represented in region 1 in the fluid-fixed frame. Now we change the position variables from "point 1/point 2" to "point/separation" via

$$\tilde{\mathbf{x}}' = \tilde{\mathbf{x}} + \mathbf{s} \tag{7.24}$$

so that

$$\begin{aligned} \tilde{x}' &= \tilde{x} + s_x \\ \tilde{y}' &= \tilde{y} + s_y \\ \tilde{z}' &= \tilde{z} + s_z \end{aligned} \tag{7.25}$$

Then,

$$A = \frac{\pi}{(4\pi^2 Ra_o hU)^2 \tau \varepsilon_\mu} \iiint \iiint \left\langle \tilde{v}_3^1(\tilde{\mathbf{x}}) \tilde{v}_3^1(\tilde{\mathbf{x}}+\mathbf{s}) \right\rangle e^{-i[(k_{x3nk}-k''_{x3n''k''})\tilde{x} - k''_{x3n''k''}s_x + (m-m'')\frac{\tilde{y}}{R} - m''\frac{s_y}{R}]}$$
$$\times \cos\left(\frac{\mu\pi z}{h}\right)\left[\cos\left(\frac{\mu\pi z}{h}\right)\cos\left(\frac{\mu\pi s_z}{h}\right) - \sin\left(\frac{\mu\pi z}{h}\right)\sin\left(\frac{\mu\pi s_z}{h}\right)\right] d\tilde{x}\, d\tilde{y}\, dz\, ds_x\, ds_y\, ds_z \tag{7.26}$$

The sine term will vanish in the z integration. In flow problems with no boundaries, the standard step at this point would be to recognize the expectation of the v product as the correlation function $\left\langle \tilde{v}_3^1(\tilde{\mathbf{x}}) \tilde{v}_3^1(\tilde{\mathbf{x}}+\mathbf{s}) \right\rangle = R_{vv}^1(\mathbf{s})$ and claim it to be a function only of the separation vector $\mathbf{s}$ (and not of the position vector $\tilde{\mathbf{x}}$). In bounded flows this is an approximation that we assume to be acceptable since the length scale turns out to be small (typically 2% to 4% of fan radius).

We still have to deal with convergence of the x integral. Recall that we are considering only a block of flow that is finite in the x direction and then taking the limit as the block size increases to infinity. For this, we employ a "top hat" function $J(\tilde{x})$ which = 1 for $-U\tau < \tilde{x} < U\tau$ and 0 otherwise. Then the correlation is written

$$\left\langle \tilde{v}_3^1(\tilde{\mathbf{x}}) \tilde{v}_3^1(\tilde{\mathbf{x}}+\mathbf{s}) \right\rangle = R_{vv}^1(\mathbf{s}) \times J(\tilde{x}) \tag{7.27}$$

Use of this function permits us to separate the separation and position integrals as follows

$$A = \frac{\pi}{(4\pi^2 Ra_o hU)^2 \varepsilon_\mu} \iiint R_{vv}^1(\mathbf{s}) e^{i(k''_{x3n''k''}s_x + m''\frac{s_y}{R})} \cos\left(\frac{\mu\pi s_z}{h}\right) ds_x\, ds_y\, ds_z$$
$$\times \int_0^h \int_{-\pi R}^{\pi R} \frac{1}{\tau} \int_{-U\tau}^{U\tau} e^{-i[(k_{x3nk}-k''_{x3n''k''})\tilde{x} + (m-m'')\frac{\tilde{y}}{R}]} \cos^2\left(\frac{\mu\pi z}{h}\right) d\tilde{x}\, d\tilde{y}\, dz \tag{7.28}$$

where the effect of the top hat function appears in the limits of the $\tilde{x}$ integral. In the first line of Eq. 7.28, we can replace the cosine with an exponential because the correlation function is even in s_z. (In the parallel derivation involving $R_{uv}^1(\mathbf{s})$, which we do not show here, it too is even in s_z, although odd in the x and y separation variables.) In the second line, the z integral yields $h\varepsilon_\mu$ so that

$$A = \frac{\pi}{(4\pi^2 Ra_o U)^2 h} \iiint R_{vv}^1(\mathbf{s}) e^{i(k''_{x3n''k''}s_x + \frac{m''}{R}s_y + \frac{\mu\pi}{h}s_z)} ds_x\, ds_y\, ds_z$$
$$\times \int_{-\pi R}^{\pi R} \frac{1}{\tau} \int_{-U\tau}^{U\tau} e^{-i[(k_{x3nk}-k''_{x3n''k''})\tilde{x} + (m-m'')\frac{\tilde{y}}{R}]} d\tilde{x}\, d\tilde{y} \tag{7.29}$$

The $\tilde{y}$ integral produces a Kroneker delta

$$\int_{-\pi R}^{\pi R} e^{-i(m-m'')\frac{\tilde{y}}{R}}\, d\tilde{y} = 2\pi R\delta_{mm''} \tag{7.30}$$

so that the $\tilde{x}$ integral becomes, after applying Eq. 3.17 for k_{x3nk},

$$\frac{1}{\tau}\int_{-U\tau}^{U\tau} e^{-i(n-n'')\frac{B_1\Omega\tilde{x}}{U}}\, d\tilde{x} = 2U\delta_{nn''} \tag{7.31}$$

in the limit as τ approaches infinity. With these results, A further reduces to

$$A = \frac{\delta_{nn''}\,\delta_{kk''}}{4\pi^2 R\, a_o^2\, U\, h}\iiint R_{vv}^1(\mathbf{s}) e^{i(k''_{x3n''k''}s_x + \frac{m''}{R}s_y + \frac{\mu\pi}{h}s_z)}\, ds_x\, ds_y\, ds_z \tag{7.32}$$

The 2 Kroneker deltas eliminate the n,n'' and k,k'' cross terms as claimed above in conjunction with Eq. 7.19. If the fluid medium were unbounded, this integral could be recognized as the 3D turbulence spectrum from the standard form

$$\int R_{vv}^1(\mathbf{s}) e^{i\mathbf{k}\cdot\mathbf{s}}\, d\mathbf{s} = (2\pi)^3 \phi_{vv}^1(\mathbf{k}) \tag{7.33}$$

We assume that this is an adequate approximation for the bounded case under consideration, so that

$$\frac{\pi\varepsilon_\mu}{\tau}\left\langle V_{3\mu qk}^1(\omega_o + nB_1\Omega) V_{3\mu qk''}^{1*}(\omega_o + n''B_1\Omega)\right\rangle = \frac{2\pi\delta_{nn''}\delta_{kk''}}{Ra_o^2 Uh}\phi_{vv}^1(\mathbf{k}) \tag{7.34}$$

where the wavenumber components are

$$\begin{aligned} k_1 &= k_{x3nk} \\ k_2 &= m/R \\ k_3 &= \mu\pi/h \end{aligned} \tag{7.35}$$

Finally, we normalize the turbulence spectra according to

$$\begin{aligned} \phi_{uu}^1(\mathbf{k}) &= R^3 W_1^2 \Phi_{uu}^1(\mathbf{K}) \\ \phi_{vv}^1(\mathbf{k}) &= R^3 W_1^2 \Phi_{vv}^1(\mathbf{K}) \\ \phi_{uv}^1(\mathbf{k}) &= R^3 W_1^2 \Phi_{uv}^1(\mathbf{K}) \end{aligned} \tag{7.36}$$

for the 2 turbulence components entering the rotor from region 1, and

$$\begin{aligned} \phi_{uu}^2(\mathbf{k}) &= R^3 W_2^2 \Phi_{uu}^2(\mathbf{K}) \\ \phi_{vv}^2(\mathbf{k}) &= R^3 W_2^2 \Phi_{vv}^2(\mathbf{K}) \\ \phi_{uv}^2(\mathbf{k}) &= R^3 W_2^2 \Phi_{uv}^2(\mathbf{K}) \end{aligned} \tag{7.37}$$

for the 2 components entering the stator from region 2. Also, we have normalized the wavenumbers by R so that the axial wavenumbers

$$K_{11} = k^1_{x3nk}\, R \equiv \hat{k}^1_{x3nk} \qquad K_{12} = k^2_{x3nk}\, R \equiv \hat{k}^2_{x3nk} \tag{7.38}$$

for regions 1 and 2, respectively. Here the subscript 11 denotes x-wavenumber in region 1 and subscript 12 denotes x-wavenumber in region 2. The circumferential and spanwise wavenumbers are

$$\begin{aligned} K_2 &= m = q + nB_1 - kB_2 \\ K_3 &= \mu\pi \big/ H_D \end{aligned} \tag{7.39}$$

Now we can write down the 6 required source terms. Since we only need the $n = n''$ and $k = k''$ terms, we eliminate the Kroneker deltas. For region 1,

$$\begin{aligned} \frac{\pi\varepsilon_\mu}{\tau}\left\langle \left| V^1_{3\mu qk}(\omega_o + nB_1\Omega)\right|^2 \right\rangle &= \frac{2\pi M_1^2 A_1}{H_D M_{x1}} \frac{R}{a_o} \Phi^1_{vv}(\mathbf{K}) \\ \frac{\pi\varepsilon_\mu}{\tau}\left\langle \left| U^1_{4\mu qk}(\omega_o + nB_1\Omega)\right|^2 \right\rangle &= \frac{2\pi M_1^2 A_1}{H_D M_{x1}} \frac{R}{a_o} \Phi^1_{uu}(\mathbf{K}) \\ \frac{\pi\varepsilon_\mu}{\tau}\left\langle \left| U^1_{4\mu qk}(\omega_o + nB_1\Omega) V^{1*}_{3\mu qk}(\omega_o + nB_1\Omega)\right| \right\rangle &= \frac{2\pi M_1^2 A_1}{H_D M_{x1}} \frac{R}{a_o} \Phi^1_{uv}(\mathbf{K}) \end{aligned} \tag{7.40}$$

and for region 2,

$$\begin{aligned} \frac{\pi\varepsilon_\mu}{\tau}\left\langle \left| V^2_{3\mu qk}(\omega_o + nB_1\Omega)\right|^2 \right\rangle &= \frac{2\pi M_2^2 A_2}{H_D M_{x2}} \frac{R}{a_o} \Phi^2_{vv}(\mathbf{K}) \\ \frac{\pi\varepsilon_\mu}{\tau}\left\langle \left| U^2_{4\mu qk}(\omega_o + nB_1\Omega)\right|^2 \right\rangle &= \frac{2\pi M_2^2 A_2}{H_D M_{x2}} \frac{R}{a_o} \Phi^2_{uu}(\mathbf{K}) \\ \frac{\pi\varepsilon_\mu}{\tau}\left\langle \left| U^2_{4\mu qk}(\omega_o + nB_1\Omega) V^{2*}_{3\mu qk}(\omega_o + nB_1\Omega)\right| \right\rangle &= \frac{2\pi M_2^2 A_2}{H_D M_{x2}} \frac{R}{a_o} \Phi^2_{uv}(\mathbf{K}) \end{aligned} \tag{7.41}$$

where $H_D = h/R$. $M_1 = W_1/a_1$ and $M_2 = W_2/a_2$ are the Mach numbers in regions 1 and 2 and M_{x1} and M_{x2} are their axial components. $A_1 = a_1/a_o$ and $A_2 = a_2/a_o$.

Choice of Turbulence Spectrum

Since we do not have an algebraic form for turbulence spectra in ducted flow, we will simply adapt the Liepmann spectrum (Ref. 14) that has been used with some success in earlier studies. Unpublished analyses by Pratt & Whitney show that this spectrum matches wake data remarkably well. The forms for the Liepmann spectrum are

$$\phi_{uu}(\mathbf{k}) = \frac{2\overline{u^2}\ell^5}{\pi^2}\frac{k_2^2 + k_3^2}{\left[1+\ell^2(k_1^2+k_2^2+k_3^2)\right]^3}$$
$$\phi_{vv}(\mathbf{k}) = \frac{2\overline{u^2}\ell^5}{\pi^2}\frac{k_1^2 + k_3^2}{\left[1+\ell^2(k_1^2+k_2^2+k_3^2)\right]^3} \qquad (7.42)$$

and

$$\phi_{uv}(\mathbf{k}) = \frac{2\overline{u^2}\ell^5}{\pi^2}\frac{k_1 k_2}{\left[1+\ell^2(k_1^2+k_2^2+k_3^2)\right]^3} \qquad (7.43)$$

In our application of these spectra, we use a sum over the discrete spanwise μ modes from 0 to ∞ rather than an integral from -∞ to ∞ over a continuous wavenumber. As suggested by Figure 15, we are approximating the integral by a sum. Since we need only the right half of the discrete approximation, we must avoid over-emphasizing the $\mu = 0$ term. Thus, we take ½ the $\mu = 0$ term and the full values for the $\mu > 0$ terms. With this approach, the shaded area of the discrete cells approximates the area under the right side of the continuous curve.

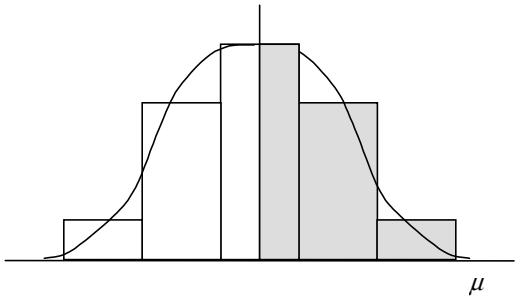

Figure 15. Sketch to explain conversion of continuous wavenumber integration to discrete summation

Working Forms for Sound Power Spectra

We are now prepared to assemble the results from the above sections to obtain the forms for programming. Sound power spectrum levels are obtained from Eq. 7.11 by multiplying by duct cross section area $2\pi Rh$, multiplying by bandwidth $\Delta\omega_o = 2\pi\overline{BW}$, and dividing by the power reference: 10^{-12} watts. Furthermore, since we use only positive frequencies for calculations, we multiply by 2 to account for the lower half of the spectrum.

The result for upstream sound power is at frequency denoted by n'' is

$$PWR^1_{\mu q}(\omega_o + n'B_1\Omega) = 5.8838\times10^{14}\left(\frac{R}{in.}\right)^3\left(\frac{\overline{BW}}{Hz}\right)$$

$$\times\Bigg\{\ \frac{M_1^2 A_1^2}{P_1 M_{x1}}\sum_{k'}F^1_{n'k'}\sum_n\sum_k\ \Big[\ \left|C(1,1,n',k';1,3,n,k)\right|^2\Phi^1_{vv}(\mathbf{K})+\left|C(1,1,n',k';1,4,n,k)\right|^2\Phi^1_{uu}(\mathbf{K})$$

$$+2\,\mathrm{Re}[C(1,1,n',k';1,3,n,k)C^*(1,1,n',k';1,4,n,k)]\Phi^1_{uv}(\mathbf{K})\ \Big]$$

$$+\frac{M_2^2 A_1 A_2}{P_1 M_{x2}}\sum_{k'}F^1_{n'k'}\sum_n\sum_k\ \Big[\ \left|C(1,1,n',k';2,3,n,k)\right|^2\Phi^2_{vv}(\mathbf{K})+\left|C(1,1,n',k';2,4,n,k)\right|^2\Phi^2_{uu}(\mathbf{K})$$

$$+2\,\mathrm{Re}[C(1,1,n',k';2,3,n,k)C^*(1,1,n',k';2,4,n,k)]\Phi^2_{uv}(\mathbf{K})\ \Big]\Bigg\}$$

(7.44)

This is summed over all of the *n,k* source modes *and* over all of the *k'* modes scattered into for a given frequency $\omega_0+n'B_1\Omega$. Power level in dB is $10\log_{10}$ of this quantity. A_r denotes ambient speed of sound normalized by speed of sound for a sea level standard day. P_r is similarly defined for pressure.

The corresponding form for downstream sound power follows immediately:

$$PWR^3_{\mu q}(\omega_o + n'B_1\Omega) = 5.8838\times10^{14}\left(\frac{R}{in.}\right)^3\left(\frac{\overline{BW}}{Hz}\right)$$

$$\times\Bigg\{\ \frac{M_1^2 A_1 A_3}{P_3 M_{x1}}\sum_{k'}F^3_{n'k'}\sum_n\sum_k\ \Big[\ \left|C(3,2,n',k';1,3,n,k)\right|^2\Phi^1_{vv}(\mathbf{K})+\left|C(3,2,n',k';1,4,n,k)\right|^2\Phi^1_{uu}(\mathbf{K})$$

$$+2\,\mathrm{Re}[C(3,2,n',k';1,3,n,k)C^*(3,2,n',k';1,4,n,k)]\Phi^1_{uv}(\mathbf{K})\ \Big]$$

$$+\frac{M_2^2 A_2 A_3}{P_3 M_{x2}}\sum_{k'}F^3_{n'k'}\sum_n\sum_k\ \Big[\ \left|C(3,2,n',k';2,3,n,k)\right|^2\Phi^2_{vv}(\mathbf{K})+\left|C(3,2,n',k';2,4,n,k)\right|^2\Phi^2_{uu}(\mathbf{K})$$

$$+2\,\mathrm{Re}[C(3,2,n',k';2,3,n,k)C^*(3,2,n',k';2,4,n,k)]\Phi^2_{uv}(\mathbf{K})\ \Big]\Bigg\}$$

(7.45)

The working forms for the turbulence spectra are

$$\left.\begin{aligned}
\Phi^1_{vv}(\mathbf{K}) &= \varepsilon_\mu \left(\frac{\overline{u^2}}{W^2}\frac{2L^5}{\pi^2}\right)\frac{K_{11}^2+K_3^2}{\left[1+L^2(K_1^2+K_2^2+K_3^2)\right]^3}\\
\Phi^1_{uu}(\mathbf{K}) &= \varepsilon_\mu \left(\frac{\overline{u^2}}{W^2}\frac{2L^5}{\pi^2}\right)\frac{K_2^2+K_3^2}{\left[1+L^2(K_1^2+K_2^2+K_3^2)\right]^3}\\
\Phi^1_{uv}(\mathbf{K}) &= \varepsilon_\mu \left(\frac{\overline{u^2}}{W^2}\frac{2L^5}{\pi^2}\right)\frac{K_{11}K_2}{\left[1+L^2(K_1^2+K_2^2+K_3^2)\right]^3}
\end{aligned}\right\} \qquad \left\{\begin{aligned}
K_{11} &= \hat{k}^1_{x3nk}\\
K_2 &= m = q + nB_1 - kB_2\\
K_3 &= \mu\pi \big/ H_D
\end{aligned}\right. \tag{7.46}$$

for flow entering the rotor from region 1. Note that the intensity and scale for region 1 are to be used. $\varepsilon_\mu = ½$ for $\mu=0$ and $=1$ for $\mu>0$. L is turbulence integral length scale normalized by duct effective radius R, i.e. $L = \ell/R$.

For turbulence entering the stator from region 2,

$$\left.\begin{aligned}
\Phi^2_{vv}(\mathbf{K}) &= \varepsilon_\mu \left(\frac{\overline{v^2}}{W^2}\frac{2L^5}{\pi^2}\right)\frac{K_{12}^2+K_3^2}{\left[1+L^2(K_1^2+K_2^2+K_3^2)\right]^3}\\
\Phi^2_{uu}(\mathbf{K}) &= \varepsilon_\mu \left(\frac{\overline{u^2}}{W^2}\frac{2L^5}{\pi^2}\right)\frac{K_2^2+K_3^2}{\left[1+L^2(K_1^2+K_2^2+K_3^2)\right]^3}\\
\Phi^2_{uv}(\mathbf{K}) &= \varepsilon_\mu \left(\frac{\overline{u^2}}{W^2}\frac{2L^5}{\pi^2}\right)\frac{K_{12}K_2}{\left[1+L^2(K_1^2+K_2^2+K_3^2)\right]^3}
\end{aligned}\right\} \qquad \left\{\begin{aligned}
K_{12} &= \hat{k}^2_{x3n,k}\\
K_2 &= m = q + nB_1 - kB_2\\
K_3 &= \mu\pi \big/ H_D
\end{aligned}\right. \tag{7.47}$$

where intensity and scale for region 2 are to be used. Under the assumption of isotropic turbulence, we have taken the u- and the v-intensities to be the same.

The equations of Sections 6 and 7 have been programmed in Fortran in code CupBB. Cases that exhibit the physical effects of interest typically run 4 to 6 hours on a 1 GigaHz personal computer. However, if high frequencies (significantly beyond the spectrum peak) are calculated, the running time can be much longer.

SECTION 8
VERIFICATION AND APPLICATION OF THEORY

This section provides verification of the new broadband coupling theory and then presents a series of calculated power spectra to demonstrate the capability of code CupBB and to demonstrate the importance of unsteady coupling and flow turning. Conclusions will be summarized in Section 9.

Verification

As described in the background section (Section 2), the new theory is a combination and extension of preceding theoretical treatments of tone and broadband noise generation. Reference 1 addressed unsteady coupling for tone noise in a 2D environment, with turning included via actuator disks. References 2 and 3 addressed broadband noise generation by isolated (uncoupled) cascades. Geometry and mean flow were uniform in the spanwise direction but use of a true 3D turbulence spectrum was enabled by Glegg's Wiener-Hopf cascade analysis. In the combined theory of this report, the turbulence spectrum, cascade response, and actuator disk response are 3D with respect to unsteady perturbations. However, the mean flow and the geometry are constant in the spanwise direction.

Because broadband coupling has not been treated previously in the literature, there are no test cases for verification. However, 3 tests were executed to provide some confidence in the code. First, note that the coupling system described in Section 6 must reduce to the tone system of Ref. 1 in the case of zero spanwise wavenumber. This has been carefully checked so as to verify (in the special case of $\mu = 0$, i.e. 2D waves) the coupling, the treatment of actuator disks, and frequency and mode scattering.

The second verification was to run the new code with effects of coupling and flow turning "turned off" and to compare results with the older code (BBCascade) from Refs. 2 and 3, which does not treat coupling and flow turning. The comparisons are very satisfactory as shown in Figures 16 and 17 for turbulent flow into a stator and rotor of a 22 inch diameter fan. CupBB computations are denoted by solid symbols and BBCascade computations by continuous curves. Results are nearly identical at all frequencies computed. Agreement was not necessarily expected at the lowest frequencies because the 2 codes treat boundary conditions differently. CupBB uses a modal description of the inflow and of the acoustic waves. This results from enforcing periodicity in the ϕ direction and flow tangency on the hard inner and outer duct walls. In contrast, BBCascade does not enforce either of these boundary conditions and hence uses continuous wavenumbers rather than modes. Further numerical experiments, to be reported in the future, show differences at low frequencies for cases where the turbulence scale approaches the blade or vane span. In any case, it is believed that Figures 16 and 17 verify correct behavior of the isolated cascade application of CupBB.

The third verification was to run the new code with all features enabled and check for qualitative agreement with test data. Results shown in Figure 18 are for the same ADP scaled model case presented in Section 2, Figure 6. Recall for that figure that the turbulence intensity and scale were adjusted to provide a "best fit" since we are attempting to represent the fan annulus by a single representative radius via the rectilinear theory. Because the modeling with the new theory includes more features, it was necessary to re-check the data fit and adjust the

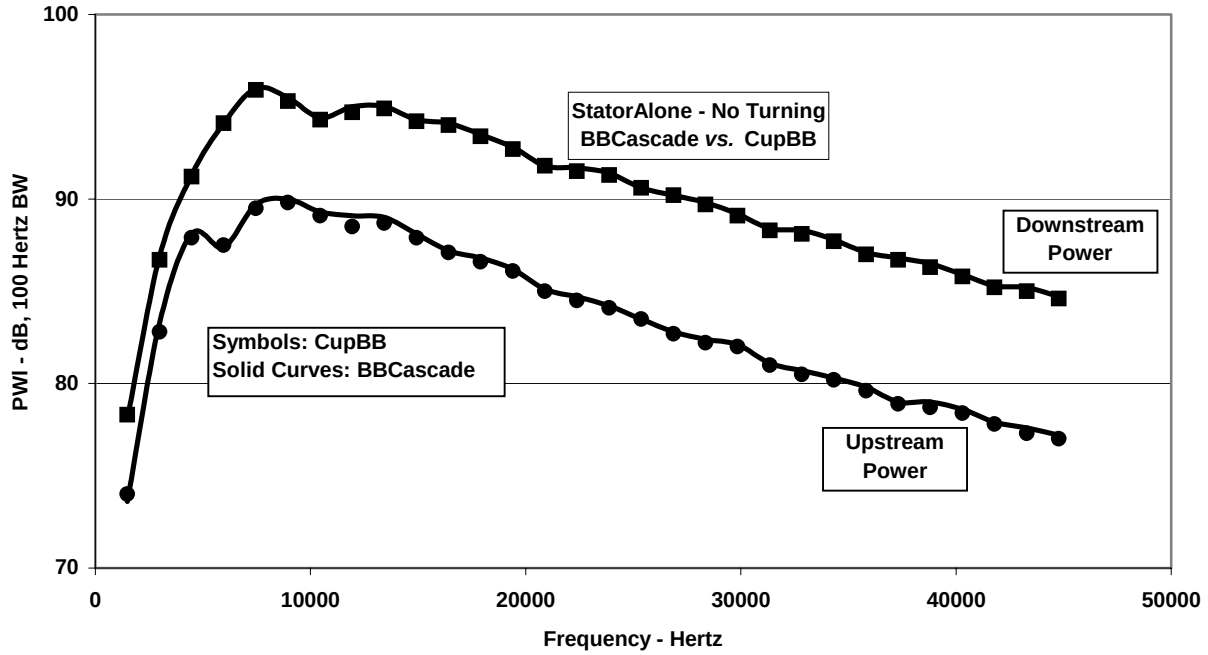

Figure 16. Comparison of old and new codes for isolated stator cascade. Turbulence RMS level was 1.0% of the mean velocity and the integral scale was 1.0% of the fan mean radius

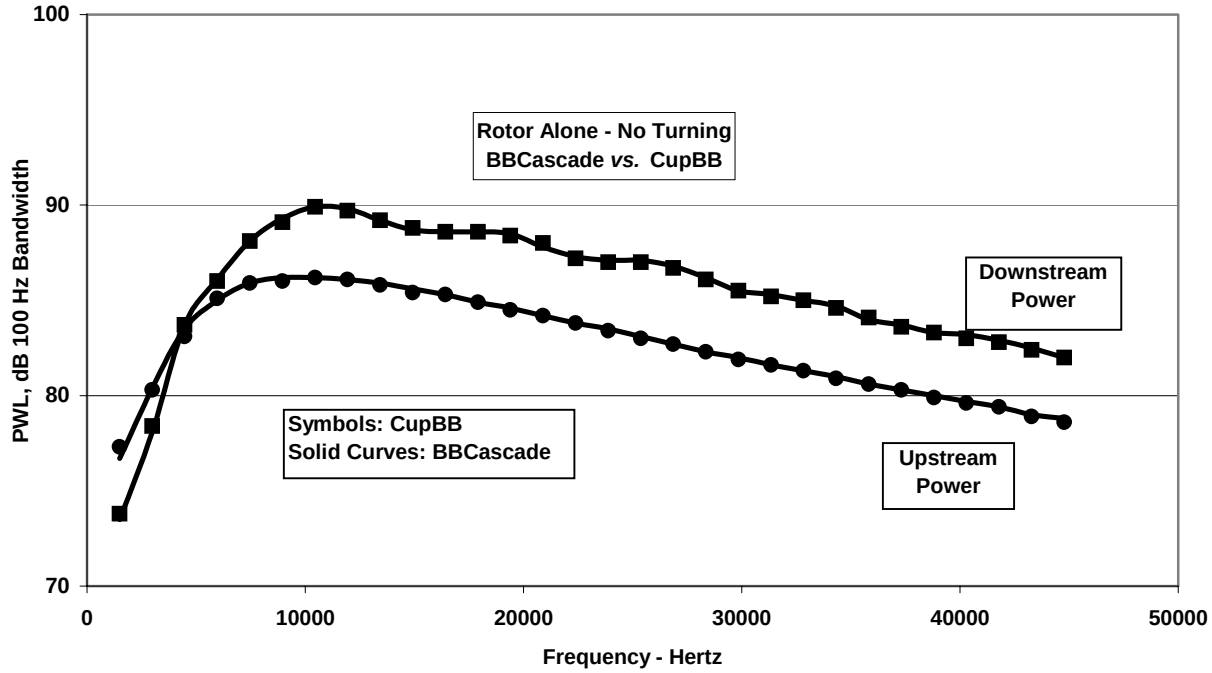

Figure 17. Comparison of old and new codes for isolated rotor cascade. Turbulence RMS level was 1.0% of the mean velocity and the integral scale was 1.0% of the fan mean radius

turbulence properties, as required. Intensity was reduced from 2.0% to 1.8% and the integral scale was reduced from 3.5% to 3.2% of radius. It was decided to match the downstream data as closely as possible and to let the upstream calculation follow, since other sources could be contributing to inlet noise. The match to the downstream spectrum shape is excellent,

considering that the only free parameter governing shape is turbulence scale. This shows the merit of using a 3D turbulence spectrum and a 3D cascade response function. Earlier schemes based on 2D cascade theory and correlation length concepts don't do this well.

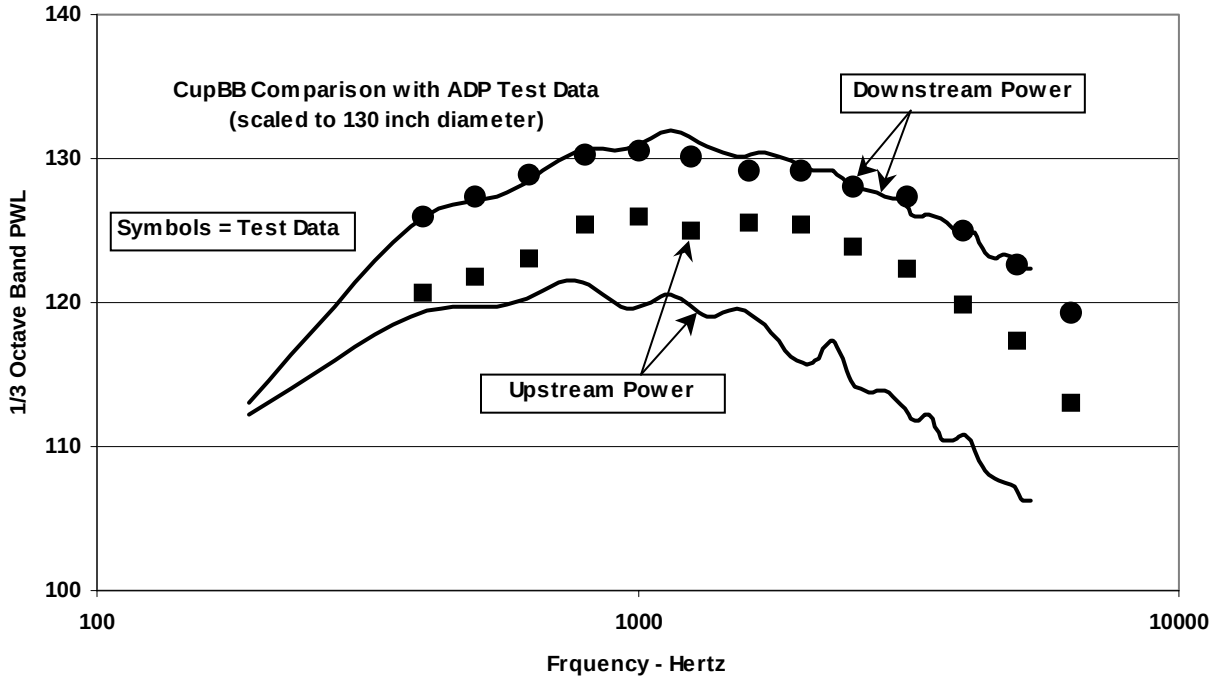

Figure 18. Calculation with fully coupled theory compared with scaled model ADP data from Figure 6. Relative to the isolated cascade calculation, the turbulence intensity was reduced from 2.0% to 1.8% and the integral scale was reduced from 3.5% to 3.2% of radius.

The significant under prediction in inlet noise should not be considered a failing of this theory. Rather it is an indication that turbulent inflow at the stator is an unlikely source of inlet noise, now that we have a reasonable model for rotor transmission loss. Recall that, when the isolated cascade theory was first brought on line, we were pleased with the upstream/downstream split (in comparison with data as shown in Figure 6). This seems naïve now that the modeling is more complete. The earlier results ignored the effect of the rotor with the result that conclusions regarding upstream noise were probably incorrect. For this case, trailing edge noise from the rotor may dominate in the upstream direction.

For reference, the remaining input used for the calculations if Fig. 18 are given below. They represent conditions at the 85% radius for a run of ADP Fan#1 at 722 ft/sec tip speed.

Radius and Hub/tip ratio:	55.25 in and 0.479
Number of blades and vanes:	18 and 45
Gap/chord rotor and stator:	1.0 and 0.8
Axial spacing between rows:	2 full rotor chords
Axial Mach# and tip Mach#:	0.49 and 0.55
Pressure ratio:	1.242
Number of "Harmonics":	NH = 14
Number of freq offsets:	# ω_o's = 2
qStep:	1

Regarding the independent mode subsets explained in previous sections, it can be seen that calculations in Figure 18 were made with 2 sets of 14 frequencies. The first set was half way

between the BPF harmonics and the second set was interlaced with centers at the BPF harmonics. All of the cut on radial modes were included at each frequency. For circumferential orders, criteria are checked for both acoustic and vortical waves and then the more stringent criterion is used. On the acoustic side, all cut on waves are included plus the cut off waves between blade rows that only decay to a prescribed level across the rotor/stator gap. On the vortical side, the turbulence spectrum is examined and all waves are included with levels down to a prescribed fraction of the spectrum peak at each frequency. The "prescribed levels" just mentioned are found by checking for convergence of the spectrum results.

Since this calculation was very time consuming, various short cuts were explored as described in the next section. All of the remaining figures were generated with variations on the ADP input given above.

Variations in Computational Parameters

First, we needed to verify that the number of frequencies (*n*'s) in the system equations can be truncated without compromising accuracy. Figure 19 was computed with the same input as for Figure 18 except that *NH* was varied through the values 2, 6, 10, and 14. Note that input waves range over positive and negative *n*'s so that $2NH+1$ input frequencies are required. (From symmetry, we can compute only the positive *NH* output frequencies and then double the result.) Even though the rotor scatters up and down in frequency, the figure shows that calculations are accurate up to whatever frequency is included in the coupled sub-sets. Apparently, up-scattering is more important than down-scattering.

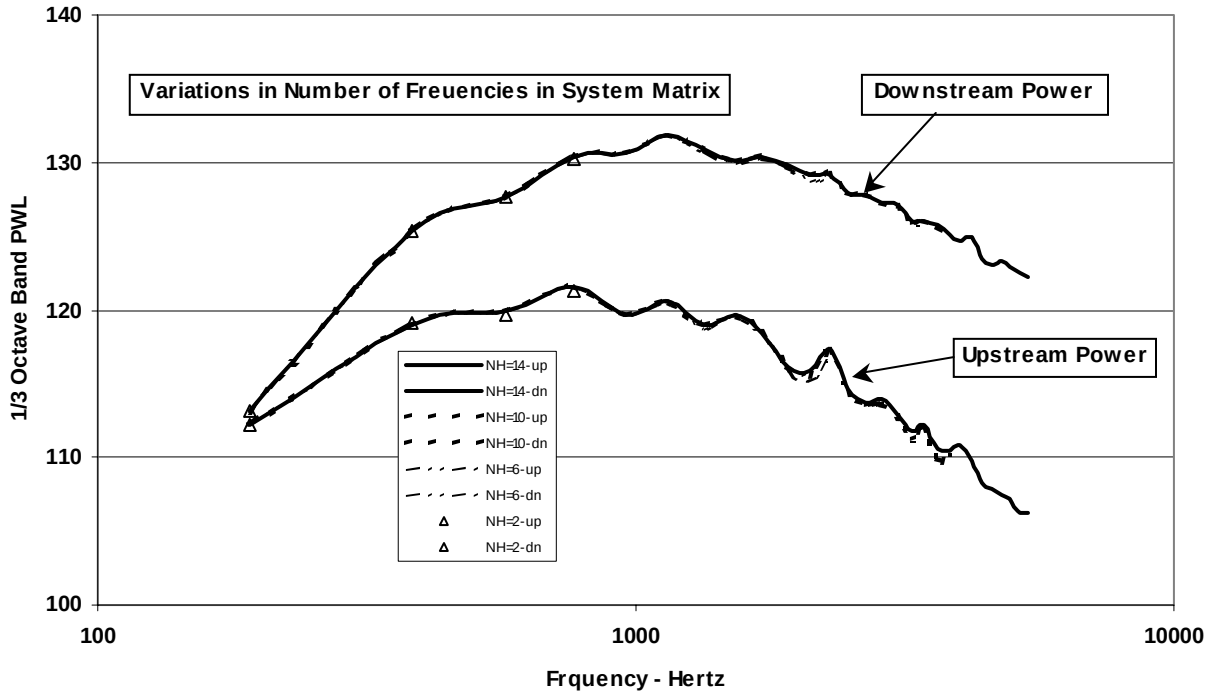

Figure 19. Effect of varying *NH* on computed results at lower frequencies. For *NH* = 2, the curves stop at 764 Hz, for *NH* = 6 at 2292 Hz for *NH* = 10 at 3821 Hz, and for *NH* = 14 at 5349.

An experiment was performed to determine if modal averaging could be used to reduce computational effort. Figure 20 was generated by stepping the *q* index in jumps of *qStep* and

then multiplying the results by *qStep*. It can be seen that skipping every other circumferential mode (*qStep* = 2) has negligible effect at all frequencies. Even skipping in steps of 5 produces good results from the peak of the spectrum and up in frequency. This is important information since computation time goes inversely with *qStep*. Jumping in steps of 10 produces unreliable results and biases the results toward higher levels. Based on these results, the remaining calculations for this report were made with *qStep* = 2.

It also seems likely that some radial orders could be skipped for further computational efficiency but this has not yet been verified. Simply skipping every other radial mode and then multiplying by 2 did not provide good results. Hence, a more refined scheme for radial mode averaging will be developed in future work.

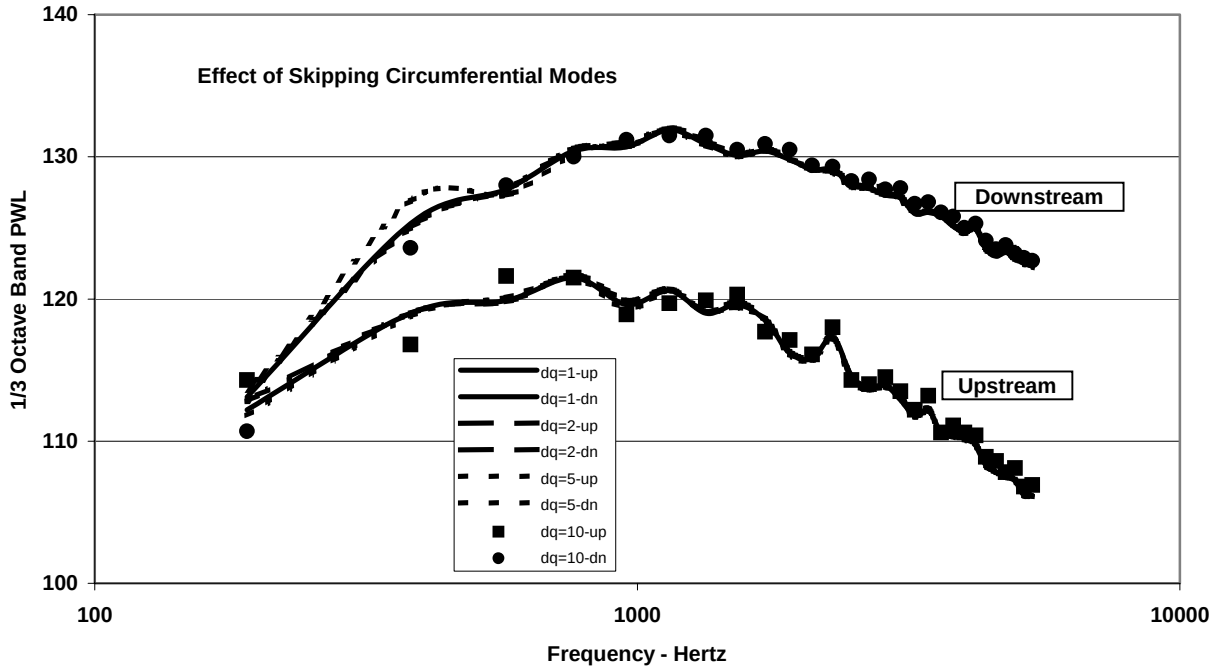

Figure 20. Effect of modal averaging with qStep = 1, 2, 5, and 10. For qStep=1, all circumferential modes are included. For qStep=2, every other mode is skipped and the results are doubled, etc.

Importance of Coupling and Flow Turning

Figure 21 was prepared for a direct comparison of the earlier isolated cascade technology and the new methodology with all features included. The solid curves, are the data-matched results from Figure 18 and include all of the new capability in CupBB. The dotted curves are the result of an isolated stator calculation with CupBB. (Thus, the dotted curves are equivalent to calculations with the earlier code BBCascade of Refs 2 and 3.) It can be seen that the full methodology increases downstream noise by about 3 dB at all frequencies and increases the upstream/downstream split (or differential) from about 5 dB to about 10 dB.

A slight variation on this result is shown in Figure 22. Here we represent the stator by the cascade plus the stator actuator disk (dotted curves). The solid curves result from adding the rotor cascade (with its actuator disk) while maintaining the mean flow and turbulence at the

stator. Again the aft noise increased and the upstream/downstream split is increased. However, the aft increase is about 2 dB rather than the 3 dB of Figure 21.

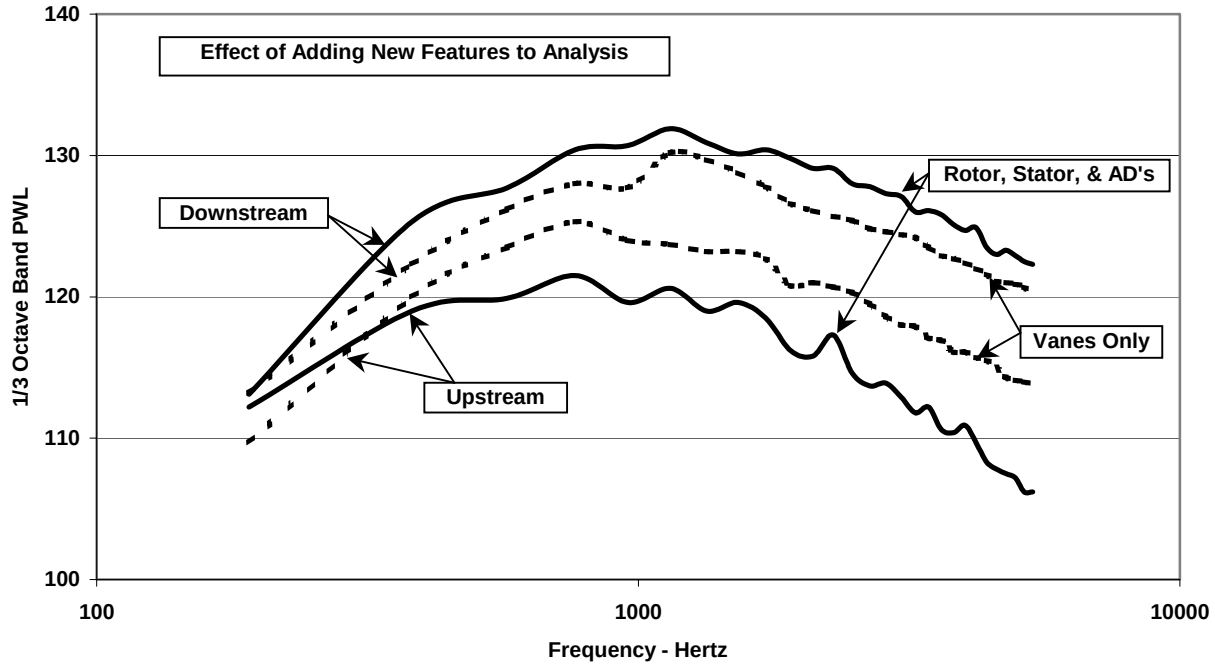

Figure 21. Calculations with CupBB for stator inflow turbulence. Isolated stator calculation compared to calculaton with all features included (blades, vanes, and actuator disks). This compares coupled *vs* uncoupled technology.

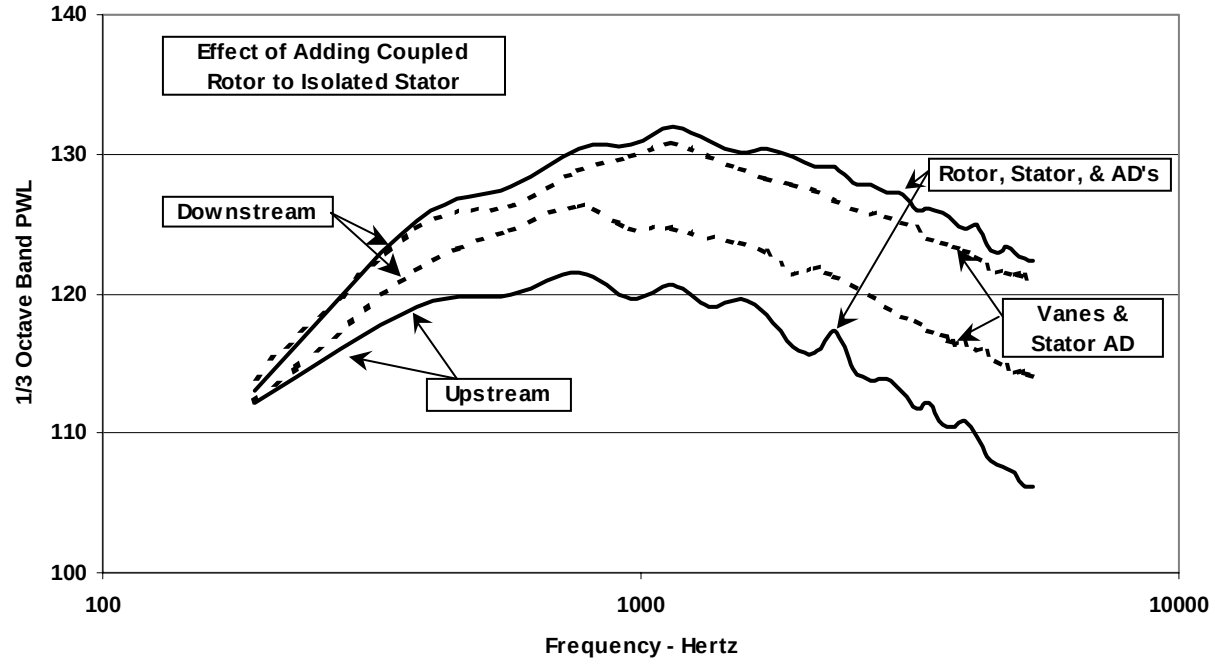

Figure 22. Same as Figure 21 except that the actuator disk is included in the isolated stator calculation.

CupBB treats rotor inflow turbulence as well. The sample calculation in Figure 23 compares the previous stator results with noise computed for the rotor with the same normalized intensity and scale for the turbulence. Both inlet and aft levels increase suggesting greater radiation efficiency by the rotor. Note the spectrum shapes for rotor and stator noise are almost the same although the high frequency parts of the spectra are a little flatter for the rotor inflow. Of course, we expect average turbulence intensity at the rotor face to be considerably less than at the stator face for typical turbofans. Thus, Figure 23 does not imply that inlet noise is dominated by rotor inflow turbulence.

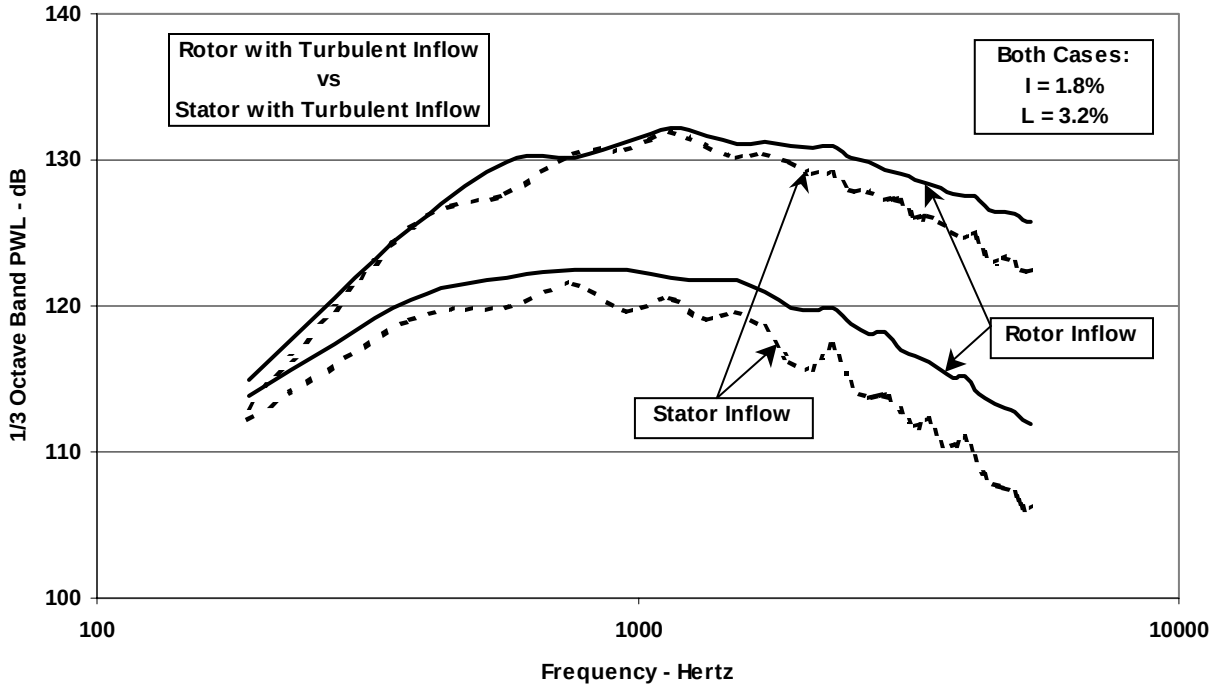

Figure 23. Noise due to rotor inflow turbulence compared with noise due to stator inflow turbulence. All of the model features were included for both calculations: 2 blade rows and turning via the actuator disks. The same normalized turbulence parameters were used for both cases.

Finally, in a form parallel to Figure 22, we evaluate the effect of the stator on rotor noise. The dotted curves in Figure 24 are for a rotor, represented by a cascade plus actuator disk, with turbulent inflow. The solid curves result from adding the stator (with actuator disk) on the downstream side without changing the rotor mean flow or inflow turbulence. The effect is significant and again indicates that isolated blade row calculations are too simplistic for reliable fan broadband noise prediction.

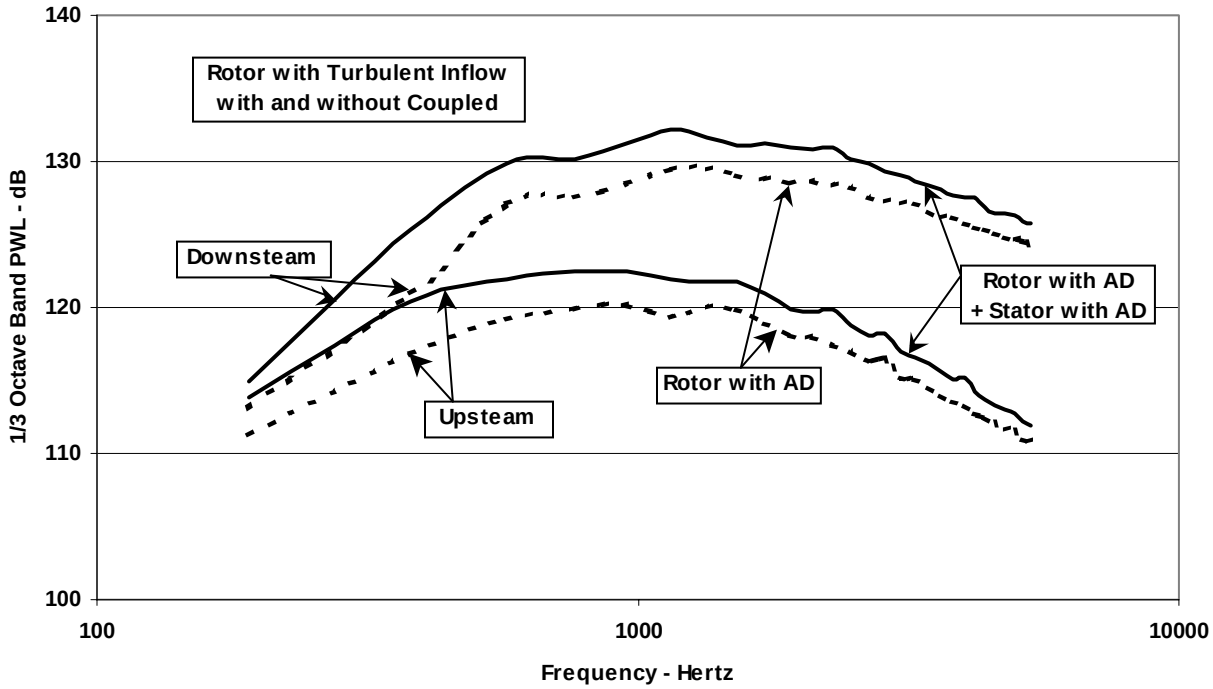

Figure 24. Comparison of calculations for rotor inflow turbulence with and without a coupled stator.

SECTION 9
CONCLUDING REMARKS

Earlier methods for predicting turbulent inflow noise from fans treated rotors and stators as isolated blade rows in a uniform background flow. This report extends that capability by adding the effects of scattering by the adjacent blade row and turning of the mean flow by the rotor and stator. Essential elements of the theory include: unsteady acoustic and vortical responses of rectilinear cascades via S. A. L. Glegg's Wiener-Hopf theory, unsteady actuator disks to represent the effect of changes in mean flow on perturbation waves, full unsteady vortical and acoustic coupling of the rotor and stator, and turbulence represented by its 3D wavenumber spectrum. The modeling requires that geometry and mean flow be constant in the spanwise direction. Although this is a limitation, the benefit is that the cascade unsteady loading and acoustic/vortical response are mutually consistent and fully 3 dimensional.

In developing the coupling analysis, an important principle was discovered: Many modes and frequencies are involved in fan broadband noise generation. In the process of reflecting back and forth between the rotor and stator, each mode/frequency couples to many other mode/freqencies. However, the coupling is limited to independent mode subsets each of which only communicates with its own modes and not with the other mode subsets. This principle of independent mode subsets makes the coupling problem tractable. If all modes could communicate with each other, computation time would be excessive. But, by taking advantage of this principle, all of the calculations presented herein could be performed on a personal computer.

The computer code CupBB, which embodies the broadband theory, can compute noise due to turbulent inflow at the rotor or stator or both. Comparison of isolated rotor or stator calculations with fully coupled calculations indicates that coupling increases the aft noise by about 3dB and increases the upstream/downstream sound power split from about 5 dB to about 10 dB.

Based on the limited calculations presented herein, the 2 major conclusions are as follows.

1. It is unlikely that stator inflow turbulence contributes significantly to inlet noise.
2. Unsteady coupling augments noise generation to the point that it must be included in any attempt at absolute level predictions.

The analysis presented in this report is based on rectilinear, flat plate theory. Although this has its limitations, the 2 conclusions above should be reliable because the analysis is a fully consistent, 3D treatment of the unsteady flow. Trends regarding effects of adjacent blade rows and flow turning are credible. Thus, in the short term, the analysis can be used to upgrade existing isolated blade row prediction methods. In the longer term, the principles discovered here and the coupling method derived can be used as guidance in development of unsteady CFD methods that can represent the blade response and turning effects more accurately.

Because of time constraints, conclusions have not yet been drawn regarding the importance of mode trapping in fan broadband noise. The physics is modeled in the code but the computer runs required for the analysis must be performed in future work.

REFERENCES

1. Hanson, D. B., "Mode Trapping in Coupled 2D Cascades – Acoustic and Aerodynamic Results", AIAA Paper 93-4417, presented at the 15th AIAA Aeroacoustics Conference, October 25-27, 1993, Long Beach, CA.
2. Hanson, D. B. and Horan, K. P., "Turbulence/Cascade Interaction: Spectra of Inflow, Cascade Response, and Noise", AIAA/CEAS Paper No. 98-2319 presented at the 4th AIAA/CEAS Aeroacoustics Conference, Toulouse, France, June 2-4, 1998.
3. Hanson, D. B., "Theory for Broadband Noise of Rotor and Stator Cascades with Inhomogeneous Inflow Turbulence – Including Effects of Lean and Sweep", NASA/CR-2001-210762, May 2001.
4. Glegg, S. A. L., "The Response of a Swept Blade Row to a Three Dimensional Gust", J. Sound and Vibration, Vol. 227(1), pp. 29-64, 1999.
5. Topol, D. A., "TFaNS Tone Fan Noise Design/Prediction System, Volume I: System Description, CUP3D Technical Documentation and Manual for Code Developers," NASA/CR-1999-208882, March 1999.
6. Tyler, J.M. & Sofrin, T. S., "Axial Flow Compressor Noise Studies", SAE Transactions, Vol. 70, 1962, pp. 309-332.
7. Smith, S. N., "Discrete Frequency Sound Generation in Axial Flow Turbomachines", Aeronautical Research Council Reports and Memoranda, R&M 3709, HMSO, London, 1973.
8. Ganz, U. W., Joppa, P. D., Patten, T. J., and Scharpf, D. F., "Boeing 18-Inch Fan Rig Broadband Noise Test", NASA/CR-1998-208704, September 1998.
9. Owczarek, J. A., "Analysis of an Axial Compressor Blade Vibration Based on Wave Reflection Theory", J. Engineering for Gas Turbines and Power, January 1984, pp. 57-64.
10. Mengle, V. G., Acoustic Spectra and Detection of Vibrating Rotor Blades, Including Row-to-Row Interference, AIAA 90-3987, October, 1990.
11. Hall, K. C. & Silkowski, P. D., "The Influence of Neighboring Blade Rows on the Unsteady Aerodynamic Response of Cascades", ASME Paper 95 GT-35.
12. Topol, D. A., Holhubner, S. C., and Mathews, D. C., "A Reflection Mechanism for Aft Fan Tone Noise," AIAA Paper No. 87-2699, October 19-21, 1987.
13. Goldstein, M. E., *Aeroacoustics*, McGraw-Hill, New York, 1976.
14. Liepmann H. W., "Extension of the Statistical Approach to Buffeting and Gust Response of Wings of Finite Span", Journal of the Aeronautical Sciences, March 1955.

APPENDIX A

GLEGG'S CASCADE THEORY FOR PRESSURE WAVES ADAPTED TO DUCT COORDINATES AND THE *n, k* INDEX NOTATION

Section 6 of this report requires forms for the acoustic and vortical responses of stators and rotors to excitation by input acoustical and vortical waves. This appendix provides the acoustic response and Appendix B provides the vortical response.

Glegg developed his theory in "cascade coordinates" in which the x axis is aligned with the flow direction. In this appendix we adapt his scheme to "duct coordinates", which have been chosen for the coupled cascade application. In duct coordinates the x axis is aligned with the duct axis, the y axis with the tangential direction (positive in the direction of rotor rotation), and the z axis coincides with the leading edge of the reference vane (or blade). Also, we replace the usual interblade phase angle, common in unsteady cascade analysis, with the n,k index notation commonly used in fan acoustic interaction theory. Glegg's theory accounts for sweep, but, in this report, we deal strictly with unswept blade rows.

First, we will review Glegg's theory (in cascade coordinates) and then transform his equations to duct coordinates. As shown in Figure A-1, geometry is constant in the z direction and the background flow is uniform: $\mathbf{U}=(W,0,0)$, as expressed in cascade coordinates. Airfoils are unloaded flat plates. Cascade gap, chord, and stagger angle are g, c, and θ.

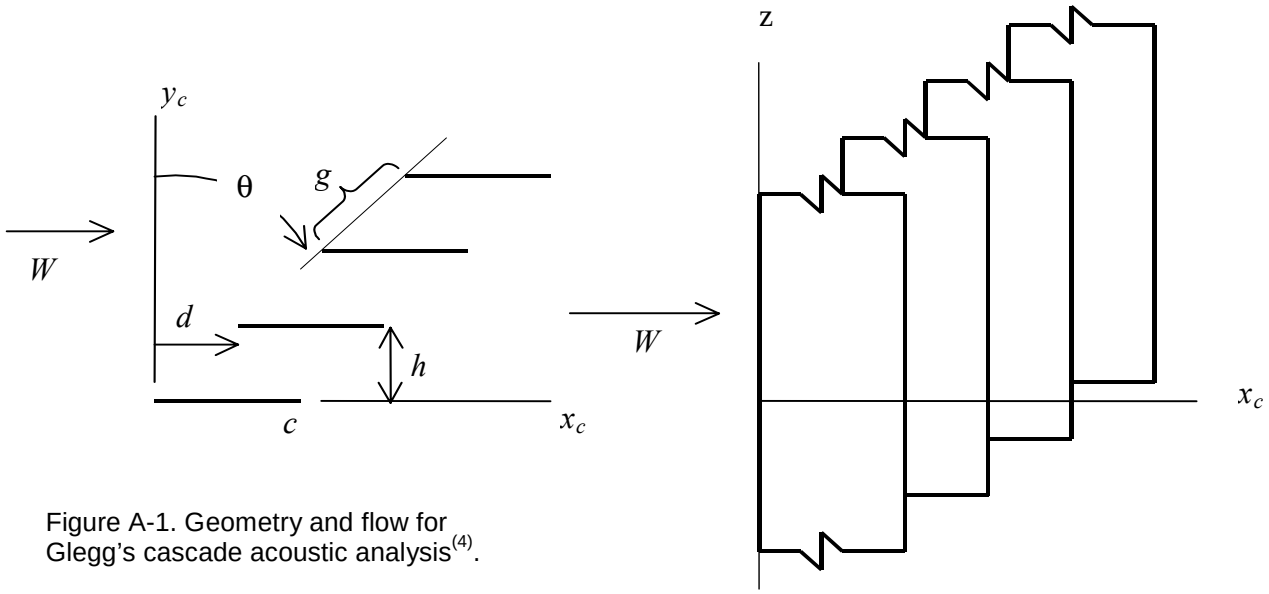

Figure A-1. Geometry and flow for Glegg's cascade acoustic analysis[4].

The unsteady flow is harmonic in space and time with upwash given by Equation A-1

$$w(\mathbf{x},t) = w_o\, e^{i(\gamma_o x_c + \alpha y_c + \nu z - \omega t)} \tag{A-1}$$

This represents a plane wave that is harmonic in time with frequency $\omega/2\pi$ and upwash complex amplitude w_o. It is also harmonic in space with x_c, y_c, and z wavenumbers equal to

γ_o, α, and ν. By use of Wiener-Hopf analysis, Glegg derived an equation equivalent to the following for the velocity potential of acoustic waves scattered by the cascade in response to the input wave of Equation A-1

$$\phi^{\pm}(\mathbf{x},t) = \pm\frac{\pi w_o c^2}{\beta s_e}\sum_{k=-\infty}^{\infty}\frac{\zeta_k^{\pm} D(\lambda_k^{\pm})}{\sqrt{\kappa_e^2 - f_k^2}}\, e^{i[-\lambda_k^{\pm}(x_c - y_c d/h) + (\sigma - 2\pi k) y_c/h + \nu z]} e^{-i\omega t} \qquad \text{(A-2)}$$

where the upper/lower sign applies to upstream/downstream going waves and

$$M = W/a \qquad \beta = \sqrt{1 - M^2} \qquad \text{(A-3)}$$

$$s_e = \sqrt{d^2 + \beta^2 h^2} \qquad \tan\chi_e = d/\beta h \qquad \lambda_k^{\pm} = \kappa M + \eta_k^{\pm} \qquad \text{(A-4)}$$

$$\zeta_k^{\pm} = \beta\sqrt{\kappa_e^2 - (\eta_k^{\pm})^2} \qquad \kappa_e^2 = \kappa^2 - (\nu/\beta)^2 \qquad \kappa = \omega/(a\beta^2) \qquad \text{(A-5)}$$

$$\eta_k^{\pm} = -f_k \sin\chi_e \pm \cos\chi_e\sqrt{\kappa_e^2 - f_k^2} \qquad f_k = (\sigma - 2\pi k + \kappa M d)/s_e \qquad \text{(A-6)}$$

and $\sigma = \gamma_o d + \alpha h$ is the interblade phase angle. D is the Fourier transform of the discontinuity in potential across the blade and wakes (in the form of an infinite product) and is the major result of Glegg's derivation. We adhere to Glegg's notation closely although we use k for the scattering index where Glegg used m, and θ for stagger, where Glegg used χ, and ω for radian frequency where Glegg used ω'. Also, the D function of this report is non-dimensional; to obtain the D function of Glegg's report, multiply the non-dimensional version by $w_o c^2$.

The velocity, pressure, and density perturbations associated with the acoustic wave can be obtained from Equation A-2 via

$$\mathbf{u} = \nabla\phi \qquad p = -\rho_r D\phi/Dt \qquad \rho' = p/a_r^2 \qquad \text{(A-7)}$$

where ρ_r and a_r are the ambient density and speed of sound in a region of the flow denoted by the subscript r. This leads to the following form for pressure in the scattered waves

$$p^{\pm}(\mathbf{x},t) = \pm\frac{i\pi\rho_r w_o c^2}{\beta s_e}\sum_{k=-\infty}^{\infty}\frac{(\omega + W\lambda_k^{\pm})\zeta_k^{\pm} D(\lambda_k^{\pm})}{\sqrt{\kappa_e^2 - f_k^2}}\, e^{i[-\lambda_k^{\pm}(x_c - y_c d/h) + (\sigma - 2\pi k) y_c/h + \nu z]} e^{-i\omega t} \qquad \text{(A-8)}$$

The formulation above gives the acoustic waves scattered by a cascade for a single planar wave input per Equation A-1. Scattering index k runs over an infinite range but, as usual in this kind of formulation, only a finite number of waves are cut on (propagate undiminished); the remaining waves decay exponentially and, thus, carry no acoustic energy. Cuton is governed by the argument of the square root $\sqrt{\kappa_e^2 - f_k^2}$; when the frequency is high enough, the argument is positive and the waves are cut on.

To apply Glegg's theory in duct coordinates (as used in the main body of this report), we transform the exponential in Eq. A-1 to

$$e^{i(k_x x + k_y y + \nu z - \omega t)} \tag{A-9}$$

where x is the axial duct coordinate and the tangential duct coordinate is $y=R\,\phi$. Furthermore, to deal directly with circumferential modes, we recognize that $k_y y = m\phi$. This, with $\phi = y/R$, gives

$$k_y = m/R \tag{A-10}$$

and the working form for the exponential in this appendix:

$$e^{i(k_x x + m\phi + \nu z - \omega t)} \tag{A-11}$$

Later on, we will find expressions for s_e, $\zeta_k^{\pm}$, $\lambda_k^{\pm}$, and $\sqrt{K_e^2 - f_k^2}$ in terms of k_x, m, and ω.

Since the analysis of this report tracks scattering by the rotor and stator, we need a notation that includes the rotor and stator scattering indices. Consistent with the presentation in Section 4, circumferential mode order is indexed on q, n, and k via

$$m = q + nB_1 - kB_2 \tag{A-12}$$

where n is the rotor scattering index, k is the stator scattering index, and q is the mode offset index. Axial wavenumber, with our n, k subscripts was given in Eq. 5-10

$$k_{xnk}^{\pm} = \frac{1}{R\beta_x^2}\left[M_x(-\hat{\omega} + mM_y) \mp \sqrt{(-\hat{\omega} + mM_y)^2 - \beta_x^2(m^2 + \hat{\nu}^2)} \right] \tag{A-13}$$

where we have normalized frequency by radius and speed of sound

$$\hat{\omega} = \frac{\omega R}{a_r} \tag{A-14}$$

and spanwise wavenumber by radius

$$\hat{\nu} = \nu R \tag{A-15}$$

The reader can verify that Eq. A-13 can also be obtained from Glegg's wavenumbers by coordinate transformation as in the following section.

Stator Scattering

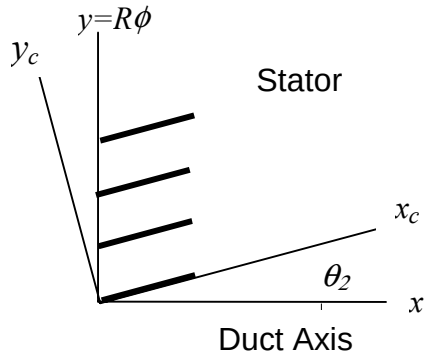

The connection between Glegg's cascade coordinates and our duct coordinates is a simple rotation about their common z axis as shown at the left. The transformation is given by

$$x = x_c \cos\theta_2 - y_c \sin\theta_2$$
$$y = x_c \sin\theta_2 + y_c \cos\theta_2$$
and (A-16)
$$x_c = \; x\cos\theta_2 + y\sin\theta_2$$
$$y_c = -x\sin\theta_2 + y\cos\theta_2$$

These equations are shown for the coordinate transformations but apply to transformation of the wavenumbers as well. Note in Equation A-2 that the axial wavenumbers are $-\lambda_k^{\pm}$. Hence, from the 3rd line of Equation A-16,

$$\lambda_{nk}^{\pm} = -k_{xnk}^{\pm} \cos\theta_2 - \frac{m}{R}\sin\theta_2 \tag{A-17}$$

where we have included an n subscript $\lambda_{nk}^{\pm}$ to help track scattered waves. This leads to an alternative form for the effect of the convective derivative in Eq. A-7 $\omega + W\lambda_{nk}^{\pm}$ (times -*i*)

$$\omega + W\lambda_{nk}^{\pm} = \omega - W(k_{xnk}^{\pm}\cos\theta_2 + \frac{m}{R}\sin\theta_2) = -\frac{a_r}{R}(-\hat{\omega} + M_x k_{xnk}^{\pm} R + M_y m) \tag{A-18}$$

or

$$\omega + W\lambda_k^{\pm} = -\frac{a_r}{R}\Lambda_{nk}^{\pm} \tag{A-19}$$

where $\Lambda_{nk}^{\pm} = -\hat{\omega} + M_x k_{xnk}^{\pm} R + M_y m$ is the same as defined in Section 5.

We can also apply the transformation of Eq. A-16 in the reverse direction to verify the form of the tangential wavenumber in the duct system derived from Glegg's forms. Note in Eq. A-2 that the y_c wavenumber in the cascade system is $\lambda_{nk}^{\pm}\tan\theta_2 + (\sigma - 2\pi k)/h$. Thus,

$$\frac{m}{R} = -\lambda_{nk}^{\pm}\sin\theta_2 + \left(\lambda_{nk}^{\pm}\tan\theta_2 + \frac{\sigma - 2\pi k}{h}\right)\cos\theta_2 \tag{A-20}$$

or, in terms of vane gap, g_2

$$\frac{m}{R} = k_y = \frac{\sigma - 2\pi k}{g_2} \tag{A-21}$$

since $h = g\cos\theta$. This is the well known form from Smith's theory (Ref. 7). Another expression required below is easily derived

$$s_e = \beta_x g_2 \tag{A-22}$$

where

$$\beta_x = \sqrt{1 - M_x^2} \tag{A-23}$$

To deal with the square root in the denominator of Equation A-2, we substitute definitions from Eqs. A-3 to A-6 and re-arrange to find

$$\sqrt{K_e^2 - f_k^2} = \frac{1}{R\beta\beta_x}\sqrt{(-\hat{\omega} + mM_y)^2 - \beta_x^2(m^2 + \hat{\nu}^2)} \tag{A-24}$$

The square root on the right side is the discriminator for cutoff. It appears frequently so we give it a special symbol

$$R_{nk} = \sqrt{(-\hat{\omega} + mM_y)^2 - \beta_x^2(m^2 + \hat{\nu}^2)} \tag{A-25}$$

Then,

$$\sqrt{K_e^2 - f_k^2} = \frac{1}{R\beta\beta_x}R_{nk} \tag{A-26}$$

A convenient form for $\zeta_k^{\pm}$ can be developed by similar manipulations. It must be treated with some care because the definition implies a square root of a square root, where the branch must be defined in the case of cutoff. From the definitions in Eqs. A-3 to A-6, we force the following form

$$\zeta_k^{\pm} = \beta\sqrt{K_e^2 - (\eta_k^{\pm})^2} = \beta\sqrt{K_e^2 - f_k^2 + f_k^2 - (\eta_k^{\pm})^2} \tag{A-27}$$

Insert the definition of $\eta_k^{\pm}$ to get

$$\zeta_k^{\pm} = \beta\sqrt{\left(K_e^2 - f_k^2\right) + f_k^2 - \left[f_k^2\sin^2\chi_e \mp 2f_k\sqrt{K_e^2 - f_k^2}\,\sin\chi_e\cos\chi_e + \left(K_e^2 - f_k^2\right)\cos^2\chi_e\right]} \tag{A-28}$$

and collect terms to find

$$\zeta_k^{\pm} = \beta\sqrt{\left(K_e^2 - f_k^2\right)\sin^2\chi_e \pm 2\sqrt{K_e^2 - f_k^2}\,\sin\chi_e\;f_k\cos\chi_e + f_k^2\cos^2\chi_e} \tag{A-29}$$

or simply

$$\zeta_k^{\pm} = \beta\left(\sqrt{K_e^2 - f_k^2}\,\sin\chi_e \pm f_k\cos\chi_e\right) \tag{A-30}$$

Again we add the n subscript and non-dimensionalize on R

$$\zeta_k^{\pm} = \hat{\zeta}_{nk}^{\pm} / R \tag{A-31}$$

Then, by substituting definitions from above, we find the non-dimensional form to be

$$\hat{\zeta}_{nk}^{\pm} = \frac{1}{\beta_x^2}\left[R_{nk} \sin\theta_2 \pm (\beta^2 m + \hat{\omega} M_y)\cos\theta_2 \right] \tag{A-32}$$

In obtaining a working form for the scattered acoustic pressure, we need to distinguish clearly between input waves and output waves using our " *n, k* " notation. We will use unprimed indices to indicate input waves and primed indices for output waves. The general form for mode order of waves input to the stator is

$$m = q + nB_1 - kB_2 \tag{A-33}$$

where q is the mode offset index, n relates to scattering at the rotor and k relates to scattering at the stator. Interblade phase angle of the input waves is related to mode order by

$$\sigma = \frac{2\pi m}{B_2} \tag{A-34}$$

Thus, in the " *n, k* " notation,

$$\sigma = \frac{2\pi}{B_2}(q + nB_1 - kB_2) \tag{A-35}$$

We temporarily denote the scattering index (of the output waves) as k''. In Glegg's (and Smith's) scattering theory, the scattering index appears only in combination with the interblade phase angle (of the input wave) as $\sigma - 2\pi k''$. We can relate this to the circumferential mode order of the output wave via

$$\sigma - 2\pi k'' = \frac{2\pi}{B_2}[q + nB_1 - (k + k'')B_2] = \frac{2\pi m''}{B_2} \tag{A-36}$$

where we have defined

$$m'' = q + nB_1 - (k + k'')B_2 \tag{A-37}$$

We modify our notation for Glegg's D function to $D_{nkk'}^{\pm}$ which indicates input mode n,k and output mode n,k'. When we put all of this together, the adapted form for the pressure waves becomes

$$p^{\pm}(\mathbf{x},t) = \frac{\mp i\,\pi\,\rho_r\,a_r\,c_2^2}{g_2\,R} w_{nk} \sum_{k''=-\infty}^{\infty} \frac{\Lambda_{n,k+k''}^{\pm}\,\hat{\zeta}_{n,k+k''}^{\pm}\,D_{n,k,k+k''}^{\pm}}{R_{n,k+k''}}\, e^{i[k_{xn,k+k''}^{\pm}x + m''\phi + \nu z - \omega t]} \tag{A-38}$$

Since the sum runs over all values of k'', it can be re-indexed via $k' = k + k''$ with the result

$$p^{\pm}(\mathbf{x},t) = \frac{\mp i\,\pi\,\rho_r\,a_r\,c_2^2}{g_2\,R} w_{nk} \sum_{k'=-\infty}^{\infty} \frac{\Lambda_{nk'}^{\pm}\,\hat{\zeta}_{nk'}^{\pm}\,D_{nkk'}^{\pm}}{R_{nk'}}\, e^{i[k_{xnk'}^{\pm}x + m'\phi + \nu z - \omega t]} \tag{A-39}$$

where $m' = q + nB_1 - k'B$. For the duct simulation in the main body of the report, the endwall are at $z = 0$ and $z = h$ and the z dependence of the upwash is given by cosines as in Eqs. 3.10 and 5.7. Of course, cosines are linear combinations of Glegg's upwash form in Eq. A-1 so that we can use

$$w(\mathbf{x},t) = w_o\, e^{i(\gamma_o x_c + \alpha y_c - \omega t)} \cos(\frac{\mu \pi z}{h}) \tag{A-40}$$

where μ is the radial mode index running from 0 to ∞. Now Eq. A-39 can simply be modified to give the response associated with Eq. A-40

$$p^{\pm}(\mathbf{x},t) = \frac{\mp i\,\pi\,\rho_r\, a_r\, c_2^2}{g_2\, R} w_{nk} \sum_{k'=-\infty}^{\infty} \frac{\Lambda^{\pm}_{nk'}\, \hat{\zeta}^{\pm}_{nk'}\, D^{\pm}_{nkk'}}{R_{nk'}}\, e^{i[k^{\pm}_{x\,nk'} x + m'\phi - \omega t]} \cos(\frac{\mu \pi z}{h}) \tag{A-41}$$

This can be written as

$$p^{\pm}(\mathbf{x},t) = \sum_{k'=-\infty}^{\infty} p^{\pm}_{nkk'} \tag{A-42}$$

where $p_{nkk'}$ is the form used in Section 6 to develop the system of scattering equations.

$$p^{\pm}_{nkk'} = \frac{\mp i\pi\,\rho_r\, a_r\, \hat{c}_2}{\bar{g}_2} w_{nk}\, \frac{\Lambda^{\pm}_{nk'}\, \hat{\zeta}^{\pm}_{nk'}\, D^{\pm}_{nkk'}}{R_{nk'}}\, e^{i[k^{\pm}_{x\,nk'} x + m'\phi - \omega t]} \cos(\frac{\mu \pi z}{h}) \tag{A-43}$$

We have defined $\hat{c}_2 = c_2/R$ and $\bar{g}_2 = g_2/c_2$. Note that in the main body of this report the stator input and output frequencies are $\omega_o + nB_1\Omega$.

Rotor Scattering

Coupling between rotor and stator is done in the stator reference frame at mode order $m = q + nB_1 - kB_2$ and frequency $\omega_o + nB_1\Omega$. Thus, the input order and frequency for the rotor are the same as for the stator problem. However, to apply the cascade theory, we must transform the input to the rotor frame where the mode order stays the same but frequency shifts because of rotation. Mode order m results in interblade phase angle

$$\sigma = \frac{2\pi m}{B_1} \tag{A-44}$$

Consider the kinematic phase of the input wave

$$\psi = m\phi - \omega t \tag{A-45}$$

Transformation to the rotor frame via $\phi = \phi_r + \Omega t$ gives

$$\psi = m\phi_r - (\omega - m\Omega)t \tag{A-46}$$

The rotor scatters mode order on the n index, so we denote the output wave modes as

$$m'' = q + (n + n'')B_1 - kB_2 \tag{A-47}$$

However, in the rotor-fixed frame, scattering does not change frequency; hence kinematic phase of the scattered waves becomes

$$\psi'' = m''\phi_r - (\omega - m\Omega)t \tag{A-48}$$

Thus, frequency in the rotor frame becomes

$$\omega_r = \omega - m\Omega \tag{A-49}$$

or, in normalized form

$$\hat{\omega}_r = \hat{\omega} - mM_T \tag{A-50}$$

Axial wavenumber for the rotor can be obtained from Eq. A-13 by replacing $\hat{\omega}$ by $\hat{\omega}_r$ and M_y by (M_y-M_T).

$$k_{xnk}^{\pm} = \frac{1}{R\beta_x^2}\left[M_x[-\hat{\omega}_r + m(M_y - M_T)] \mp \sqrt{[-\hat{\omega}_r + m(M_y - M_T)]^2 - \beta_x^2(m^2 + \hat{\nu}^2)} \right] \tag{A-51}$$

However, it can be seen from Eq. A-48 that

$$-\hat{\omega}_r + m(M_y - M_T) = -\hat{\omega} + mM_y \tag{A-52}$$

and axial wavenumber reverts to the form used for the stator in Eq. A-13

$$k_{xnk}^{\pm} = \frac{1}{R\beta_x^2}\left[M_x(-\hat{\omega} + mM_y) \mp \sqrt{(-\hat{\omega} + mM_y)^2 - \beta_x^2(m^2 + \hat{\nu}^2)} \right] \tag{A-53}$$

This is as it must be since the wavenumbers are related to physical lengths of the waves that would be the same in any coordinate system. A similar approach shows that $\sqrt{K_e^2 - f_n^2}$ has the same form for the stator, i.e. $\sqrt{K_e^2 - f_k^2} = R_{nk}/R\beta\beta_x$ where, as before

$$R_{nk} = \sqrt{(-\hat{\omega} + mM_y)^2 - \beta_x^2(m^2 + \hat{\nu}^2)} \tag{A-54}$$

The derivation for $\zeta_n^{\pm}$ proceeds the same as for the stator down to Eq. A-30:

$$\zeta_n^{\pm} = \beta\left(\sqrt{K_e^2 - f_n^2}\, \sin\chi_e \pm f_n \cos\chi_e \right) \tag{A-55}$$

except that now, of course, χ_e applies to rotor geometry and flow. We add the k subscript for clarity and normalize on R as follows

$$\zeta_n^{\pm} = \hat{\zeta}_{nk}^{\pm} / R \tag{A-56}$$

Substitution of the appropriate definitions leads to the following as the normalized form for the rotor

$$\hat{\zeta}_{nk}^{\pm} = \frac{1}{\beta_x^2}\left[R_{nk} \sin\theta_1 \pm (\beta_1^2 m + \hat{\omega}_r (M_y - M_T)) \cos\theta_1 \right] \tag{A-57}$$

where again the upper/lower sign goes with the up/downstream-going acoustic wave. Here,

$$\beta_1^2 = 1 - M_x^2 - (M_y - M_T)^2 \tag{A-58}$$

is related to the relative Mach number at the rotor.

As stated above, interblade phase angle for input waves is

$$\sigma = \frac{2\pi m}{B_1} \tag{A-59}$$

where m for the input wave is still $m=q+nB_1-kB_2$. We temporarily use n'' as the rotor scattering index. Then the factor in Glegg's equations containing the scattering index becomes

$$\sigma + 2\pi n'' = \frac{2\pi}{B_1}[q + (n+n'')B_1 - kB_2] = \frac{2\pi m''}{B_1} \tag{A-60}$$

Here we have defined

$$m'' = q + (n+n'')B_1 - kB_2 \tag{A-61}$$

The pressure in the rotor frame can now be written

$$p^{\pm}(\mathbf{x},t) = \frac{\mp i\pi\, \rho_r\, a_r c_1^2}{g_1 R} w_{nk} \sum_{n''=-\infty}^{\infty} \frac{\Lambda_{n+n'',k}^{\pm}\, \hat{\zeta}_{n+n'',k}^{\pm}\, D_{n,k,n+n''}}{R_{n+n'',k}}\, e^{i[k_{x,n+n'',k}^{\pm} x + m''\phi_r + \nu z - \omega_r t]} \tag{A-62}$$

We re-index this via $n'=n+n''$, note that the application in the main body of this report uses $\omega = \omega_o + nB_1\Omega$, and then return to the stator frame via $\phi_r = \phi - \Omega t$ to find

$$p^{\pm}(\mathbf{x},t) = \frac{\mp i\pi\, \rho_r\, a_r c_1^2}{g_1 R} w_{nk} \sum_{n'=-\infty}^{\infty} \frac{\Lambda_{n'k}^{\pm}\, \hat{\zeta}_{n'k}^{\pm}\, D_{nkn'}}{R_{n'k}}\, e^{i[k_{xn'k}^{\pm} x + m'\phi + \nu z - (\omega_o + n' B_1 \Omega) t]} \tag{A-63}$$

As with the stator scattering equations, $\Lambda_{n'k}^{\pm}$ gives the effect of the convective derivative. This is the same in the rotor and stator frames since, by definition, it is the derivative "following a particle". The equivalence can be seen in our notation as follows. The convective derivative in the rotor frame produces

$$\frac{D_r}{D_r t} = i\left[-\omega_r + U k_{xn'k}^{\pm} + (V - \Omega R)\frac{m'}{R} \right] \tag{A-64}$$

since the transverse velocity in the rotor frame is $V-\Omega R$. In the stator frame

$$\frac{D}{Dt} = i\left[-\omega + Uk^{\pm}_{xn'k} + V\frac{m'}{R}\right] = i\left[-(\omega_o - n'B_1\Omega) + Uk^{\pm}_{xn'k} + V\frac{m'}{R}\right] \tag{A-65}$$

These are the same since $\omega_r = \omega - m'\Omega$. In a form parallel to Eq. A-40 for the stator waves, we write

$$p^{\pm}(\mathbf{x},t) = \sum_{n'=-\infty}^{\infty} p^{\pm}_{nkn'} \tag{A-66}$$

where

$$p^{\pm}_{nkn'} = \frac{\mp i\pi\rho_r a_r \hat{c}_1}{\bar{g}_1} w_{nk} \frac{\Lambda^{\pm}_{n'k}\hat{\zeta}^{\pm}_{n'k} D_{nkn'}}{R_{n'k}} e^{i[k^{\pm}_{xn'k}x + m'\phi + \nu z - (\omega_o + n'B_1\Omega)t]} \tag{A-67}$$

For the upwash in a ducted system we again use Eq. A-40 so that Eq. A-67 becomes

$$p^{\pm}_{nkn'} = \frac{\mp i\pi\rho_r a_r \hat{c}_1}{\bar{g}_1} w_{nk} \frac{\Lambda^{\pm}_{n'k}\hat{\zeta}^{\pm}_{n'k} D_{nkn'}}{R_{n'k}} e^{i[k^{\pm}_{xn'k}x + m'\phi - (\omega_o + n'B_1\Omega)t]} \cos\left(\frac{\mu\pi z}{h}\right) \tag{A-68}$$

This gives the scattering by the rotor represented in the stator reference frame. It is the desired form for setting up the scattering equations in Section 6. It can be seen that the rotor scatters frequencies $\omega_o + nB_1\Omega$ into frequencies $\omega_o + n'B_1\Omega$.

APPENDIX B

GLEGG'S CASCADE THEORY FOR VORTICAL WAVES ADAPTED TO DUCT COORDINATES AND THE n, k INDEX NOTATION

This appendix develops equations needed in Section 6 for vortical waves shed by a cascade due to excitation by both acoustic and vortical waves. Results are provided in the contexts of both stator and rotor.

Glegg has extended the Wiener-Hopf theory of Ref. 4 to include vortical response (via a personal communication). The output velocity perturbation can be written in a series over the scattering index k as follows

$$\mathbf{v}(\mathbf{x},t) = \sum_{k=-\infty}^{\infty} \mathbf{V}_k \, e^{i(\gamma_c x_c + \alpha y_c + \nu z - \omega t)} \tag{B-1}$$

where x_c and y_c are Glegg's cascade coordinates (x and y in his notation) and γ_c and α are the associated wavenumbers (corresponding to convection).

$$\gamma_c = \omega / W \tag{B-2}$$

$$\alpha = (\sigma - 2\pi k - \gamma_c d)/h \tag{B-3}$$

and ν is the z wavenumber. Glegg's result for the velocity vector amplitudes is

$$\mathbf{V}_k = \frac{-2\pi i K(\gamma_c) w_o c}{h(\gamma_c^2 + \alpha^2 + \nu^2)} (\alpha\gamma_c \mathbf{i}_c + \zeta_c^2 \mathbf{j}_c + \alpha\nu \mathbf{k}_c) \tag{B-4}$$

where

$$\zeta_c^2 = -(\gamma_c^2 + \nu^2) \tag{B-5}$$

When $\mathbf{V}_k$ is represented in duct coordinates via Eqs. A-16, the resulting x, y, z components are

$$u_k = \frac{-2\pi i K(\gamma_c) w_o c}{h(\gamma_c^2 + \alpha^2 + \nu^2)} (\alpha\gamma_c \cos\theta - \zeta_c^2 \sin\theta) \tag{B-6}$$

$$v_k = \frac{-2\pi i K(\gamma_c) w_o c}{h(\gamma_c^2 + \alpha^2 + \nu^2)} (\alpha\gamma_c \sin\theta + \zeta_c^2 \cos\theta) \tag{B-7}$$

$$w_k = \frac{-2\pi i K(\gamma_c) w_o c}{h(\gamma_c^2 + \alpha^2 + \nu^2)} (\alpha\nu) \tag{B-8}$$

Stator Waves

For the vortical waves, we apply the strategy already developed in Appendix A for pressure waves. Mode order of the input waves is

$$m = q + nB_1 - kB_2 \tag{B-9}$$

with associated interblade phase angle

$$\sigma = \frac{2\pi m}{B_2} \tag{B-10}$$

Since the stator scatters on the k index, we write the mode order of the scattered waves as

$$m'' = q + nB_1 - (k + k'')B_2 \tag{B-11}$$

Then the y_c wavenumber can be expressed in terms of duct coordinates wavenumbers via Eq. A-16 with the result

$$\alpha_{n,k+k''} = -k_{x3n,k+k''} \sin\theta_2 + \frac{m''}{R}\cos\theta_2 \tag{B-12}$$

Now the velocity perturbations controlling upwash (in the duct coordinate system) are

$$u(\mathbf{x},t) = \frac{-2\pi i K(\gamma_c)}{h/c}\, w_{nk} \sum_{k''=-\infty}^{\infty} \frac{\alpha_{n,k+k''}\gamma_c \cos\theta_2 - \zeta_c^2 \sin\theta_2}{\gamma_c^2 + \alpha_{n,k+k''}^2 + \nu^2}\, e^{i(k_{x3n,k+k''}x + m''\phi + \nu z - \omega t)} \tag{B-13}$$

and

$$v(\mathbf{x},t) = \frac{-2\pi i K(\gamma_c)}{h/c}\, w_{nk} \sum_{k''=-\infty}^{\infty} \frac{\alpha_{n,k+k''}\gamma_c \sin\theta_2 + \zeta_c^2 \cos\theta_2}{\gamma_c^2 + \alpha_{n,k+k''}^2 + \nu^2}\, e^{i(k_{x3n,k+k''}x + m''\phi + \nu z - \omega t)} \tag{B-14}$$

Eqs. B-13 and B-14 are in a mixed notation, using wavenumbers from both the duct system and the cascade system. This turns out to be convenient for coding.

Again, we shift the k'' index via $k' = k + k''$ to arrive at the final forms for vortical waves shed by the stator

$$u(\mathbf{x},t) = \sum_{k'=-\infty}^{\infty} u_{nkk'} \tag{B-15}$$

and

$$v(\mathbf{x},t) = \sum_{k'=-\infty}^{\infty} v_{nkk'} \tag{B-16}$$

where

$$u_{nkk'} = \frac{-2\pi i K(\gamma_c)}{h/c}\, \frac{\alpha_{nk'}\gamma_c \cos\theta_2 - \zeta_c^2 \sin\theta_2}{\gamma_c^2 + \alpha_{nk'}^2 + \nu^2}\, w_{nk}\, e^{i(k_{x3nk'}x + m'\phi + \nu z - \omega t)} \tag{B-17}$$

$$v_{nkk'} = \frac{-2\pi i K(\gamma_c)}{h/c}\, \frac{\alpha_{nk'}\gamma_c \sin\theta_2 + \zeta_c^2 \cos\theta_2}{\gamma_c^2 + \alpha_{nk'}^2 + \nu^2}\, w_{nk}\, e^{i(k_{x3nk'}x + m'\phi + \nu z - \omega t)} \tag{B-18}$$

where in the main body of this report $\omega = \omega_o + nB_1\Omega$. As the notation implies, these represent scattering by the stator of an n,k input wave into an n,k' output wave.

Rotor Waves

Here we find forms analogous to Eqs. B-17 and B-18 for scattering by the rotor. Input waves have mode order $m = q + nB_1 - kB_2$ and frequency ω in the stator coordinate system. Mode order m results in interblade phase angle

$$\sigma = \frac{2\pi m}{B_1} \tag{B-19}$$

Consider the kinematic phase of the input wave

$$\psi = m\phi - \omega t \tag{B-20}$$

Transformation to the rotor frame via $\phi = \phi_r + \Omega t$ gives

$$\psi = m\phi_r - (\omega - m\Omega)t \tag{B-21}$$

The rotor scatters on the n index, so we denote the output wave mode orders as

$$m'' = q + (n + n'')B_1 - kB_2 \tag{B-22}$$

However, in the rotor-fixed frame, the frequency does not change so that the kinematic phase of the scattered waves becomes

$$\psi'' = m''\phi_r - (\omega - m\Omega)t \tag{B-23}$$

Then the α wavenumber is

$$\alpha_{n+n'',k} = -k_{x3n+n'',k}\sin\theta_1 + \frac{m''}{R}\cos\theta_1 \tag{B-24}$$

and the relevant velocity perturbations (in the rotor frame) are

$$u(\mathbf{x},t) = \frac{-2\pi i K(\gamma_c)}{h/c}\, w_{nk} \sum_{n''=-\infty}^{\infty} \frac{\alpha_{n+n'',k}\,\gamma_c\cos\theta_1 - \zeta_c^2\sin\theta_1}{\gamma_c^2 + \alpha_{n+n'',k}^2 + \nu^2}\, e^{i(k_{x3n+n'',k}\,x + \nu z + \psi'')} \tag{B-25}$$

and

$$v(\mathbf{x},t) = \frac{-2\pi i K(\gamma_c)}{h/c}\, w_{nk} \sum_{n''=-\infty}^{\infty} \frac{\alpha_{n+n'',k}\,\gamma_c\sin\theta_1 + \zeta_c^2\cos\theta_1}{\gamma_c^2 + \alpha_{n+n'',k}^2 + \nu^2}\, e^{i(k_{x3n+n'',k}\,x + \nu z + \psi'')} \tag{B-26}$$

Transformation back to the stator frame yields

$$\psi'' = m''\phi - (\omega + m''\Omega - m\Omega)t \tag{B-27}$$

We shift the n'' index via $n' = n + n''$ to arrive at the final forms for vortical waves shed by the rotor. Frequency becomes $\omega_r = \omega + (n' - n)\Omega$ and

$$u(\mathbf{x},t) = \sum_{n'=-\infty}^{\infty} u_{nkn'} \tag{B-28}$$

and

$$v(\mathbf{x},t) = \sum_{n'=-\infty}^{\infty} v_{nkn'} \tag{B-29}$$

where

$$u_{nkn'} = \frac{-2\pi i K(\gamma_c)}{h/c} \frac{\alpha_{n'k}\,\gamma_c \cos\theta_1 - \zeta_c^2 \sin\theta_1}{\gamma_c^2 + \alpha_{n'k}^2 + \nu^2} w_{nk}\, e^{i\{k_{x3n'k}x + m'\phi + \nu z - [\omega + (n'-n)B_1\Omega]t\}} \tag{B-30}$$

$$v_{nkn'} = \frac{-2\pi i K(\gamma_c)}{h/c} \frac{\alpha_{n'k}\,\gamma_c \sin\theta_1 + \zeta_c^2 \cos\theta_1}{\gamma_c^2 + \alpha_{n'k}^2 + \nu^2} w_{nk}\, e^{i\{k_{x3n'k}x + m'\phi + \nu z - [\omega + (n'-n)B_1\Omega]t\}} \tag{B-31}$$

And here the notation indicates scattering by the rotor of an $n,\ k$ input wave into an $n',\ k$ output wave. These forms are adapted to the coupling analysis in the main body of the report, $\omega_o + nB_1\Omega$ and hence Eqs. B-30 and B-31 become

$$u_{nkn'} = \frac{-2\pi i K(\gamma_c)}{h/c} \frac{\alpha_{n'k}\,\gamma_c \cos\theta_1 - \zeta_c^2 \sin\theta_1}{\gamma_c^2 + \alpha_{n'k}^2 + \nu^2} w_{nk}\, e^{i[k_{x3n'k}x + m'\phi + \nu z - (\omega_o + n'B_1\Omega)t]} \tag{B-32}$$

$$v_{nkn'} = \frac{-2\pi i K(\gamma_c)}{h/c} \frac{\alpha_{n'k}\,\gamma_c \sin\theta_1 + \zeta_c^2 \cos\theta_1}{\gamma_c^2 + \alpha_{n'k}^2 + \nu^2} w_{nk}\, e^{i[k_{x3n'k}x + m'\phi + \nu z - (\omega_o + n'B_1\Omega)t]} \tag{B-33}$$

APPENDIX C
ACTUATOR DISK THEORY

In Section 6, equations were derived for the rotor and stator as scattering elements. For example, the stator element consists of 2 sub-elements: the vane cascade in uniform flow and an actuator disk whose role is to account for changes in the mean flow that affect the acoustic environment. Section 6 gave the derivation for the cascade scattering and showed how the cascade is coupled to the actuator disk; this appendix provides the derivation of the actuator disk equations for application in Section 6.

The actuator disks in the scattering theory account for turning of the mean flow at the rotor and stator through conservation of mass and momentum. In the conservation equations, the flow quantities are written as sums of steady and perturbation (or unsteady) parts. When the steady and unsteady parts are separated, the steady flow is considered to be prescribed or known from a separate aerodynamic analysis. The steady flow provides coefficients for the unsteady equations so that jumps in the mean flow cause jumps in the perturbation flow. The jumps are effectively modal reflection and transmission coefficients that can be found by inverting a linear system.

There are 4 wave types:

T=1: Upstream-going pressure waves
T=2: Downstream-going pressure waves
T=3: Vortical (downstream-going) waves
T=4: Vortical (downstream-going) waves

and 4 conservation equations:

Conservation of mass
Conservation of axial momentum
Conservation of tangential momentum
Conservation of radial momentum

These are satisfied on a mode-by-mode basis using the standard wave set from the main text. Each of the 4 wave types as input scatters out 4 wave types. Thus, whereas the cascades scatter on mode order and wave type, the actuator disks scatter only on wave type. The actuator disks do not scatter on mode order because they have no variation in geometry in the tangential direction.

In the following sections, we apply the conservation equations, one at a time, by linearizing them and applying the standard wave sets from Section 5. These lead to 4 by 4 matrix systems for each circumferential mode order (each n, k combination) that are solved by inversion.

CONSERVATION OF MASS

For conservation of mass, ρu is matched on both sides of the actuator disk:

$$(\rho u)_a = (\rho u)_b \tag{C-1}$$

We write this in terms of steady and unsteady parts (with the tilde's):

$$(\rho_a + \tilde{\rho}_a)(U_a + \tilde{u}_a) = (\rho_b + \tilde{\rho}_b)(U_b + \tilde{u}_b) \tag{C-2}$$

and focus on the first order unsteady terms, which become

$$\rho_a \tilde{u}_a + \frac{U_a}{a_a^2}\tilde{p}_a = \rho_b \tilde{u}_b + \frac{U_b}{a_b^2}\tilde{p}_b \tag{C-3}$$

after applying $\tilde{p} = \tilde{\rho} a^2$. Now, we define

$$C_a = \frac{a_o}{p_o}\left(\rho_a \tilde{u}_a + \frac{U_a}{a_a^2}\tilde{p}_a\right) \tag{C-4}$$

for matching at the actuator disk with a similar form C_b for region b. The normalization via a_o/p_o is for convenience. a_o and p_o are reference values for the sound speed and ambient pressure which will drop out of the formulas later.

We interpret Eq. C-4 to apply on a mode-by-mode basis and express the perturbation quantities as the sum over all wave types. For example, the contribution of the upstream-going pressure (Type 1) in region a is denoted by the coefficient A_1^a, which is stands for the defining pressure component $A_1^a(n,k)$ in Eq. 6.1. The contribution from the associated axial velocity component in Eq. C-4 is proportional to A_1^a via the second line of Eq. 5.11.

For $\mu = 0$:

$$\begin{aligned} C_a = {} & \frac{a_o}{p_o}\left[\rho_a \frac{p_o}{\rho_a a_a}\left(\frac{-\hat{k}_{x1nk}^a}{\Lambda_{1nk}^a}\right) + \frac{M_x^a}{a_a}p_o\right]A_1^a \\ & + \frac{a_o}{p_o}\left[\rho_a \frac{p_o}{\rho_a a_a}\left(\frac{-\hat{k}_{x2nk}^a}{\Lambda_{2nk}^a}\right) + \frac{M_x^a}{a_a}p_o\right]A_2^a \\ & + \frac{a_o}{p_o}\left[\rho_a a_o\left(\frac{-m}{\hat{k}_{x3nk}^a}\right)\right]A_3^a \end{aligned} \tag{C-5}$$

where the first line comes from the upstream-going pressure wave, the second from the downstream-going pressure wave, and the third from the vorticity wave. Because we are matching on a mode-by-mode basis, we have dropped the n,k subscripts, the exponential, and the cosine, which are common to all terms.

For $\mu > 0$:

$$
\begin{aligned}
C_a = & \frac{a_o}{p_o}\left[\rho_a \frac{p_o}{\rho_a a_a}\left(\frac{-\hat{k}^a_{x1nk}}{\Lambda^a_{1nk}}\right) + \frac{M^a_x}{a_a} p_o\right] A^a_1 \\
& + \frac{a_o}{p_o}\left[\rho_a \frac{p_o}{\rho_a a_a}\left(\frac{-\hat{k}^a_{x2nk}}{\Lambda^a_{2nk}}\right) + \frac{M^a_x}{a_a} p_o\right] A^a_2 \\
& + [0] A^a_3 \\
& + \frac{a_o}{p_o}[\rho_a a_o] A^a_4
\end{aligned}
\tag{C-6}
$$

All of the matching is at $x = 0$; reference planes are shifted later via exponentials. We compress the notation and write Eq. C-4 as

$$
C_a = C_{1a} A^a_1 + C_{2a} A^a_2 + C_{3a} A^a_3 + C_{4a} A^a_4 \tag{C-7}
$$

where

$$
\begin{aligned}
C_{1a} &= \frac{a_o}{a_a}\left[\frac{-\hat{k}^a_{x1nk}}{\Lambda^a_{1nk}} + M^a_x\right] \\
C_{2a} &= \frac{a_o}{a_a}\left[\frac{-\hat{k}^a_{x2nk}}{\Lambda^a_{2nk}} + M^a_x\right]
\end{aligned}
\tag{C-8}
$$

For $\mu = 0$

$$
C_{3a} = \gamma \frac{p_a}{p_o}\left(\frac{a_o}{a_a}\right)^2 \left[\frac{-m}{\hat{k}^a_{x3nk}}\right] \tag{C-9}
$$

and for $\mu > 0$

$$
\begin{aligned}
C_{3a} &= 0 \\
C_{4a} &= \gamma \frac{p_a}{p_o}\left(\frac{a_o}{a_a}\right)^2
\end{aligned}
\tag{C-10}
$$

where γ, the ratio of specific heats, entered from $\gamma p_a = \rho_a a_a^2$. The same argument leads to the conserved quantity on the b side of the actuator disk (for $\mu > 0$)

$$
C_b = C_{1b} A^b_1 + C_{2b} A^b_2 + C_{3b} A^b_3 + C_{4b} A^b_4 \tag{C-11}
$$

Now we equate C_a and C_b. Furthermore, we identify the 4 waves approaching the actuator disk from each side as input waves and place them on the right hand side of the equation and the 4 waves leaving the actuator disk as scattered waves and place them on the left side. The input waves are the upstream-going pressure wave on the b side and the downstream-going pressure wave and the vorticity waves on the a side. The scattered waves are on the upstream-going wave on the a side and the downstream-going pressure and vorticity waves on the b side.

$$C_{1a}A_1^a - C_{2b}A_2^b - C_{3b}A_3^b - C_{4b}A_4^b = C_{1b}A_1^b - C_{2a}A_2^a - C_{3a}A_3^a - C_{4a}A_4^a \qquad \text{(C-12)}$$

This (or the corresponding equation for $\mu = 0$) is the first of the actuator disk equations and represents conservation of mass.

CONSERVATION OF AXIAL MOMENTUM

We treat conservation of axial momentum in similar fashion. The unlinearized conservation equation is

$$L\sin\alpha_m + (p + \rho u^2)_a = (p + \rho u^2)_b \qquad \text{(C-13)}$$

where the first term is the axial component of loading on the disk. The critical step here is to separate the total loading on the blade row into the steady part, which is handled via the actuator disk, and the unsteady part, which is handled via unsteady cascade theory. Then, when we express the variables in Eq. C-13 in terms of steady and unsteady parts, the unsteady loading (on the actuator disk) is by definition equal to zero and the first order perturbation equation is

$$(1+(M_x^a)^2)\tilde{p}_a + 2\rho_a U_a \tilde{u}_a = (1+(M_x^b)^2)\tilde{p}_b + 2\rho_b U_b \tilde{u}_b \qquad \text{(C-14)}$$

We define

$$F_a = \frac{1}{p_o}\left[(1+(M_x^a)^2)\tilde{p}_a + 2\rho_a U_a \tilde{u}_a\right] \qquad \text{(C-15)}$$

and expand it in the 4 wave types, as before

$$F_a = F_{1a}A_1^a + F_{2a}A_2^a + F_{3a}A_3^a + F_{4a}A_4^a \qquad \text{(C-16)}$$

where

$$\begin{aligned} F_{1a} &= [1+(M_x^a)^2] + 2M_x^a\left(\frac{-\hat{k}_{x1nk}^a}{\Lambda_{1nk}^a}\right) \\ F_{2a} &= [1+(M_x^a)^2] + 2M_x^a\left(\frac{-\hat{k}_{x2nk}^a}{\Lambda_{2nk}^a}\right) \end{aligned} \qquad \text{(C-17)}$$

for $\mu = 0$

$$F_{3a} = 2\gamma\frac{p_a}{p_o}\frac{a_o}{a_a}M_x^a\left[\frac{-m}{\hat{k}_{x3nk}^a}\right] \qquad \text{(C-18)}$$

and for $\mu > 0$

$$\begin{aligned} F_{3a} &= 0 \\ F_{4a} &= 2\gamma\frac{p_a}{p_o}\frac{a_o}{a_a}M_x^a \end{aligned} \qquad \text{(C-19)}$$

The equations for the b side of the actuator disk are the same with b's substituted for the a's. By using the scheme described above for identifying source waves and scattered waves, the equation for conservation of axial momentum becomes

$$F_{1a}A_1^a - F_{2b}A_2^b - F_{3b}A_3^b - F_{4b}A_4^b = F_{1b}A_1^b - F_{2a}A_2^a - F_{3a}A_3^a - F_{4a}A_4^a \tag{C-20}$$

CONSERVATION OF TANGENTIAL MOMENTUM

The unlinearized equation for transverse (y direction) momentum is

$$-L\cos\alpha_m + (\rho u v)_a = (\rho u v)_b \tag{C-21}$$

Using the same arguments as in the discussion of axial momentum, the first order conserved quantity can be written

$$G_a = \frac{1}{p_o}\left[\rho_a U_a \tilde{v}_a + \rho_a V_a \tilde{u}_a + M_x^a M_y^a \tilde{p}_a\right] \tag{C-22}$$

or, in terms of the 4 wave types, as

$$G_a = G_{1a}A_1^a + G_{2a}A_2^a + G_{3a}A_3^a + G_{4a}A_4^a \tag{C-23}$$

where

$$\begin{aligned} G_{1a} &= M_x^a\left(\frac{-m}{\Lambda_{1nk}^a}\right) + M_y^a\left(\frac{-\hat{k}_{x1nk}^a}{\Lambda_{1nk}^a}\right) + M_x^a M_y^a \\ G_{2a} &= M_x^a\left(\frac{-m}{\Lambda_{2nk}^a}\right) + M_y^a\left(\frac{-\hat{k}_{x2nk}^a}{\Lambda_{2nk}^a}\right) + M_x^a M_y^a \end{aligned} \tag{C-24}$$

for $\mu = 0$

$$G_{3a} = \gamma\frac{p_a}{p_o}\frac{a_o}{a_a}\left[M_x^a + M_y^a\left(\frac{-m}{\hat{k}_{x3nk}^a}\right)\right] \tag{C-25}$$

and for $\mu > 0$

$$\begin{aligned} G_{3a} &= \gamma\frac{p_a}{p_o}\frac{a_o}{a_a}\left[M_x^a\right] \\ G_{4a} &= \gamma\frac{p_a}{p_o}\frac{a_o}{a_a}\left[M_y^a\right] \end{aligned} \tag{C-26}$$

and the conservation equation for tangential momentum has the same form as the other 2 conservation equations

$$G_{1a}A_1^a - G_{2b}A_2^b - G_{3b}A_3^b - G_{4b}A_4^b = G_{1b}A_1^b - G_{2a}A_2^a - G_{3a}A_3^a - G_{4a}A_4^a \tag{C-27}$$

CONSERVATION OF RADIAL MOMENTUM

This, the 4th conservation equation, is only applied for $\mu > 0$, where there are 4 wave types. The unlinearized equation for transverse (y direction) momentum is

$$(\rho u w)_a = (\rho u w)_b \tag{C-28}$$

Using the same arguments as in the discussion of axial momentum, the first order conserved quantity can be written $\rho_a U_a \tilde{w}_a$. We define

$$H_a = \frac{1}{p_o}[\rho_a U_a \tilde{w}_a] \tag{C-29}$$

or, in terms of the 4 wave types, as

$$H_a = H_{1a} A_1^a + H_{2a} A_2^a + H_{3a} A_3^a + H_{4a} A_4^a \tag{C-30}$$

where

$$\begin{aligned}
H_{1a} &= M_x^a \left(\frac{-i\mu\pi / H_D}{\Lambda_{1nk}^a} \right) \\
H_{2a} &= M_x^a \left(\frac{-i\mu\pi / H_D}{\Lambda_{2nk}^a} \right) \\
H_{3a} &= \gamma \frac{p_a}{p_o} \frac{a_o}{a_a} M_x^a \left[\frac{-i m}{\mu\pi / H_D} \right] \\
H_{4a} &= \gamma \frac{p_a}{p_o} \frac{a_o}{a_a} M_x^a \left[\frac{-i \hat{k}_{x4nk}^a}{\mu\pi / H_D} \right]
\end{aligned} \tag{C-31}$$

and the conservation equation for radial momentum has the same form as the other 3 conservation equations

$$H_{1a} A_1^a - H_{2b} A_2^b - H_{3b} A_3^b - H_{4b} A_4^b = H_{1b} A_1^b - H_{2a} A_2^a - H_{3a} A_3^a - H_{4a} A_4^a \tag{C-32}$$

SOLUTION OF LINEAR SYSTEM

By "solution" here, we mean finding the scattered waves for specified input waves. To this end we assemble Eqs. C-12, C-20, C-27, C-32 into matrix form

$$\begin{bmatrix} C_{1a} & -C_{2b} & -C_{3b} & -C_{4b} \\ F_{1a} & -F_{2b} & -F_{3b} & -F_{4b} \\ G_{1a} & -G_{2b} & -G_{3b} & -G_{4b} \\ H_{1a} & -H_{2b} & -H_{3b} & -H_{4b} \end{bmatrix} \begin{bmatrix} A_1^a \\ A_2^b \\ A_3^b \\ A_4^b \end{bmatrix} = \begin{bmatrix} C_{1b} & -C_{2a} & -C_{3a} & -C_{4a} \\ F_{1b} & -F_{2a} & -F_{3a} & -F_{4a} \\ G_{1b} & -G_{2a} & -G_{3a} & -G_{4a} \\ H_{1b} & -H_{2a} & -H_{3a} & -H_{4a} \end{bmatrix} \begin{bmatrix} A_1^b \\ A_2^a \\ A_3^a \\ A_4^a \end{bmatrix} \tag{C-33}$$

Solution to this equation is

$$\begin{bmatrix} A_1^a \\ A_2^b \\ A_3^b \\ A_4^b \end{bmatrix} = \begin{bmatrix} C_{1a} & -C_{2b} & -C_{3b} & -C_{4b} \\ F_{1a} & -F_{2b} & -F_{3b} & -F_{4b} \\ G_{1a} & -G_{2b} & -G_{3b} & -G_{4b} \\ H_{1a} & -H_{2b} & -H_{3b} & -H_{4b} \end{bmatrix}^{-1} \begin{bmatrix} C_{1b} & -C_{2a} & -C_{3a} & -C_{4a} \\ F_{1b} & -F_{2a} & -F_{3a} & -F_{4a} \\ G_{1b} & -G_{2a} & -G_{3a} & -G_{4a} \\ H_{1b} & -H_{2a} & -H_{3a} & -H_{4a} \end{bmatrix} \begin{bmatrix} A_1^b \\ A_2^a \\ A_3^a \\ A_4^a \end{bmatrix} \tag{C-34}$$

or simply

$$\begin{bmatrix} A_1^a \\ A_2^b \\ A_3^b \\ A_4^b \end{bmatrix} = \begin{bmatrix} K_{11} & K_{12} & K_{13} & K_{14} \\ K_{21} & K_{22} & K_{23} & K_{24} \\ K_{31} & K_{32} & K_{33} & K_{34} \\ K_{41} & K_{42} & K_{43} & K_{44} \end{bmatrix} \begin{bmatrix} A_1^b \\ A_2^a \\ A_3^a \\ A_4^a \end{bmatrix} \tag{C-35}$$

APPLICATION OF SOLUTION

The objective of this analysis is to create rotor and stator acoustic elements that can be represented in the coupling system of Figure 13. For example, when the stator cascade (with uniform flow corresponding to region 2) is combined with an actuator disk at the trailing edge to turn the flow from the θ direction to axial, the result is the stator acoustic element. This is done by using Eqs. 6-13 and 6-14, which amounts to 4 equations for the input/output behavior of the actuator disk, and a similar set of 4 equations for the input output behavior of the stator cascade. Setting the output of the cascade (on the downstream side) to the input of the actuator disk (on the upstream side) and the output of the actuator disk to the input of cascade permits us to eliminate 4 equations. The result is Eq. 6-22 which represents the input/output characteristics of the combined stator element.

APPENDIX D
LIST OF SYMBOLS

a_r, a_o	speed of sound in region r , speed of sound on standard day at sea level
c_1 , c_2	chord of rotor and stator cascades
g	cascade gap
h	duct height in main part of report, gap perpendicular to blades in Appendices A & B
j	index for counting frequency from one mode sub-set to another
k	scattering index for stator
m	circumferential mode order
n	scattering index for rotor
p	acoustic pressure
p_r, p_o	pressure in region r, pressure on standard day at sea level
q	mode offset index
r	subscript (or superscript) for region (See Section 5). Also denotes rotor.
t	time
u, v, w	axial, tangential, and radial components of perturbation velocity
x, y, z	coordinates in "duct system" (x axis aligned with axis of rotor rotation)
x_c, y_c, z	coordinates in "cascade system" (x_c axis aligned with airfoil chord and mean flow)
w	upwash velocity component
A_r	$= a_r / a_o$
$A_T^r(n,k)$	modal coefficient in state vector. See Section 6. T is wave type, r is region, and n and k are the rotor and stator scattering indices.
$B_T^r(n,k)$	modal coefficient for source vector (related to turbulence in Section 7).
B_1 , B_2	Number of blades in rotor, vanes in stator
D	Glegg's potential jump. See Eq. A-2 of this report and Ref. 4.
E	Cutoff discriminator. See Eq. 7.10.
F_{nk}	Ratio of modal sound power to modal sound pressure, see Eq. 7.9.
H_D	h/R , annulus height/effective radius
I	acoustic intensity
K	Glegg's vorticity factor. See Eq. B-4 and Ref. 4.
L	turbulence scale/R
M_x, M_y	axial and tangential Mach numbers of mean flow, U/a_r and V/a_r
$P_T^r(\ )$	See Section 5
P_r	$= p_r / p_o$
R	"effective radius" of fan; used for scaling
$S_{T'T}^{r'r}(\ )$	scattering coefficient, see Section 5
T	wave type. See Section 5.
U	axial component of mean velocity
V	tangential component of mean velocity
W	mean velocity
A	state vector, see Section 6
B	source vector, see Section 6
S	scattering/coupling matrix, see Section 6

α chordwise wavenumber in cascade coordinate system

β $\sqrt{1-M^2}$

β_x $\sqrt{1-M_x^2}$

γ ratio of specific heats, 1.4 for air

$\delta_{i,j}$ Kroneker delta, = 1 for $i = j$ and = 0 for $i \neq j$

$\delta(\ )$ Dirac delta or impulse function

ε_μ = 1 for $\mu = 0$ and = ½ for $\mu > 0$

$\bar{\varepsilon}_\mu$ = 2 for $\mu = 0$ and = 1 for $\mu > 0$

ϕ = y/R, tangential angle in duct coordinates

μ radial mode order

ν radial wavenumber = $\mu\pi/H_D$

λ result of convective derivative acting on exponentials, see Eq. 3-7

σ interblade phase angle

θ stagger angle

ρ density

τ one half the time for the block of flow under consideration to pass through the cascade, see discussion in conjunction with Eqs. 7-25 – 7-29

ω 2π times frequency

ω_0 offset frequency

Ω angular speed of rotor

Λ $\lambda R / a_r$

superscripts

$(\ )^r$ region =1 upstream of rotor, =2 between rotor and stator, =3 downstream of stator

$(\ )^*$ complex conjugate

subscripts

$(\ )_T$ denotes wave type, see Section 5

overbars and hats

$\overline{(\ )}$ normalization by chord

$\tilde{(\ )}$ normalization by R

REPORT DOCUMENTATION PAGE

Form Approved
OMB No. 0704-0188

1. AGENCY USE ONLY (*Leave blank*)	2. REPORT DATE	3. REPORT TYPE AND DATES COVERED
	December 2003	Final Contractor Report

4. TITLE AND SUBTITLE

Broadband Noise of Fans—With Unsteady Coupling Theory to Account for Rotor and Stator Reflection/Transmission Effects

5. FUNDING NUMBERS

WU–781–30–11–00
NAS3–27727
AST Task 13

6. AUTHOR(S)

Donald B. Hanson, Consultant

7. PERFORMING ORGANIZATION NAME(S) AND ADDRESS(ES)

Pratt & Whitney
400 Main Street
East Hartford, Connecticut 06108

8. PERFORMING ORGANIZATION REPORT NUMBER

E–12989–1

9. SPONSORING/MONITORING AGENCY NAME(S) AND ADDRESS(ES)

National Aeronautics and Space Administration
Washington, DC 20546–0001

10. SPONSORING/MONITORING AGENCY REPORT NUMBER

NASA CR—2001-211136-REV1

11. SUPPLEMENTARY NOTES

Project Manager, Dennis L. Huff, Structures and Acoustics Division, NASA Glenn Research Center, organization code 5940, 216–433–3913.

12a. DISTRIBUTION/AVAILABILITY STATEMENT

Unclassified - Unlimited
Subject Category: 71 Distribution: Nonstandard

Available electronically at http://gltrs.grc.nasa.gov/GLTRS

This publication is available from the NASA Center for AeroSpace Information, 301–621–0390.

12b. DISTRIBUTION CODE

13. ABSTRACT ***(Maximum 200 words)***

This report examines the effects on broadband noise generation of unsteady coupling between a rotor and stator in the fan stage of a turbofan engine. Whereas previous acoustic analyses treated the blade rows as isolated cascades, the present work accounts for reflection and transmission effects at both blade rows by tracking the mode and frequency scattering of pressure and vortical waves. The fan stage is modeled in rectilinear geometry to take advantage of a previously existing unsteady cascade theory for 3D perturbation waves and thereby use a realistic 3D turbulence spectrum. In the analysis, it was found that the set of participating modes divides itself naturally into "independent mode subsets" that couple only among themselves and not to the other such subsets. This principle is the basis for the analysis and considerably reduces computational effort. It also provides a simple, accurate scheme for modal averaging for further efficiency. Computed results for a coupled fan stage are compared with calculations for isolated blade rows. It is found that coupling increases downstream noise by 2 to 4 dB. Upstream noise is lower for isolated cascades and is further reduced by including coupling effects. In comparison with test data, the increase in the upstream/downstream differential indicates that broadband noise from turbulent inflow at the stator dominates downstream noise but is not a significant contributor to upstream noise.

14. SUBJECT TERMS

Fan noise; Broadband noise; Rotor-stator; Acoustics; Turbomachinery

15. NUMBER OF PAGES

94

16. PRICE CODE

17. SECURITY CLASSIFICATION OF REPORT	18. SECURITY CLASSIFICATION OF THIS PAGE	19. SECURITY CLASSIFICATION OF ABSTRACT	20. LIMITATION OF ABSTRACT
Unclassified	Unclassified	Unclassified	